Macro-Fiber Composites for Sensing, Actuation and Power Generation

by

Henry A. Sodano

Thesis Submitted to the Faculty of the
Virginia Polytechnic Institute and State University
in partial fulfillment of the requirements for the degree of

Master of Science

in

Mechanical Engineering

Dr. Daniel J. Inman, Chair
Dr. Donald J. Leo
Dr. Gyuhae Park

July 28, 2003

Blacksburg, Virginia

Keywords: Piezoelectric, macro-fiber composite, self-sensing, inflatable structures, power harvesting

Macro-Fiber Composites for Sensing, Actuation and Power Generation

Henry A. Sodano

Abstract

The research presented in this thesis uses the macro-fiber composite (MFC) actuator that was recently developed at the NASA Langley Research Center for two major themes, sensing and actuation for vibration control, and power harvesting. The MFC is constructed using piezofibers embedded in an epoxy matrix and coated with Kapton skin. The construction process of the MFC affords it vast advantages over the traditionally used piezoceramic material. The MFC is extremely flexible, allowing it to be bonded to structures that have curved surface without fear of accidental breakage or additional surface treatment as is the case with monolithic piezoceramic materials. Additionally the MFC uses interdigitated electrodes that capitalize on the higher d_{33} piezoelectric coupling coefficient, allowing it to produce higher forces and strain than typical monolithic piezoceramic materials. The research presented in this thesis investigates some potential applications for the MFC as well as additional topics in power harvesting.

This first study performed was to determine if the MFC is capable of being used as a sensor for structural vibration. The MFC was incorporated into a self-sensing circuit and used to provide collocated control of an aluminum beam. It was found that the MFC makes a very accurate sensor and was able to provide the beam with over 80% vibration suppression at its second resonant frequency. Following this work, the MFC was used as both a sensor and actuator to apply multiple-input-multiple-output vibration control of an inflated satellite component. The control system used a positive position feedback (PPF) controller and two pairs of sensors and actuators in order to provide global vibration suppression of an inflated torus. The experiments

found that the MFC and control system was very effective in attenuating the vibration of the first mode but ineffective at higher modes. It was found the positioning of the sensors and actuators on the structure contributed heavily to the controller's performance at higher modes. A discussion of the reasons for the controller's ineffectiveness is supplied and a solution using self-sensing techniques for collocated vibration suppression is investigated.

Subsequent to the research in vibration sensing and control, the ability to use piezoelectric materials to convert ambient vibration into usable electrical energy was tested and quantified. First, a model of a power harvesting beam is developed using variational methods and is validated on a composite structure containing four separate piezoelectric wafers. It is shown that the model can accurately predict the power generated from the vibration of a cantilever beam regardless of the load resistance or excitation frequency. The damping effects of power harvesting on a structure are also demonstrated and discussed using the model. Next, the ability of the piezoelectric material to recharge a battery and a quantification of the power generated are investigated. After determining that the rechargeable battery is compatible with the power generated through the piezoelectric effect, the MFC was compared with the traditional monolithic PZT for use as a power harvesting material. It was found that the MFC produces a very low current, making it less efficient than the PZT material. Furthermore, because of the low current generation of the MFC, it was unable to charge batteries because of their need for relatively large current. Due to the MFC being incapable of charging batteries, only the PZT was used to and the charge times for several nickel metal hydride batteries ranging from 40 to 1000mAh are supplied.

Acknowledgments

First I would like to extend my sincerest thanks to my advisor Dr. Daniel J. Inman for his support throughout my work, insight and lighthearted nature that has made working in CIMSS truly a pleasure. Additionally, Dr. Inman's sense of humor provides a good laugh and smile during every conversation. I would also like to graciously thank Dr. Gyuhae Park who provided me with the inspiration and encouragement to successfully complete all of my research efforts without significant pain. Without his contributions to this work and his ability to see the long term goals, the research presented in this thesis would have never been completed so timely. The research that we have completed together has also left what I am sure will be a lifelong friendship. I would also like to extend my thanks to my committee member Dr. Donald J. Leo for his advice throughout this work and giving me a chance to perform research at CIMSS, without Dr. Inman's invitation to do summer research I am sure that I would not have had such a pleasurable experience as a graduate student.

I would also like to thank my family for their support and love throughout my undergraduate and graduate studies. Their encouragement convinced me that a graduate degree was the best direction for me to take, which I am now sure was the correct choice. In addition, I would like to thank my loving girlfriend Lisa Franks for her support and encouragement when I though that I was beat. Without her I would have far more grey hairs than I gained in the last year. Finally, I must extend thanks to all the members of CIMSS, so many of which have provided me with insight and ideas for successfully completing this research effort.

Table of Contents

List of Tables

List of Figures

Nomenclature

α = proportional damping constant

a = acceleration

A = amplitude of vibration

β = proportional damping constant

b = width of beam

c = modulus of elasticity

C_p = capacitance of piezoelectric

C = damping matrix

δ = variation

d = displacement

d_{ij} = piezoelectric constant relating voltage and stress

D = Electric Displacement

E = electric field

e = piezoelectric coupling coefficient

f = external force

F = applied force

K = stiffness

L = length of beam

m = total number of data points

M = mass

η = efficiency

n = data point index

P = power

ψ = location of electrical potential

q = electrical charge

ρ = density

r = temporal coordinate of displacement

R = resistance

ε = dielectric constant

S = strain

t = thickness of beam or time

t_p = thickness of piezoelectric

T = kinetic energy or stress in piezoelectric constitutive equations

θ = piezoelectric coupling matrix

u = displacement

U = potential energy

v = voltage

V = volume, chapter 4

V = voltage drop across load resistance, chapter 5

V.I. = variational indicator

Φ = mode shapes

ω = natural frequency

ζ = damping ratio

Superscript

E = parameter at constant electrical field (short circuit)

S = Value taken at constant strain

T = parameter at constant stress or transpose

Subscript

p = piezoelectric

s = structure

Chapter 1

Introduction

1.1 Introduction to Piezoelectricity

Piezoelectric materials have the unique ability to interchange electrical energy and mechanical strain energy or force. Due to this characteristic of the material, it has been found to be very effective for use in dynamic applications involving vibration suppression and sensing. However these materials have been used in numerous other applications including sonar, audio buzzers, air ultrasonic transducers (e.g. television remote controls) and piezoceramic ignition systems (www.piezo.com). While these materials have found notable applications, piezoelectrics devices have not found the market (except for push button igniter systems) that will allow the production rates of the material to have substantial growth causing the cost to be dragged down and become cost effective in numerous other applications.

1.1.1 History of Piezoelectricity

In 1880, the first experiment displaying the piezoelectric effect was performed on specially prepared crystals (quartz, topaz, tourmaline, cane sugar and Rochelle salt) and published by Pierre and Jacques Curie. The crystals were subjected to a mechanical stress and a conclusive measurement of surface charge was made. This discovery was termed piezoelectricity to distinguish it from other areas of phenomenological experience such as “contact electricity”

(friction generated static electricity) and "pyroelectricity" (electrical energy generated from the heating of crystals). The Currie brothers asserted that there was a one to one correspondence between the electrical effects of temperature change and mechanical stress. This prediction allowed the brothers to use their understanding of the microscopic and crystallographic origins of piezoelectricity to effectively choose the crystals for use in the experiments as well as the cuts of these crystals.

While the Currie brothers were able to predict that electricity could be generated from an applied stress (direct piezoelectricity), they did not predict the opposite effect, know as converse piezoelectricity. Direct piezoelectricity illustrates that when a mechanical stress is applied to the material an electric charge results, this converse phenomena illustrates that the application of an electrical field creates a mechanical stress. The converse piezoelectric effect was later mathematically proven in 1881 by Lippman using the fundamental thermodynamic principles. The converse piezoelectric effect was quickly confirmed by the Curies and quantitative proof of the complete reversibility of electro-elasto-mechanical deformations in piezoelectric crystals was later obtained.

After its discovery and until the early 1900's, piezoelectricity was mainly a topic of scientific interest. The early twentieth century was producing many new machines, none of which incorporated piezoelectricity. The reason for the lack of applications, was primarily because piezoelectricity was an obscure science and the recently developed mathematics describing this phenomenon were very complicated and hard to understand. However, in 1916 during World War I, Paul Langevin of France developed the first engineering use for piezoelectricity by developing an ultrasonic submarine detector. The device was termed the "Langevin type transducer," later to be perfected and lead to sonar devices which are used extensively to this day. The Langevin type transducer was constructed of and array of thin quartz crystals sandwiched between two metal plates. When the quartz crystals were excited through the piezoelectric effect, the plates emitted high frequency sound waves into the water. A second quartz device was then used to detect the return of the sound wave. The time required for the sound wave to leave the first transducer and return to the second contained information revealing the depth of the submarine.

Following the development of Langevin's transducer, a conference was held in 1917 under the direction of Robert A. Milliken and sponsored by the National Research Council. At

this conference the early sonar device was revealed to the public. One of the researchers invited to this conference was Walter G. Cady, who had an interest in submarine detection. After hearing the news and learning of piezoelectric materials, he became so intrigued that he embarked on a lifelong journey developing piezoelectric principles and applications. From 1917 through the 1940's Cady's work as well as others led to a period of intense development of piezoelectric devices. During this period of intense piezoelectric research, numerous applications were developed that we now find common including microphones, accelerometers, ultrasonic transducers, bender element actuators and phonograph pick-ups.

With the amount of research and number of applications involving piezoelectric materials growing, the production quantity and feasibility of the products was limited by material performance. Beginning the mid 1930's, there were some advances in the production of materials with higher piezoelectric properties, leading to the development of the crystal ADP (ammonium-dihydrogen-phosphate). ADP possessed the rugged characteristic of the quartz crystal and the strong piezoelectric characteristics of Rochelle salt (Inman et al., 2000). In addition to ADP several other piezoelectric crystals were identified, a few of the more effective ones are EDT (ethylene diamine tartrate), DKT (dipotoassium tartrate) and $BaTiO_3$ (Barium Titanium Oxide). The advances made in these crystals lead to the development of wave filters for use in multi-channel telephony work at Bell telephone Laboratories. However, while these new crystals held vast improvements over there predecessors they still left room for further development.

The next step in the development of high performance piezoelectric materials occurred during World War II. In the U.S., Japan and the Soviet Union, isolated research groups were developing advanced capacitor materials and found that certain ceramics prepared by sintering metallic oxide powders, exhibited dielectric constants up to 100 times greater than those of the commonly cut crystals of the time. In addition, ferroelectric materials were constructed to have similar improvements in piezoelectric properties. The most notable of these early ferroelectric materials was Barium titanate that had piezoelectric properties similar to that of Rochelle salt but was not water soluble, could withstand higher operating temperatures and was capable of being manufactured in many different shapes and sizes due to its ceramic substance. This discovery of an easily manufactured piezoelectric ceramic with far greater performance than any other to date sparked a new period of intense research and development of piezoelectric devices.

The greater research efforts began to produce ceramic materials with better piezoelectric properties than Barium titanate, leading to the development of numerous materials, the most notable of these being lead metaniobate (PMN) and lead zerconate titanate (PZT). These two materials are still among the most used for piezoelectric applications today. Following the development of the piezoceramic was the piezoelectric semiconductor film and piezoelectric polymers. The most notable of the piezo-polymers is the polyvinylidene fluoride film (PVDF), which is still heavily used.

During this new found search for piezoelectric materials, processing and production methods were dominated by industrial groups in the United States who secured an early position in the market with strong patents. However, after the war, advances were made in individual private companies who felt the newly developed products would produce the most profit with strong patents and secrete processes. This closed research market for piezoelectric devices caused the amount of new market development in the United States to be substantially limited.

While the United States were working with a closed flow of ideas between companies, Japanese companies and universities formed a group of researchers dedicated to the open flow of ideas and applications involving piezoelectric materials, deemed the Barium Titanate Application Research Committee, in 1951. This organization allowed technical challenges and new market areas to be overcome and developed with far greater ease than the closed flow of ideas seen in the U.S. Due to this type of research the Japanese began to lead the piezoelectric market and in 1951 the successful test of a fish-finder allowed them gain the upper hand in the world market of piezoelectric products. The continuing effort of the Japanese groups led to the development of unpatented piezoelectric materials with performance close to that of PZT. This new freely available piezoelectric material was all that they needed to begin filling and opening new markets for there continued production of creative products.

The success of the Japanese has led other nations to develop heavy research programs in the area of piezoelectrics and other smart materials. The increase in research is reflected through the steady rise in piezo patents granted as well as the substantial rise of publications in this area from Russia, China and India. This increase in research with piezoelectric materials will certainly bring about new innovative products and materials as it has in the past. For a more detailed account of the history of piezoelectric materials see www.piezo.com and Inman and Cudney (2000).

1.1.2 Piezoceramic Fiber Actuators

Since the development of piezoceramic materials they have been used extensively in the fields of sensing and actuation. However, these materials have several properties that limit their application in real systems. Due to the ceramic nature of the monolithic piezoelectric material they are very brittle, making them vulnerable to accidental breakage during handling and bonding procedures. In addition, they have very poor ability to conform to curved surfaces and are very dense and stiff causing mass loading and localized stiffness to be a factor when working with very flexible or lightweight structures. These limitations have motivated researchers to develop alternative methods of manufacturing the piezoceramic to better suit it for the next generation of piezoelectric applications.

To resolve the inadequacy of the monolithic piezoceramic material for many applications, the idea of using a composite material consisting of an active piezoceramic fibrous phase embedded in a polymeric matrix phase was investigated. Typically when in fiber form crystalline materials have much higher strengths, where the decrease in volume fraction of flaws leads to and increase in specific strength (Williams et al., 2002). In addition to this added strength of the base material, the flexibility of the polymer matrix allows the piezoceramic fibers to have greatly increased conformability to curved surfaces and provides a protective shell around the piezoelectric material. This polymer shell allows the piezofiber to withstand impacts and harsh environments far better than monolithic piezoelectric materials. The result of configuring the piezofiber inside a polymer matrix is an actuator that can be incorporated into or bonded to more realistic structures.

Several actuators that incorporate piezofiber technology are commercially available or under development at research institutes, namely the 1-3 composites by Smart Materials Corp. (http://www.smart-material.com), active fiber composite (AFC) actuators developed by MIT (Bent, 1993a, 1993b, 1994, 1995, 1997 and Janos et al., 1998), and macro-fiber composite (MFC) actuators constructed at NASA Langley Research Center (Wilkie et al, 2000). In the following sections I will give a brief introduction to each of these different actuators, for a more detailed description of each of these materials, consult their corresponding references. In addition the company responsible for the 1-3 composite actuators, Smart Materials Corp. was given the contract from NASA to market the MFC and information regarding these actuator can be found on the website www.smart-material.com.

1-3 Composites

The 1-3 composite actuator from Smart Material Corp. consists of piezoelectric rods embedded in a polymer matrix. The piezoelectric ceramic material is aligned through the longitudinal direction while the polymer phase is continuous in all three directions, hence its name 1-3 composite. These actuators are constructed using a patented soft mold process that was invented at the Fraunhofer Research Facility in Germany. This process consists of copying a reusable soft mold from a positive form of the final structure then filling the mold with the piezoceramic material. Once the mold is filled with the piezoelectric material it is fired to sinter the piezoceramic. Using this process the active pixels can be constructed in either round (70 micron diameter with 50-micron spaces) or rectangular (80 microns with 120 micron spaces) as shown in Figure 1.1. This soft molding process holds many advantages over the previously used die-and-fill, injection molding or dicing techniques due to the molds being reusable, allowing thousands like actuators to be made. In addition, the fabrication is relatively easy and cost effective because of the simplicity of the mold construction when compared to the other options for fiber construction. Once the brittle fibers are formed a polymer matrix is added to the remaining spaces to protect the fibers from breakage. Subsequent to this process is the addition of metal electrodes for poling of the device, later to be used as a means of applying an electric field or measuring the current produced during sensing.

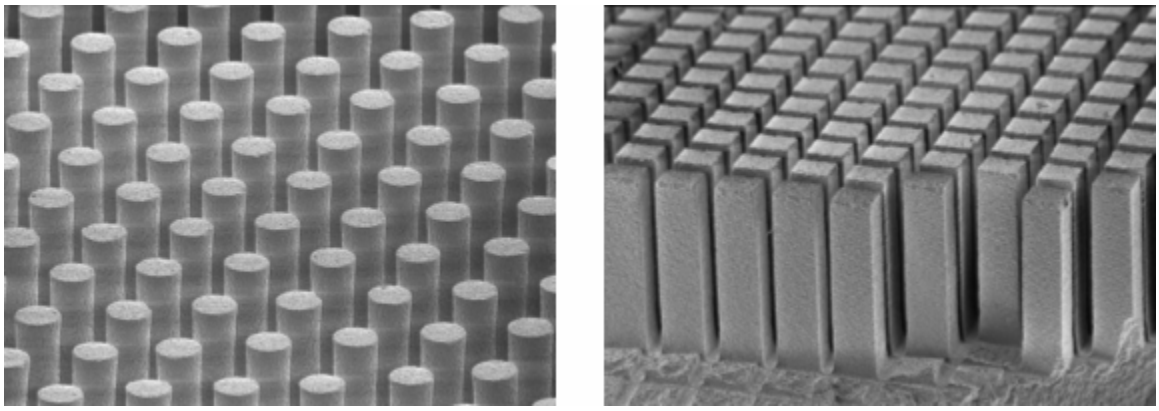

a) b)

Figure 1.1: 1-3 composite actuators by Smart Materials Corp. piezoceramic rods with a) round fibers and b) rectangular fibers (http://www.smart-material.com).

These actuators provide several advantages over the monolithic piezoceramic due to lower acoustic impedance, higher coupling coefficients providing more effective conversion of

electrical energy into mechanical energy and vice versa, reduced lateral coupling due to isolated fibers, greater flexibility through the polymer matrix and higher bandwidths up to 10 Mhz (Gebhardt et al., 1999). These advantages have made the 1-3 composite actuators a popular choice for ultrasound applications, including medical ultrasound, flow control, sonar, non-destructive testing and broadband transceivers. In addition to these applications, the 1-3 composite is used for attenuation of acoustic waves in smart composite panels. This is achieved by sandwiching the actuator inside of two composite panels. When this arrangement is attached to a structure such as an aircraft fuselage it can be used to attenuate noise levels, function as pressure sensors or reduce the broadband vibration levels inside the fuselage of an aircraft by 20 dB (http://www.msiusa.com).

Active Fiber Composites

The active fiber composite (AFC) actuator developed at MIT's Active Materials and Structures Lab is another type of piezoceramic fiber composite actuator that has seen much attention due to its wide range of potential applications. This actuator is constructed of unidirectional aligned piezoceramic fibers surrounded by a polymer matrix. The AFC can also be adapted such that inactive glass fibers are inserted into the polymer matrix to add additional structural strength. A photomicrograph of the cross section of an AFC with glass fiber reinforcement added is shown in Figure 1.2, where the piezoceramic fibers are 130 microns in diameter and the S-glass fiber have a diameter of 5 microns.

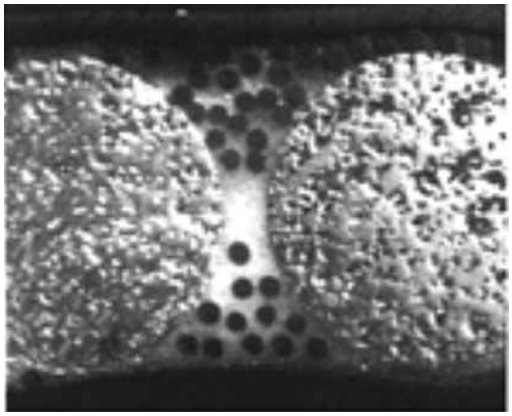

Figure 1.2: Cross section of the AFC with glass rods (Williams, R. 2002).

The piezoceramic fibers are produced through a patented injection molding process (Gentilman et al., 2003). The procedure combines either PZT or PMN powder with a wax based

binder, and then the material is granulated as feedstock for the injection molding process. Once this is completed the feedstock is heated to the specified viscosity and rapidly injected at high pressure into a cooled mold. Due to the incompressible nature of the material, when injected into the mold the fibers obtain a constant density throughout and alleviate issues of voids and internal defects that occur during dry pressing or low pressure forming methods. The homogeneous density of the material produces like microstructures, dimensions and electromechanical properties after firing.

After the production of the piezoceramic fibers an electrode is layer is placed on the top and bottom of the fibers to facilitate the application or an electric field of the collection of current during sensing. The AFC uses interdigitated electrodes that allow the electrical potential to form along the length of the fiber; therefore capitalizing on the higher d_{33} piezoelectric coupling coefficient, a schematic to help visualize the electric field developed along the fibers is shown in Figure 1.3. The metallic electrodes are normally formed using photolithography, which is a very accurate process, however it is a time consuming and expensive process that etches copper strips onto a thin Kapton® film. A second method can be used to avoid this process that consists of screen-printing silver ink onto a thin Kapton® sheet. While this method is quick and inexpensive it is also inaccurate and produces variations in electrode pattern, in addition to having a limited ductility resulting in a shorter lifespan of the final product (Williams, R. 2002).

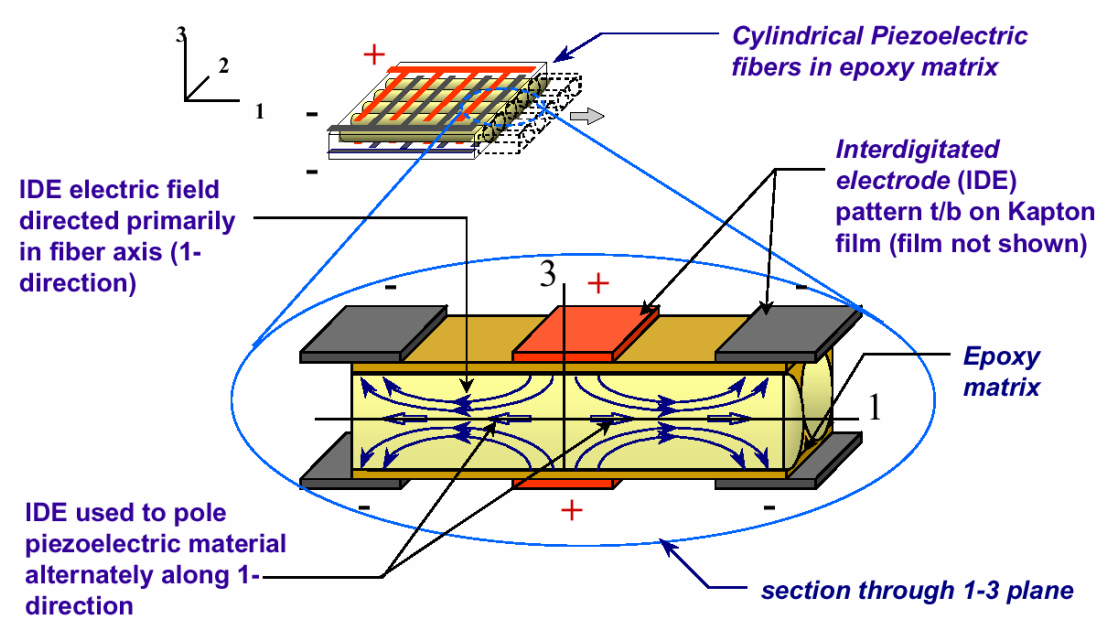

Figure 1.3: Schematic of the cross section of an AFC actuator (Wilkie, 2000).

The final assembly of the AFC is fairly complicated; Figure 1.4 helps to visualize this process. The process begins with the bottom electrode being placed on the aluminum vacuum plate using the locator pins. The piezoelectric fibers are then laid out carefully on the bottom electrode making sure that the fibers are in a single layer and are as parallel to one another as possible. With the piezoceramic fibers laid out the glass fibers or other material can be included if desired, in order to increase the strength of the actuator. The next step is to insert the Kapton® molds along the edges of the electrodes to retain and form the polymer matrix that will be added. With the Kapton molds in place an epoxy resin doped with an air release agent is applied to the fibers and any inactive material that was added, then the top electrode is aligned on top of the fibers using the positioning holes. With the final layout of the actuator positioned, the plate is placed in a press, where heat and pressure are applied to aid in the curing of the epoxy resin. This process utilizes the vacuum port, which minimizes the amount of void formation in the actuator.

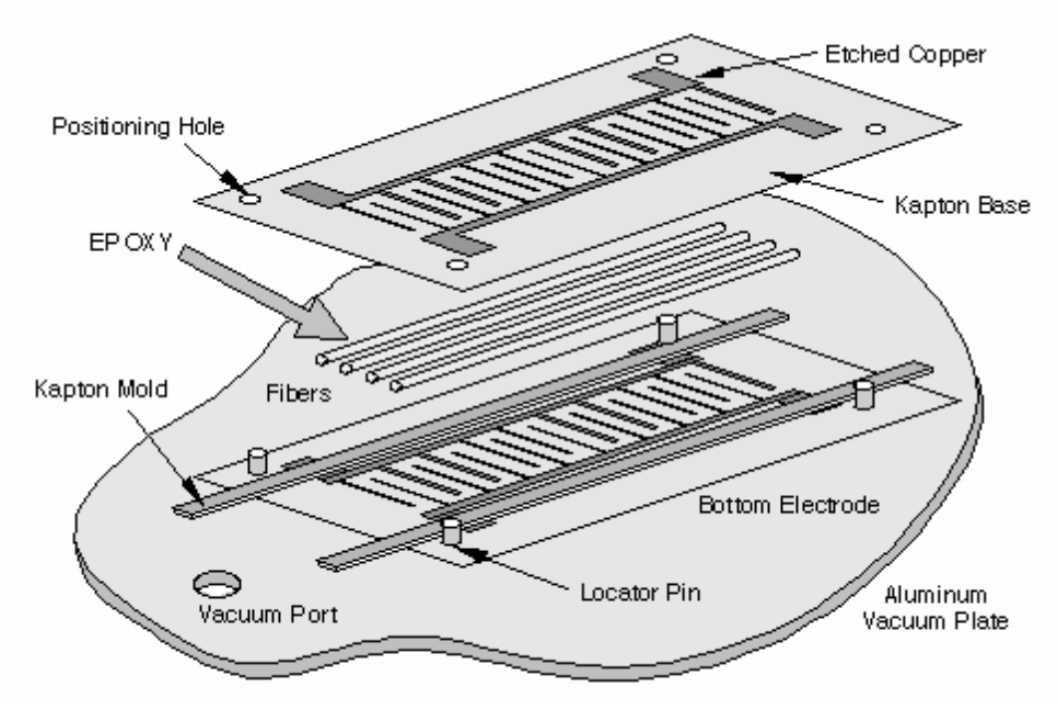

Figure 1.4: Schematic of the manufacturing process of the active fiber composite (Williams, R. 2002).

The final product is an actuator that has increased flexibility, durability and electro-mechanical coupling due the interdigitated electrodes that capitalize on the higher d_{33} coefficient. This type of technology has many possible structural applications; however, the assembly can be

avoided and the fiber can be incorporated directly into any laminated composite material. One of the major considerations for use of this property is to incorporate the fibers into the rotor blades of a helicopter. The helicopter blades experience large aerodynamic loads and in turn induce large vibration and noise issues. With the active fiber embedded inside the rotor blade the vibration and noise levels inside the helicopter could be significantly reduced providing increased comfort to the pilot and passengers of the aircraft.

Macro-Fiber Composites

The third and last type of piezoceramic fiber actuator that will be discussed is the macro-fiber composite (MFC) actuator that was developed at the NASA Langley Research Center. The MFC is similar to the AFC because both consist of the same three primary components; active piezoceramic fibers aligned in a unidirectional manner, interdigitated electrodes, and an adhesive polymer matrix, the layers of the MFC are shown in Figure 1.5. However, the MFC has one difference that greatly affects the manufacturing process and the performance of the actuator, it has rectangular fibers. A photomicrograph of the cross section of an MFC showing the rectangular fibers is shown in Figure 1.6, where the fiber's length and height are 356 and 178 micron respectively (Wilkie, 2000).

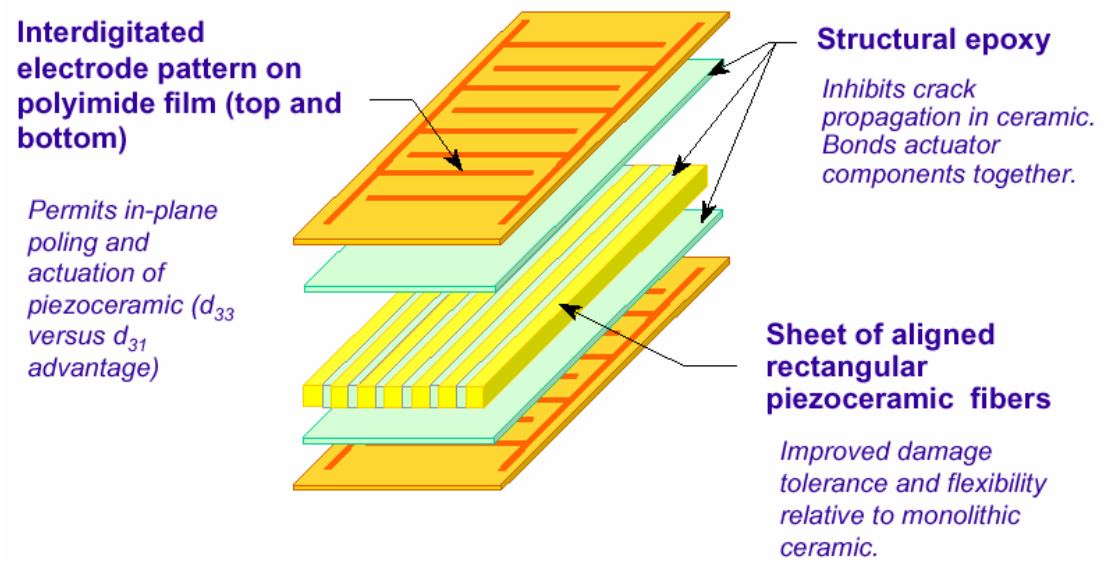

Figure 1.5: Schematic showing the order of different layers in the macro-fiber composite actuator.

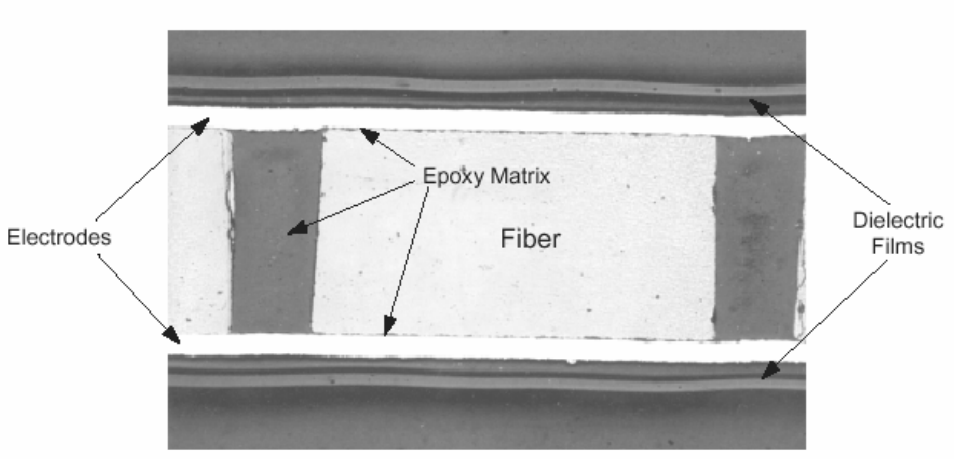

Figure 1.6: Photomicrograph of the cross section of a macro-fiber composite actuator (Wilkie, 2000).

The fibers of the MFC have a rectangular cross section due to the method used to form the fibers. Instead of forming them through an injection molding process as done in fabrication of the AFC, they are machined from low cost piezoceramic wafers and a computer controlled dicing saw, this process is shown in Figure 1.7. It can also be seen in Figure 1.7 that the piezoceramic wafer is laid on top of a blue surface, this is the polymer carrier film that is used to hold the fibers in place during handling and machining of the fibers.

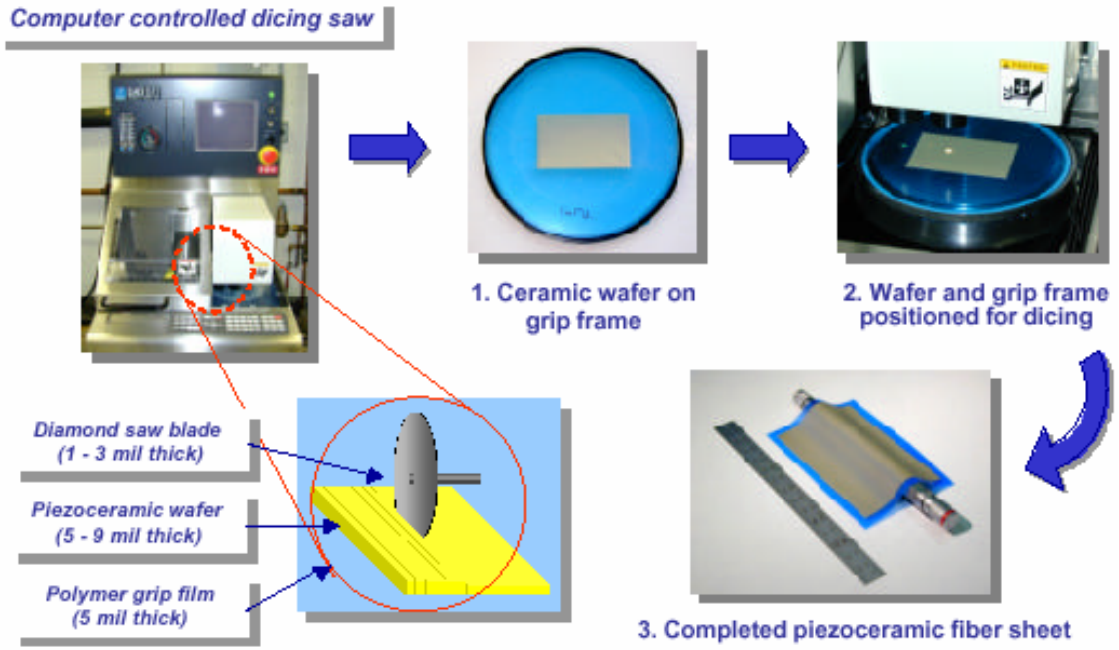

Figure 1.7: Fabrication process of the macro-fiber composite piezofibers (Williams, 2000).

The other two components of the MFC are the polymer matrix and the interdigitated electrodes. The interdigitated electrodes are made using a photoresist-and-etch process on commercially available copper-clad polyimide film. After the piezoceramic wafer has been cut it is then transferred and fixed to the bottom electrode film using a thermosetting epoxy adhesive that functions as the polymer matrix material. The sheet is then slightly heated to allow the epoxy to secure the piezoceramic fibers and ensure they are properly aligned. Once the fibers are secure the polymer carrier sheet is removed and a layer of thermosetting epoxy is added to the top before applying the top electrode sheet, this process of bonding the electrode layer is shown in Figure 1.8. After all layers of the MFC are stacked together the entire assembly is placed inside of a vacuum press were heat and pressure is applied to reject the formation and growth of voids in the epoxy matrix.

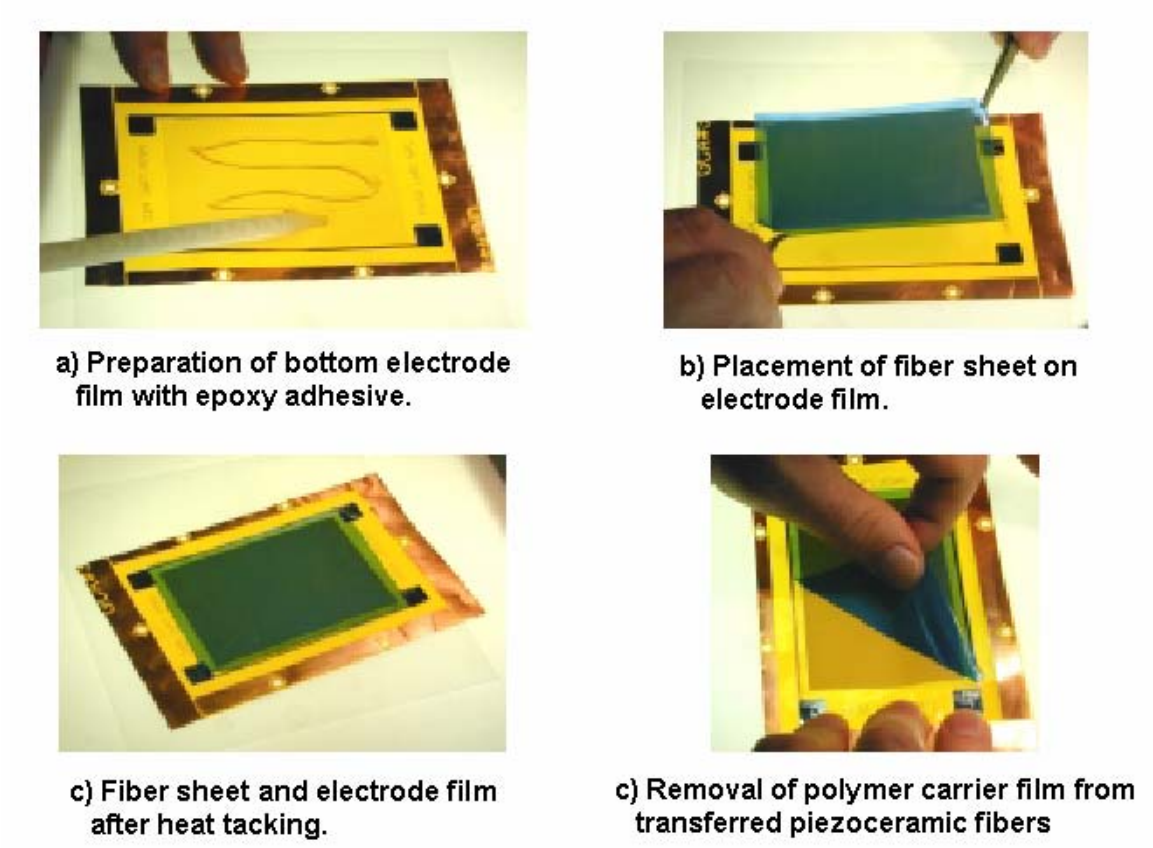

Figure 1.8: Integration of the active fibers and the interdigitated electrodes (Willie, 2000).

Like the AFC, the MFC is extremely flexible, durable and has the advantage of higher electromechanical coupling coefficients granted through the interdigitated electrodes. However,

the manufacturing processes discussed in the previous paragraphs allow the MFC to be produced at a much lower cost than the AFC and therefore are causing the AFC to be overlooked when determining the ideal actuator for a specific application. As mentioned earlier the MFC is a new technology and has not been tested in many of it potential applications. One application that has seen a lot of interest consists of bonding MFC patches to the vertical tail of fighter aircraft. Each side of the tail fin will have five MFC actuators embedded under the fiberglass shell as shown in Figure 1.9. These actuators will function as a means for counteracting the bending and torsional stresses that are inflicted on the tail during flight as a result of buffeting loads. The MFC actuator has also seen attention for use in inflatable satellite applications. The role of MFC in these applications will be discussed in the following sections.

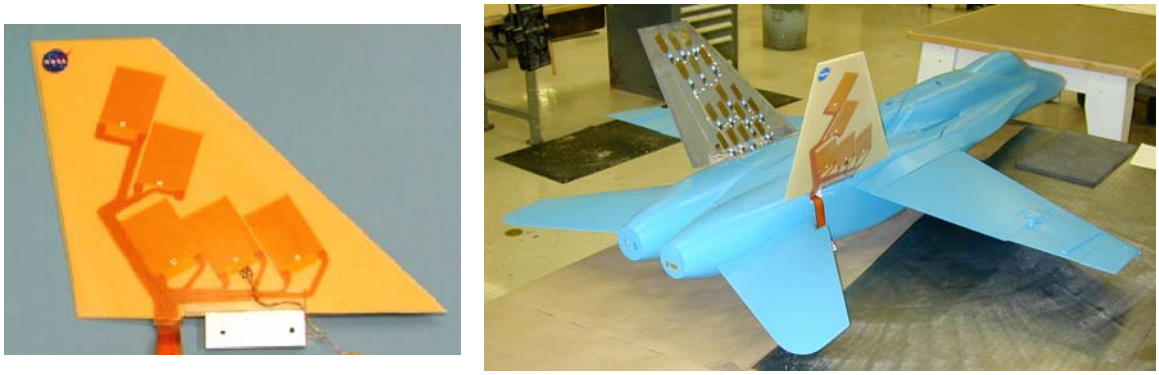

Figure 1.9: Scaled model of fighter jets vertical tail fins with MFC embedded into the fiberglass shell (Figures from NASA).

1.2 Literature Review

The following sections will discuss research that has been previously carried out in the topics of inflatable structures, vibration suppression using piezoelectric devices and power harvesting. Although much of the work reviewed in this section was carrier out using monolithic piezoelectric devices the scope of this thesis is to use piezoceramic fiber composites in these applications.

1.2.1 Inflatable Satellites

Inflatable satellites have become increasingly popular over the past few decades. These structures pose certain advantages over traditional satellites, such as minimal launch mass and volume. The satellite is compactly packaged before its launch into space and once in orbit the structure is deployed and inflated. Because the satellite is packaged for the duration of time it is in the shuttle bay, the device can be made to become far larger than any other solid satellite. This advantage is necessary for space antennas, which require very large surface areas. However, these advantages do carry a drawback; the dynamics of inflatable structures are considerably more difficult to analyze and test than a ridged structure. While there has been considerable research into the analysis of inflatable structures the amount of experimental ground testing of their dynamics had seen far less attention until recently. For the inflatable satellite to succeed, it is critical that these dynamics be understood.

History of Inflatable Satellites

The beginning of inflatable satellites was marked by the development of three inflatable devices by the Goodyear Corporation. In a period of time stretching from the late 1950's to the early 1960's, Goodyear developed an inflatable search antenna, radar calibration sphere and lenticular inflatable parabolic reflector (Freeland et al, 1998). The search antenna used a rigidizing support structure that was able to fold up into a compact, lightweight package. The third structure developed at Goodyear was the lenticular inflatable parabolic reflector that pioneered some of the inflatable satellite technology presently used, including the construction of antenna supported in a toroidal ring. These early developments in inflatable technology provided key innovations in the areas of fabrication, bonding of structural elements, packaging and deployment.

The innovative structures built at Goodyear were the first to use inflatable technology, however, none of their structures made it into space. The proof that inflatable satellites could be effectively deployed in space was demonstrated with NASA's launch of the Echo 1A satellite on August 12th 1960. The Echo 1A satellite (often referred to as the Echo 1 satellite due to a launch vehicle failure before deployment of the actual Echo 1 satellite) was a 30.5 m diameter balloon constructed of 12.7 micron thick metallized mylar, designed to act as a passive communications

reflector. One of the major reasons for using inflatable satellites is their extremely efficient use of space when packaged; this was shown with the Echo 1 that had an inflated diameter of 30.5 m and a packaged diameter of 66 cm. The Echo 1 was functional and used to redirect transcontinental and intercontinental telephone, radio and television signals. This pioneering satellite in the field of inflatable structures was followed by the Echo 2 satellite in January of 1964. However, following the launch of Echo 2 the inflatable satellite program died down and would not see another functional satellite launch for 32 years.

After the Echo Balloons program, the European Space Agency (ESA) began to show interest in inflatable structures by sponsoring the structural concept development of reflector antenna and sun shades at the Contraves Space Division in Switzerland. From the late 1970's till the early 1980's two antenna were built and tested but were never functional like the Echo 1 and 2 balloons. This program did however make progress in the field of inflatable structures. One of the antennas that they constructed was tested for the surface precision of the reflector and other mechanical characteristics. The researchers found that the 10 x 12 meter antenna had a reflection precision of a few millimeters RMS, Freeland et al. (1998) states that this accuracy is quite good for the antenna's size.

Following the ESA's inflatable satellite program, NASA began sponsoring the In-Space Technology Experiments Program's (In-STEP) Inflatable Antenna Experiment (IAE) that resulted in the launch of the next functional inflatable satellite. On May 19, 1996 the Space Shuttle Endeavour carried the Spartan 207/Inflatable Antenna Experiment (Sp207/IAE) into orbit. The inflatable satellite was constructed of Mylar reflective antenna held in place by an inflated torus and three 28 meter inflated struts; the Spartan 207/IAE in orbit is shown in Figure 1.10. The goals of this program were, a) to develop an inexpensive inflatable space structure, b) demonstrate the packaging efficiency of functional inflatable devices, c) show the reliability of the deployment of the satellite and d) develop a large reflective membrane antenna with a surface precision of a few millimeters RMS. These goals were accomplished and the inflatable antenna was successfully inflated in orbit, with the only issues arising in unexpected dynamics of the structure during deployment (Preliminary Mission Report, 1997).

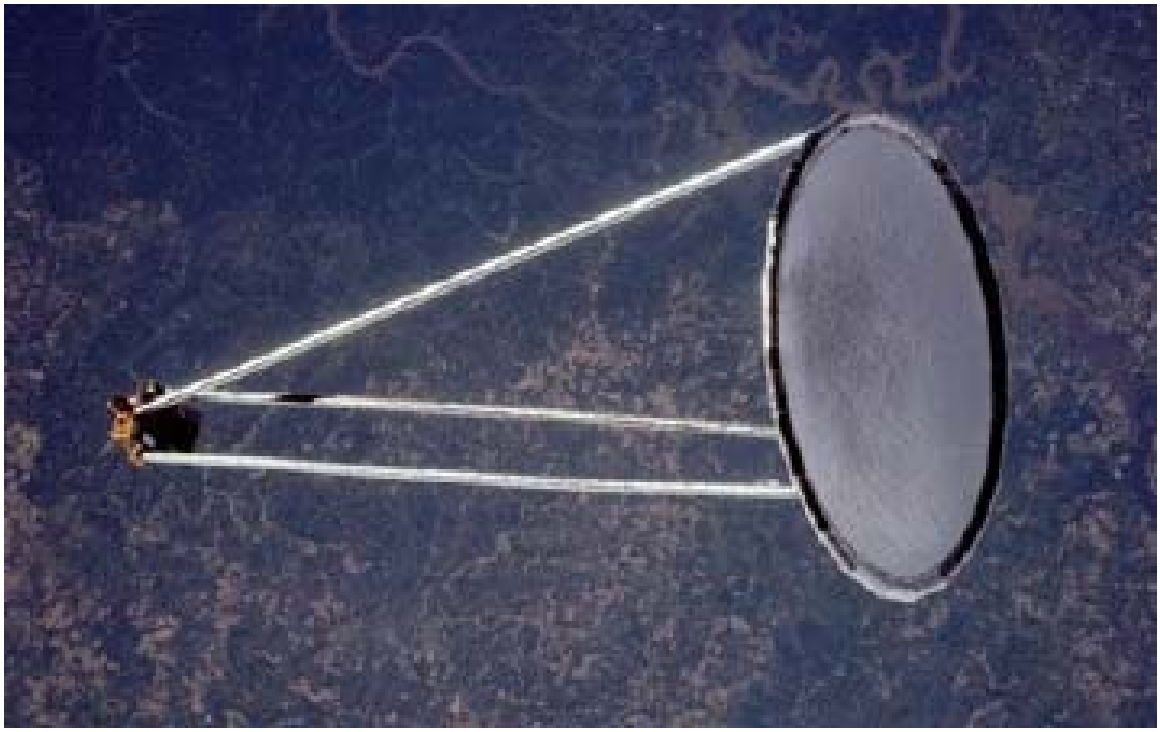

Figure 1.10: Spartan 207/Inflatable Antenna Experiment in orbit (Figure from NASA).

Dynamic Testing and Control of Inflatable Satellite Components

With the successful launch of the Spartan 207/Inflatable Antenna Experiment there has been a recent surge of research into the dynamics of inflatable structures. When in orbit the inflated structure is subject to vibrations induced mechanically by guidance systems and space debris as well as thermally induced vibrations from variable amounts of direct sunlight. However, until recently efforts to examine and understand the dynamics of these structures were performed without experimental analysis. In the absence of a complete understanding of these dynamics effective control systems cannot be implemented to ensure that the satellite will achieve its optimal performance.

Tinker (1998) investigated the dynamics of an inflatable structure for the shooting star experiment. The Shooting Star Experiment's (SSE) goal was to develop a device that could capture sunlight and use this thermal energy to heat a propellant providing thrust to the structure. However, the thrust capable of being produced is on the order of a few newtons, this requires the use of a lightweight device such as an inflatable structure. Tinker tested an inflated beam in free-

free boundary conditions to determine whether simple beam theory was applicable to inflatable structures. The inflated beam was tested at various pressures and with two different polyimide film shell thicknesses. The results of these experiments showed the inflated beam performed very similar to that of a solid beam. Next an inflated torus connected to three struts was tested in ambient conditions with three different inflation pressures, 0.25, 0.5, and 1.0 psig, in order to characterize the dynamics with a varying internal pressure. An electromagnetic shaker was mounted to the support plate and used to excite the structure. It was found that the natural frequencies and mode shapes had considerable change for each different internal pressure. This test was necessary because as the satellite passes from orbital eclipse to orbital day the internal pressure could experience significant variations. The inflated torus was also inflated in a vacuum chamber to determine whether the structure could properly inflate and hold pressure, Tinker comments that the results were very encouraging.

In later experiments, Slade et al. (2001) tested the dynamics of the inflated torus with three struts from the Pathfinder 3 Shooting Star Experiment in both ambient and vacuum conditions. The structure was suspended with free-free boundary conditions and excited using an electromagnetic shaker attached to the support plate. In order to avoid mass loading of the structure a laser vibrometer was used to capture the dynamics. It was found that the natural frequencies, damping and mode shapes significantly change between ambient and vacuum conditions. As one would expect the damping of the structure decreased in vacuum conditions. Slade et al. state that the results of this study point to a need to conduct vacuum modal surveys of inflatable articles intended for space application in order to ensure that on-orbit behavior will be well-replicated in the test environment. Following these tests Leigh et al. (2001) used the results of the tests performed at ambient conditions to determine the effectiveness of finite element software to model the inflatable structure. The finite element code MSC/NASTRAN was used to develop a model of the system for two cases; one using beam elements and the second using shell elements. The results of the model do not correlate well, but he authors state that the model shows potential to correlate well, if enough detail is observed during its creation.

Other recent studies (Agnes and Rogers, 2000) to characterize the dynamics of inflatable structures have shown to be difficult due to there extremely lightweight, flexible and high damping properties. The flexible nature of inflatable objects causes point excitation to result in only local deformations rather than exciting the global modes necessary for model verification and parameter identification. To overcome these issues Griffith and Main (2000) used a modified

impact hammer to excite the global modes of the structure while avoiding local excitation. The tip of the impact hammer was enlarged such that sufficient energy was input to the system to excite the global modes. They found that increasing the internal pressure of the torus from 0.8 psig to 1.0 psig resulted in significantly less damping and improved the coherence considerably. During the modal testing the authors used a roving accelerometer technique that causes differences in the frequency response at each location of the accelerometer due to the movement of accelerometer's mass around the system. This is an issue when dealing with inflatable structures due to their extreme lightweight, one improvement mentioned by the authors would be to use non-contacting methods of measurements such as a laser vibrometer or photogrammetry and videogrammetry. A still easier remedy to this problem would be to use a roving hammer technique, this means that the accelerometer location is stationary and the impact location is changed.

Vibration Sensing and Actuation for Control using Piezoelectric Materials

The concept of using piezoelectric materials for structural sensing and actuation is a well developed field and has seen a large amount of research interest for the last couple of decades. Bailey and Hubbard (1985) used PVDF film rather the monolithic piezoceramic to control the first bending mode of a thin steel cantilever beam. The piezo film spanned the entire length of the beam and provided the actuation energy while an accelerometer mounted at the tip of the beam supplied the feedback signal. The control law was developed using Lyapunov's second method for distributed parameter systems. Both constant-gain and constant-amplitude controllers were designed and implemented to control the first mode of the beam. The constant gain-controller was linear and provided double the baseline damping while the constant-amplitude controller was nonlinear and provided double the baseline damping for large vibrations and 40 times the baseline damping for small vibrations.

Crawley and de Luis (1985) also began experimenting with vibration control of a cantilever beam in the mid 1980's. Unlike Bailey and Hubbard (1985), Crawley and de Luis used monolithic piezoceramic elements to applied control to the aluminum beam used in their experiments. First Crawley and de Luis developed a model of the mechanical coupling of bonded segmented piezoelectric actuators to the dynamics of the structural member using a shear lag analysis. The model is used to examine how the effectiveness of the piezoelectric actuator changes with the scale of the structure and a comparison of the structural authority of various

piezoelectric materials is performed. After building the model of the system an experimental setup was constructed to validate it. Using the experimentally identified damping ratio, the model and experimental results showed excellent agreement. In addition, a simple one mode rate feedback controller was applied to the beam and was shown to increase the modal damping by an order of magnitude. Hanagud et al. (1985) also performed active vibration control on a cantilever beam in 1985 with piezoceramic elements bonded to its surface.

While a few papers were popping up prior to 1985 most were not distinctly on vibration control using piezoelectric material and as time progressed the research area began to grow producing some still widely used control theories. Fanson and Caughey (1987) developed a method for applying vibration control using piezoelectric materials termed positive position feedback (PPF). One aspect of large structures that can raise issues on the stability of an applied control system is that these large structures are basically distributed parameter systems that may have many modes of vibration. Because of these uncontrolled or unmodeled modes within the bandwidth of the controller can results in "spillover" and jeopardize the stability of the system. The previously existing control technique that provided the greatest resistance to the destabilizing effects of spillover was collocated direct velocity feedback. However, this type of control scheme did experience instability if actuator dynamics were not carefully considered. Both issues are overcome with the use of positive position feedback, which is not sensitive to spillover and does not destabilize with finite actuator dynamics. In addition, positive position feedback control algorithms provide better performance than velocity feedback because the position feedback is a state feedback were velocity feedback works essentially as a compensator. Fanson and Caughey implement the PPF controller on a cantilever beam and effectively simultaneously control the first six bending modes while achieving modal damping ratios as high as 20% of critical.

Baz et al. (1987) also developed an optimal control algorithm using a modified Independent Modal Space Control Method for piezoceramic patches. The control scheme is designed to enable the selection of the optimal location, control gains and excitation voltage. The authors found that an optimal thickness piezoceramic existed for the most efficient control of beams. The control algorithm was implemented on a steel beam while the performance of various different configurations of number of actuators, actuator thickness and actuator material were recorded. However, in the late 1980's piezoelectric devices were also used to achieve vibration control on plates. Lee et al. (1989) developed controller using PVF_2 to control the first

bending mode of a cantilever plate. The resulting controller achieved critical damping of the first mode using a collocated velocity feedback algorithm.

With the amount of research rapidly growing in the late 1980's one major element of vibration control using piezoelectrics was missing, a versatile and accurate model of the effects of piezoelectrics actuators on the dynamics of a bending beam. In 1990 two models describing the effects of piezoelectric bimorph actuators were produced. Crawley and Anderson (1990) develop techniques for modeling the induced strain actuation of beam-like components. Three models were developed and compared, one using uniform induced strain, a second using Bernoulli-Euler induced strain and a third using finite elements. It was fount that the induced strain model adapted from Crawley and de Luis (1985) was effective in induced stretching but not in induced bending, particularly for thin structures. The Bernoulli-Euler model was found to be effective for both induced bending and stretching with one exception that was modeled in the finite element code. Using the finite element code it was found that the Bernoulli-Euler model was effective when the influence of the finite bonding layer (layer of adhesive material between the structure and piezoelectric patch), characterized by Γ, was greater than 20 and the length to thickness ratio is greater than 100. It is also noted that the model is only valid for small strains due to the nonlinear hysteretic field strain and creep. The second model produced in 1990 was Hagood et al. (1990) that derives a model for the effects of dynamic coupling between a structure and the piezoelectric element bonded to it through the piezoelectric effect. The Model uses a Rayleigh-Ritz formulation to develop the general equation of motion for the piezoelectric attached to the beam. The resulting model is very accurate and can be applied to most any arrangement of piezoelectric materials. In addition, to being accurate the model allows the excitation voltage as well as the electrical boundary conditions and mechanical boundary conditions to be specified. Hagood et al. validates his model on a shunt damping system and achieves excellent results. Following the late 1980's the amount of research devoted to piezoelectric materials continued to grow substantially and still does. For more information regarding the recent advances in piezoelectrics see Chopra (2002).

Smart Material for Dynamic Testing and Control of Inflatable Satellites

Because of the advances in piezoelectric materials since the early 1990's smart materials have become a viable answer to the problems encounter during early testing of inflatable structures. Some of the issues that were faced with the previously mentioned research into the

dynamic testing of inflatable structures are as follows. Slade et al. (2000) were unable to obtain consistent results with the laser vibrometer due to a combination of influences of the free-free suspension system and shaker imposed constraints including mass loading, added damping and non-global excitation. Griffith and Main (2000) also experienced difficulties including extremely low coherence and a lack of energy input to the higher frequencies because of the flexible nature of the inflated object. To overcome these issues many researches have begun to look toward piezoelectric materials for dynamic testing of inflatable structures.

Agnes and Rogers (2000) attempted to perform a modal test on an inflatable children's swimming pool suspended vertically in a square frame. The torus was excited using both an electromagnetic shaker and PVDF patch while the response of the structure was measured using a laser vibrometer at points around the perimeter of the face of the torus. The authors used a multivariate mode indicator function (MMIF) to identify the resonant frequencies. However, further modal analysis was not performed due to significant nonlinear behavior in the system and low excitation levels on the part of the PVDF patch. Although this paper did not produce revolutionary results it, it did show that piezoelectric materials could be use for excitation of inflatable structures.

Briand et al. (2000) also used PVDF patches to test the dynamics of an inflatable torus, although the patches were used for sensing rather than excitation. The test fixture was a tire inner tube and was excited using an electromagnetic shaker. The experimental setup was able produce results with good coherence from 0-100 Hz. However, unlike the results found in Agnes and Roger (2000) a modal analysis was capable of being performed. This was the case because the PVDF patches are ideal for sensing due to their low mass and stiffness but they are not well suited for actuation due to low coupling coefficients. The results of the modal test were then compared to a finite element model with favorable results. The authors also mention the possibility of using shape memory films and fabrics to produce the actuation energy. This research showed that smart materials, namely piezoelectrics were a definite choice for sensing the dynamics of inflatable structures.

Park et al (2001) used an electromagnetic shaker to excite an inflated tire inner tube with both accelerometers and multiple PVDF patches located around the structure to effectively sense the vibration at multiple locations during one excitation period. They found that the data measured with PVDF film was consistent with that obtained from the accelerometer. Although,

the natural frequencies were almost identical for both methods, those obtained using the accelerometers were slightly less as expected due to mass loading. However, the PVDF film sensors offer several advantages when testing inflatable structures because they are lightweight and extremely flexible allowing then to conform to the torodial shell without adding additional mass or stiffness to the system. In addition to testing the torus with an electromagnetic shaker they used both a bimorph PVDF patch and a MFC to excite the torus. It was found that the MFC and PVDF patches were ineffective at exciting the lower frequencies but effective at higher frequencies, this was attributed to imperfect bonding caused by the use of double sided tape to secure the patches. The PVDF patch used in Agnes and Rogers (2000) was ineffective while this patch worked well because Park et al. constructed a multilayer bimorph PVDF actuator that produced far more strain energy than the unimorph patch. One definite advantage of the smart material actuators over the shaker input was found; they greatly reduced interference with the suspension modes of the free-free torus. The last portion of this work was to implement a Positive Position Feedback (PPF) control system using the MFC and PVDF patches to reduce the vibration of the 3^{rd} and 4^{th} out of plane bending modes. The control system resulted in approximately 50% vibration reduction, but it is speculated that more attenuation could be achieved if the actuators were permanently bonded to the structure.

Following the work previously mentioned, Park et al. (2002) performed a modal analysis on a torus constructed of Kapton with an aspect ratio that more closely matched that of the actual satellites intended for space. The torus was excited with both electromagnetic shaker and MFC. The sensing was performed using both accelerometer and PVDF film to compare the performance of each. It was found the MFC could globally excite the inflatable torus and produced better results than the shaker input due to less interference with the suspension modes of the free-free torus. It was also shown that the PVDF patch provides measurements of comparable quality to that of the accelerometer. The modal analysis accurately found the first four out of plane bending mode shape as well as the first two in plane bending mode shapes. Ruggiero et al (2002) used the same test structure to perform a modal analysis using multiple input and multiple output (MIMO) techniques in addition to developing a PPF control system to attenuate vibration in the first mode. The MIMO testing techniques are necessary because multiple actuators would be needed to globally excite the immense structures intended for space. This work showed that the MIMO testes produce results identical to those obtained earlier using one MFC for excitation. The MFC was also used to control the first mode and was shown to reduce the vibration by 70%.

While much headway has been made in the dynamic testing of inflatable structures there is still much to be learned. However, with the advances in piezoelectric actuators, materials, controls algorithms, finite element programs, structures and computational power of computers the steps necessary to understand the dynamics of inflatable devices are becoming clear.

1.2.2 Power Harvesting Using Piezoelectric Materials

The piezoelectric effect as mentioned earlier is the property that allows piezoelectric materials to convert electrical energy into mechanical strain energy and vice versa. This property of piezoelectric materials allow them to be used as mechanisms to transfer mechanical energy, usually ambient vibration into electrical energy that can then be stored and used to power other devices, this process in termed power harvesting. With the recent advances in wireless and MEMS technology, sensors can be placed almost anywhere necessary. Since these devices are wireless it becomes necessary that they have their own power supply. This power supply in most cases is the conventional battery. But problems can occur when using batteries because of there finite life span. When the battery is extinguished of all its power, the sensor must be retrieved and the battery changed. Because wireless sensors are developed so that they can be placed in remote locations such as structural sensors on a bridge or GPS tracking devices on animals in the wild, obtaining the sensor simply to replace the battery can become a very expensive task. Therefore, if a method of obtaining the untapped energy surrounding these sensors was implemented significant life could be added to the power supply. One method is to use piezoelectric materials to obtain energy lost during vibrations of the test specimen. This captured energy could then be used to prolong the life of the power supply or in the ideal case provide endless energy for the sensors lifespan.

In 1984 Hausler et al. published work that proposed an implantable physiological power supply using PVDF films. The generator would acquire power lost during respiration through the expansion and compression of the rib cage. A miniaturized prototype was constructed for testing on animals. The power harvesting device was fixed to the ribs of a mongrel dog and spontaneous breathing led to a peak voltage of 18V, which corresponds to a power output of 17μW. However, the power supplied was insufficient for operation of the desired electronics, but optimization of the PVDF film size and properties as well as a more suitable attachment to the ribs was speculated to produce electrical power output of 1mW.

Starner (1996) also explores the possibility of eliminating bulky and inconvenient power systems by acquiring the energy expended in everyday activities to power a computer or other portable electronic devices. His study surveyed various power generation methods including body heat, breath, blood pressure, finger motion, upper limb motion and walking. He calculates that approximately 67 W of power is lost during walking and that a piezoelectric device mounted inside a shoe with a conversion efficiency of 12.5 percent could achieve 8.4 W of power. Two methods of power generation are identified, piezoelectric and rotary generator, with the advantages and weakness of each outlined. One idea he explains is to place piezoelectric patches in the joints of clothing to harvest the energy lost during bending and states that about 0.33 watts could be obtained. The different possible storage devices are also listed and explained.

Umeda et al. (1996) investigate the possibility of transforming impact energy from a steel ball dropped onto a plate with a piezoelectric material attached into usable electric energy. An electrical equivalence model is developed to simulate the mechanical interaction and power generation of the steel ball impacting the plate. The model was used to determine the maximum efficiency and identify the major areas of loss in the system. It was found that most of the impact energy is converted back to kinetic energy when the ball bounces off of the plate and therefore, the efficiency decreased as the potential energy of the ball increased. They found that if it were possible for the ball to stick to the plate rather than bounce off, a maximum of 52% efficiency could be obtained. In addition, the authors determined that an optimal load resistance exists at which the maximum power will leave the piezoelectric element.

Umeda et al. (1997) continued their study by investigating the characteristics of power storage using a piezoelectric generator. The energy storage circuit was constructed of a bridge rectifier and capacitor. As with the previous case the power harvesting device was a piezoelectric vibrator that was impacted by a steel ball. To simulate the generation and storage mechanism they developed an equivalent circuit model. After examining the first impact they determined that as the capacitance increased the electrical charge increased because the duration of oscillation became longer and the output current decreased. It was also found that as the initial voltage increased the stored electrical charge decreased for all values of capacitance. After analyzing the model a prototype was built and a maximum efficiency of 35% was achieved, over 3 times that of a solar cell.

Like Starner (1996) and Hausler (1984), Kymissis et al. (1998) decided to investigate the possibility of obtaining energy lost through biological activity, by incorporating power harvesting devices into a shoe. Two different types of piezoelectric materials and a rotary generator were used. The piezo based power harvesting devices were a multiple layered PVDF patch and a piezoceramic Thunder actuator. The PVDF patch was placed in the sole of the shoe to harvest the bending energy and the Thunder actuator was located in the heel to harvest the impact energy. It was found that the PVDF patch and Thunder actuator produced an average power of approximately 1.1mW and 1.8mW of power respectively. After testing the smart materials they attached the rotary generator and were able to capture an average of 0.23W of power. The mechanical generator provided more power but was found to hinder the ability to walk comfortably. After calculating the amount of power capable of being generated they constructed an energy harvesting circuit. The circuit used a capacitor to store the charge until a sufficient amount is captured. Then the circuitry allows the power to be released to an transmitter that would send a 12-bit code. The system could transmit the code about 6-7 times every 3-6 steps.

Ottman et al. (2002) worked to develop a circuit that would maximize the power flow from the piezoelectric device. A DC-DC step down converter was implemented in coordination with a wave rectifier, capacitor and electro-chemical battery. In addition to the circuitry, an adaptive control technique was developed to continuously implement optimal power transfer theory and maximize the power flow into the battery. This active controller varied the switching frequency of the step down converter to maximize to the power plow from the piezoelectric elements and raise the current to levels more acceptable for charging batteries. The circuit and controller were built and tested on a vibrating cantilever plate with bimorph piezoelectric elements attached. It was found that when using the circuit, over four times the energy was transferred to the battery than with direct charging alone. However, if the power harvesting medium produced less than ten volts, then power flow into the battery was reduced due to losses in the additional circuit components.

1.3 Thesis Overview

The following section will detail the contributions that this work has made in several areas and provides a detailed description of the research presented in each chapter of this thesis.

1.3.1 Contributions

This Thesis has provided several contributions in various areas of research. This section will provide a brief overview of these contributions, while a more detailed version is provided in chapter six of this thesis. The macro-fiber composite (MFC) actuator is a new piezoceramic actuator that was developed at the NASA Langley Research center. Recently the MFC has become commercially available and most of the material properties have been explored. However, since it is a relatively new actuator much of the potential applications for its use have not been demonstrated. The MFC was developed as a piezoelectric actuator because of the higher strain and force produced. Because in its development stages the attention was concentrated on it actuator properties, its ability to be uses as a sensor went untested. Therefore, the first contribution of this work was to demonstrate that the MFC could be used as both a sensor and actuator. To do this a self-sensing experiment was setup and two abilities of the MFC were found. The first was that the MFC has sensing qualities comparable to that of the traditionally used piezoceramic materials and the second was that the MFC could incorporated into a self-sensing circuit and use to apply collocated control.

After finding the MFC to be an effective sensor, it was used in a MIMO control experiment to suppress the vibration of an inflated torus. Previous studies at the Center for Intelligent materials Systems and Structures have found that one MFC patch can globally excite and apply satisfactory vibration suppression of an inflated structure. However, the actual structures intend for use in space would have diameters as large as 30 meters, making it highly unlikely that one actuator could excite globally it. Therefore, control systems using multiple sensors and actuators must be implemented to control the vibration around these structures. The work presented in this thesis has developed one such control system that can be used to attenuate the vibration of the larger structures intended for space. The controller uses positive position feedback techniques and an arrangement of two separate pairs of sensors and actuators. It was found to be very effective at controlling the first mode of vibration but ineffective at higher

modes. This inability to control the higher modes was attributed to the location of the sensors and actuators and the presence of repeated modes in the structure. Therefore, the only way to arrange the sensors and actuator such that they could apply control to every mode was to make them collocated. To do this, a self-sensing circuit must be implemented and because it was found in the previous study that the MFC could be used for this application, a self-sensing control experiment was setup to show the feasibility of collocated control for inflated structures.

Next, the work of this thesis switched from vibration control to power harvesting. The first section of my research in power harvesting developed a model of a power harvesting beam. It was shown to be very accurate on a composite structure with a complex layout of piezoelectric patches. The model was found to produce excellent results independent of the load resistance and excitation frequency used. Furthermore, the model was used to show the damping effects of power harvesting on the dynamics of the structure. This model can be used as a design tool for developing power harvesting systems. With the model in hand, it can reveal the size and location of the piezoelectric as well as the amount of vibration required to generate the desired electrical signal.

One problem that is often encountered when using power harvesting systems is that the energy produced by the piezoelectric material is often not sufficient to power most electronics. Therefore, methods of accumulating the energy so that it many be used as a power source need to be developed. The method typically used to accumulate this energy, is a capacitor. However, the capacitor has characteristics that are not ideal for many practical applications. These limitations led me to develop another method of storing the power that would not limit the type of applications that could be powered. The rechargeable battery was an option that had not been explored by other researchers and possesses the qualities that were needed in a power harvesting system. Therefore, an experiment was setup using a piezoceramic plate to charge a nickel metal hydride battery. It was found that the power generated by the piezoelectric material was indeed compatible with that required by the rechargeable battery. After showing that the piezoelectric material could be used with rechargeable batteries, the ability to use MFC as power harvesting devices was tested. However, in doing this it was found that the MFC was incompatible with the requirements of the battery, due to a low current output. Therefore, because of the low current generation, it was determined that the MFC is not suitable for use as a power harvesting device. Following this finding, various capacity nickel metal hydride batteries were charged to determine the largest battery that could be effectively charged and the charge time for each with both a

resonant and random signal. This study provides a basis for other researchers to determine the ideal size battery for there intended application based on the charge time and capacity of the battery.

The advances made from the work presented in this thesis will provide future researchers with the tools necessary to use the macro-fiber composite actuator effectively in numerous applications. The sensing capabilities of the MFC were realized and its capabilities were shown in several studies including, a self-sensing actuator for collocated control and the development of a multiple sensor and actuator control scheme for the suppression of the vibration of inflatable structures allowing control systems to be extended to real scale satellites. Following the work in sensing, the ability to use the power generated by piezoelectric materials to recharge batteries was discovered and the issues regarding the effectiveness of the MFC as a power harvesting device were discussed. In addition, a model to predict the power generation of a beam with piezoelectric patches attached was derived and shown to be very accurate on a composite beam with complicated piezoelectric layout. These contributions will certainly aid researchers in the future.

1.3.2 Chapter Summary

Chapter 1 provides an introduction to previous work in the topics associated with this thesis. The history of piezoelectricity is first discussed, providing a background of the materials and its applications. The macro fiber composite (MFC), that is tested throughout this thesis is one type of piezoceramic fiber actuator. To provide a background of this type of transducer, an overview of the fabrication and typical applications of the MFC as well as two other common piezoceramic fiber actuators are given. Following this discussion, the two major topics of this thesis, dynamic testing of inflatable structures and power harvesting, have an in depth literature review. The literature review of inflatable structures includes information regarding, their history, early attempts to classify their dynamic behavior using traditional means of testing and more recent experiments performed using piezoelectric materials. Subsequent to this previous work into the use of piezoelectric devices for power harvesting is presented.

Chapter 2 begins presenting the results of my master's research. This chapter begins by providing a small introduction to self-sensing actuators and some of the research that has been carried out using them. Following the introduction, a description of the construction of the self-sensing circuit and the principles of how it works are given. The self-sensing actuator is

advantageous to use because it allows the sensor and actuator to be perfectly collocated, which is ideal for certain control techniques such as direct velocity feedback and positive position feedback (PPF) control. The collocated nature of the sensor and actuator provide the control systems used with additional stability to various parameters that would deteriorate the effectiveness of a normal control system. However, there are issues that affect the ability of the self-sensing circuit to work properly; the most substantial of these is an unbalanced circuit. To demonstrate the effect of an unbalanced circuit a simulation of a self-sensing system is performed and the result of an unbalanced circuit on the ability to measure a frequency response, generate an accurate sensing signal and control a system are shown. The simulation is followed by a description of the experimental setup used to demonstrate the MFC's ability to be used as a self-sensing actuator for collocated control. The experimental setup is detailed and the results of a collocated control experiment on an aluminum beam are presented.

In chapter 3 the ability of a MFC to be used as in a multiple sensor and actuator control experiment is investigated. Previous experiments at the Center for Intelligent Material Systems and Structures (CIMSS) to control the dynamics of an inflatable structure showed that one MFC patch can globally excite and suppress the vibration of an inflated torus. However, these tests were performed on a scaled model of the actual inflated torus intended for use in space. The actual structure would have a diameter as large a 30 meters making it highly unlikely that one actuator could globally excite such a large structure. Therefore, control techniques using multiple sensors and actuators must be developed to allow the control scheme to be extended to real scale satellites. This chapter develops one such control system using PPF control techniques and two pairs of sensors and actuators. The results of the control experiments are discussed and difficulties encountered are explained. Due to issues encountered with the location of the sensor and actuator, a control experiment to use self-sensing techniques was setup. The methods used and the results of these tests are outlined.

Following the work in sensing and control using MFC, Chapter 4 begins presenting the results of work performed in the area of power harvesting. This chapter develops a model to describe the amount of energy generated during vibration of a beam with piezoelectric patches attached. The model is formulated from variational principles and validated on a complex composite beam containing multiple piezoelectric actuators. Due to the composite structure of the beam an experimental test is performed to find the modulus of the composite material. The procedures and experimental setup used to find this parameter are provided. Subsequent to

determining the modulus of the composite material, the beam is used to validate the model and is shown to produce very accurate results. The last section of this chapter makes a comparison between power harvesting and shunt damping.

Chapter 5 continues the work in power harvesting, and goes into depth on the methods of power storage using a piezoelectric power harvesting devices. The motivation of the work in this chapter is that piezoelectric materials generate levels of power far to low to power most electronics. Therefore, methods of accumulating the energy generated to allow it to be used to power a typical electrical circuit must be found. Two methods of storage for power harvesting are tested and the relative advantages and weaknesses of each are outlined. The first method is a capacitive circuit and the second method uses a nickel metal hydride rechargeable battery. The power output of the piezoelectric has never before been used with a battery so it ability to do so is first shown. Then the relative advantages and disadvantages of each are outlined. After finding the piezoceramic was capable of charging a battery, the ability of MFC to be used as power harvesting devices is tested. After working with the MFC, an investigation into the largest size battery that can be effectively charged is performed and the results are presented.

The final chapter of this thesis is Chapter 6, and provides a brief overview of the results found throughout my master's work. Following the overview, a discussion of the contributions that my work has made and how they will affect future research is outlined. The final section of this chapter and the thesis, describes the possible future work that could be performed to further the research that I have completed.

Chapter 2

Self-Sensing Macro-Fiber Composite Actuator

2.1 Introduction to Self-sensing actuators

When designing a controller it is often advantages to the stability of the system to have collocated sensors and actuators. In this configuration, both devices experience the same dynamics allowing for more effective control in the absence of an accurate model of the system. For instance, Goh and Coughley (1985) presented results showing that in the absence of finite actuator dynamics, structures controlled with collocated velocity feedback are unconditionally stable at all frequencies. In addition, collocated control eliminates possible closed loop instabilities caused by capacitive coupling between the sensor and actuator elements. A self-sensing actuator holds the ability to perform both duties of sensing and actuation allowing it to be perfectly collocated.

The ability to use a piezoelectric device as a self-sensing actuator was first discovered and published by Dosch et al. (1992). The self-sensing actuator works through circuitry that can distinguish between the sensing signal and the control signal applied to the piezoelectric patch. In doing this the circuit can cancel the applied control voltage out and return only the sensing signal. This process allows one piezoelectric element to sense and apply actuation to the beam at the same time. To show the effectiveness of the self-sensing actuator, Dosch et al designed and used a PPF controller to suppress the first and second modes of vibration in a cantilever beam. The

controller was shown to be very effective by reducing the settling time of the first mode from 35 seconds to 0.3 seconds and the second mode from 7 seconds to 0.9 seconds.

Subsequent to the work of Dosch et al. (1992) other researches have found self-sensing piezoelectric actuators to be very useful for use in control applications. Frampton et al. (1995) used a self-sensing actuator bonded to an aircraft panel for reduction in flutter at various mach numbers. It was found that the control system was very effective for adding damping to the near flutter pole and reducing the peak response significantly. Döngi et al. (1995) also investigated the effectiveness of using a self-sensing actuator for active flutter suppression. A novel control approach based on output feedback for Active Compensation of Aerodynamic Stiffness was presented and shown to possess good robustness to a variety of properties.

While most studies use monolithic piezoceramic material for its higher coupling coefficients, piezoelectric films have also been used as self-sensing actuators. Nishigaki and Endo (2000) used self-sensing piezofilm for control of both a cantilever beam and a flexible circular ring. For the case of a cantilever beam, the fundamental equations were derived and a theoretical analysis of the control system was performed. After finding that the control system was effective for the cantilever beam, they applied it to a flexible curved ring. Their analysis was performed using Hamilton's principle and showed that self-sensing systems are also effective for curved flexible structures.

2.2 Self-Sensing Circuit Design and Considerations

2.2.1 Self-Sensing Circuit Principles

A piezoelectric patch can be used as both a sensor and actuator through the use of circuitry that can distinguish between the control and sensor signal. One of the popular circuit designs used to build a self-sensing actuator is shown in Figure 2.1. The circuit consists of three operational amplifiers that are configured as a difference amplifier; this means that the voltage differential between the two braches is the output of the circuit. The basic principles behind the operation of the self-sensing circuit are as follows. A control signal is applied to the system as shown in Figure 2.1. The control signal is then sent through an upper and lower branch of the circuit. For this explanation and to be consistent with Figure 2.1, the upper branch contains the

piezoelectric element and the lower branch contains a capacitor that whose capacitance is equal to the piezoelectric element. When the control signal is applied to the circuit, an equal voltage appears in both the upper and lower branch of the circuit because both branches have an equal capacitance; this is the most important factor for a working self-sensing circuit. However, the piezoelectric element is experiencing some kind of vibration and develops a sensing voltage through the piezoelectric effect. This sensing voltage is added to the control voltage of the upper branch. Therefore, the lower branch has only the control voltage and the upper branch has both the control voltage plus sensing voltage. Now both branches of the circuit are fed into a difference amplifier that subtracts the voltage of each branch from the other. The effect of this is to cancel the control signal that is equally present in both the upper and lower branches of the circuit and leave only the sensing signal. This sensing signal can then be used as if no control signal was ever applied.

2.2.2 Self-Sensing Circuit Considerations

While this type of circuit has many advantages for control applications, there are some issues that must be considered before it can be effectively implemented. The two major issues are operational amplifiers and unbalanced circuits. The first issue is the choice of op-amps to be used in the circuit. It is very important that the op-amps do not output a noisy signal. When working with piezoelectric materials, the magnitude of the control signal is usually much larger than that of the sensing signal, therefore, if the op-amps produce noise it will correspond to the larger control voltage and affect the circuit's ability to cancel the control signal out. If noise is generated in the op-amps it is very difficult to measure a clean and accurate sensing signal from the circuit.

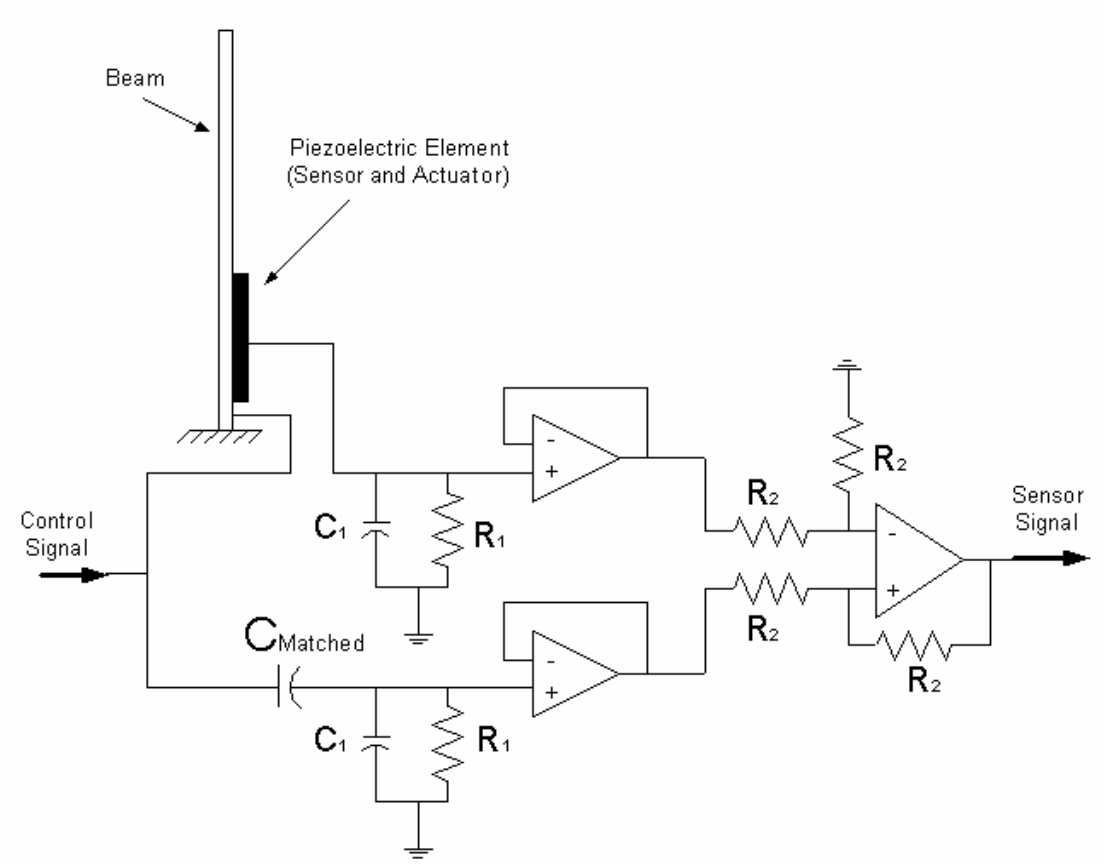

Figure 2.1: Schematic of the self-sensing circuit.

The second issue when working with a self-sensing circuit is an unbalanced bridge. An unbalanced bridge means that the value of the piezoelectric's capacitance and the matched capacitance are not exactly the same. This can occur for a number of reasons including accidental mismatch, piezoelectric aging, and ambient temperature changes. The piezoelectric material has a capacitance that is a function of temperature, frequency as well as other factors. Because the capacitance is a function of temperature the circuit can become unbalanced just from day to day operation. Furthermore, the frequency range that the actuator is operating at also affects the balance of the circuit. If the matched capacitor does not follow the same frequency dependent capacitance curve, then the circuit may be balanced at one frequency but not at another. These two factors as well as others have limited the use of self-sensing actuators in many practical applications.

To overcome these issues, researchers have attempted to design adaptive circuitry that will adjust the matched capacitance to account for these variations in capacitive values.

Vipperman and Clark (1996) developed a method of using adaptive filters coupled with LMS algorithms to provide the nonlinear magnitude compensation of the matched capacitance for a self-sensing actuator they deem a sensoriactuator. The methods used were able to reduce the error in the capacitors by as much a 20%. However, the complexity of the system makes it hard to implement and does not provide a complete solution to the problem. Okugawa and Sasaki (2002) propose the use of system identification and observer theory to estimate the state vectors and achieve self-maintenance of a self-sensing system. This system was also found to be ineffective and could not be used efficiently for its intended application.

Effects of an Unbalanced Circuit

To demonstrate the effect of an unbalanced circuit on the sensors output voltage a simulation was performed. The code for the simulation can be found in Appendix A. The simulation takes a control signal and applies it to a cantilever beam then measures the response through an electrical equivalence circuit created in MATLAB's Simulink program. This program allows the matched capacitance to be changed by a percentage of the piezoelectrics capacitance and the sensor signal plotted.

The first test was to observe the effect of the mistuned circuit on the time response of a cantilever beam. A random and chirp disturbance signal was used as an input to the system and the sensing response as the capacitance varied was recorded. Figure 2.2 shows the response to the random signal and Figure 2.3 shows the effect on a chirp signal. It is apparent from these two plots that the sensor signal begins to deteriorate as the difference in the values of the two capacitors change. The reason for the degradation of the sensor signals performance is that as the circuit becomes more unbalance the circuit cannot cancel the control signal out fully and it begins to show up in the measured response.

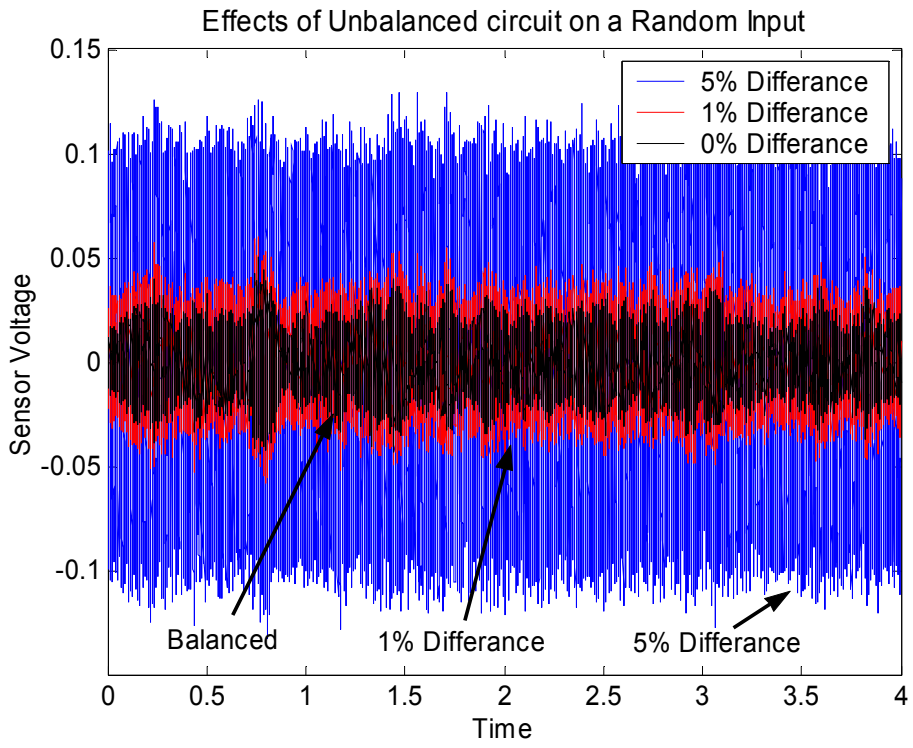

Figure 2.2: Effect of an unbalanced circuit with a random control signal on the circuit output.

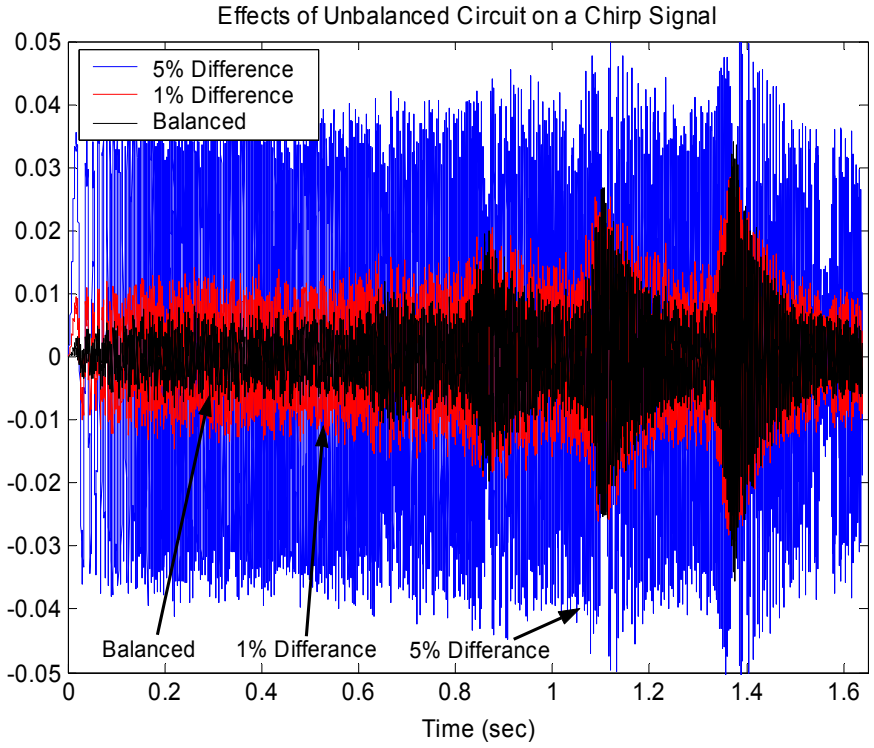

Figure 2.3: Effect of an unbalanced circuit with a chirp control signal on the circuit output.

The second simulation performed was to determine the effect of the unbalanced circuit on the frequency response function (FRF) measured by the self-sensing circuit. This was performed by applying a chirp control signal and measuring the response at each frequency. Figure 2.4 shows the effect of the matched capacitance having a value higher than the piezoelectric element and Figure 2.5 shows the effect of the matched capacitance having a lower value. It can be seen in Figure 2.4 and 2.5 that as the difference between the matched capacitance and the piezoelectric capacitance increases the FRF approaches a straight line. This occurs because as their difference becomes greater, the circuitry allows more and more of the control signal to appear in the sensor signal. Since the FRF is in the ratio of output versus the input, as the difference in capacitance becomes larger and the output becomes more and more like the input causing the FRF to approach a straight line at the value of one. Another interesting observation that is apparent in Figure 2.4 and 2.5, is the effect of the piezoelectric capacitance having a higher or lower value than the matched capacitance. If the matched value is higher than the anti-resonance occurs before the resonance frequency, but if the matched value is lower, the anti-resonance occurs after the resonance frequency.

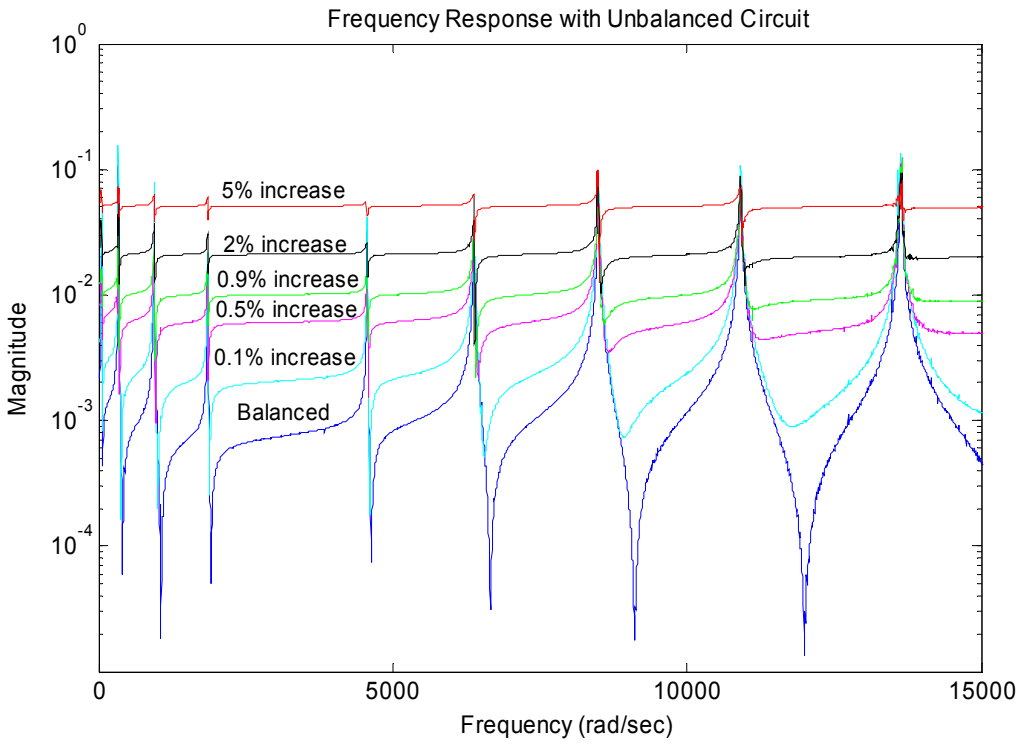

Figure 2.4: Effect of an unbalanced circuit with a higher piezoelectric capacitance than matched capacitance on the frequency response function.

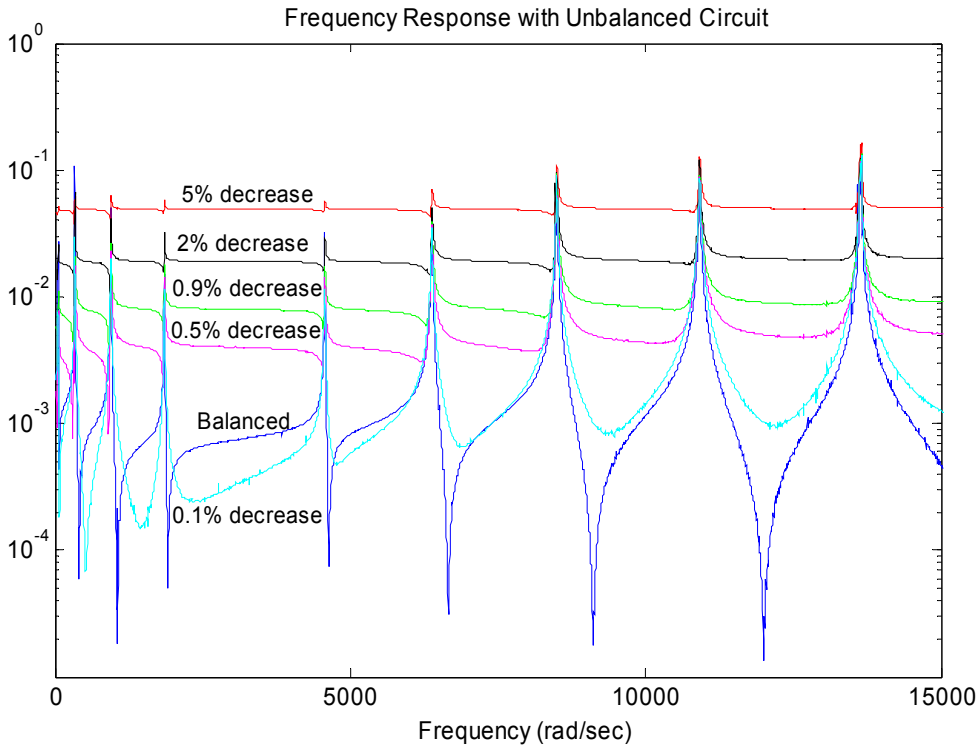

Figure 2.5: Effect of an unbalanced circuit with a lower piezoelectric capacitance than matched capacitance on the frequency response function.

Another undesired effect of an unbalanced circuit is brought about because the sensing signal is no longer accurate; this makes it difficult to implement an effective and stable control system. Figure 2.6 shows the vibration of a cantilever beam with positive position feedback (PPF) control applied. The three plots represent a balanced circuit, 1% unbalanced circuit and 5% unbalanced circuit, also in all plots of Figure 2.6 the matched capacitance is increased. It can be seen from Figure 2.6 that as the circuit becomes unbalanced the performance of the controller begins to degrade rapidly because the sensing voltage becomes hidden in the control signal. If the circuit were to become unbalance such that the matched capacitance was smaller than the piezoelectric capacitance then the stability of the system would fail at about 1% unbalance.

This simulation shows that the performance of a self-sensing circuit heavily depends on the circuit being in a balanced state. A piezoelectric element has a capacitance that is around 4ηF (depending on its dimensions), this means that a change of one percent corresponds to 40pF.

Therefore, slight changes in temperature and other parameters can drastically affect the performance of both the sensing capabilities and the control system used in conjunction with the self-sensing actuator. The importance of a balanced circuit on the effectiveness of a self-sensing actuator must never be overlooked.

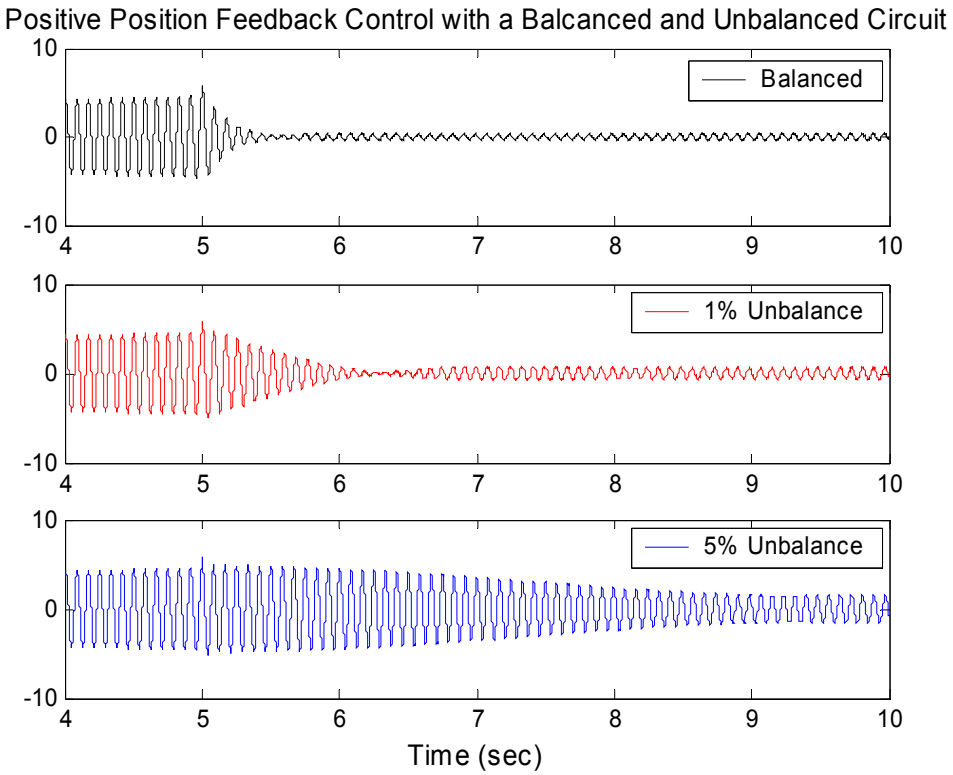

Figure 2.6: Performance of PPF controller as a self-sensing circuit becomes unbalanced.

2.3 Experimental Testing and Results

The monolithic piezoceramic patch has been used as a self-sensing actuator and has been successfully implemented in control schemes since 1992. However, the concept of using a piezofiber actuator as a self-sensing actuator has never been explored. The following sections will describe the experimental setup and results from tests performed on a macro-fiber composite (MFC) actuator. The MFC is used as a self-sensing actuator for both measuring the frequency response and providing vibration suppression to a cantilever beam excited at its second resonant frequency.

2.3.1 Experimental Setup

An MFC Patch was bonded near the root of a 558x50x4 mm cantilever aluminum beam as shown in Figure 2.7 and Figure 2.8. A monolithic piezoelectric patch was mounted approximately midway down the length of the beam and used to supply a disturbance signal for the control experiment. The MFC had dimensions of 50x42mm and the PZT had dimensions of 50x35mm. The self-sensing circuit was connected to a dSpace control board to allow for real time vibration suppression of the beam. The dSpace control board can be easily damaged in the event of a surge voltage flowing into the box. This is further complicated by the use of a PPF filter that can go unstable during tuning of the parameters and send large control voltages out that have a direct path back to the control board through the self-sensing circuit. Therefore, if the circuit does not fully cancel the control signal out, the surge voltages can potentially enter the dSpace and cause damage. Thus, the size of the control signals applied was limited. During the control experiments, if the sensing signal output from the self-sensing circuit was used to show the vibration suppression, an inaccurate measurement could be given due to errors in the circuit, such as an unbalanced bridge. Therefore, it is necessary to use a sensor separate from the control system. To measure the level of vibration before and after the application of the control signal and to provide independent verification of the closed loop results a PCB accelerometer Model U352C22 weighting 0.5 grams was placed at the tip of beam.

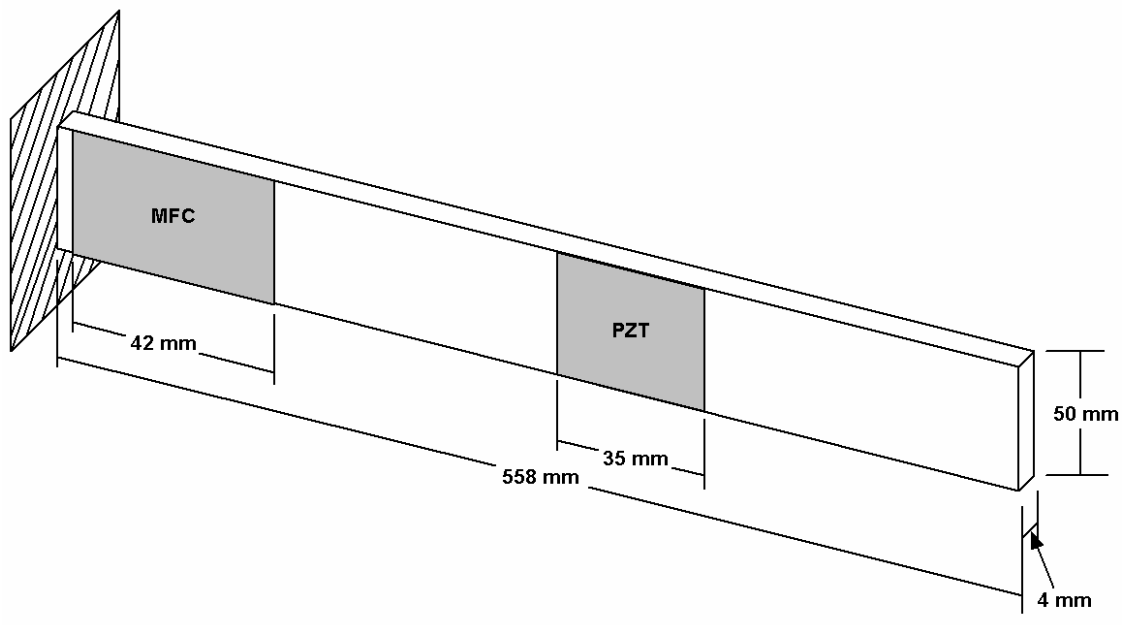

Figure 2.7: Dimensions of beam and location of MFC element.

Figure 2.8: Picture of MFC bonded to aluminum beam.

2.3.2 Self-Sensing Positive Position Feedback Control of Cantilever Beam

In past studies the MFC has only been shown to work as an actuator and not as a sensor. Therefore, before PPF control could be applied to the beam, the ability of the MFC to work as a sensor had to be identified. To do this, it was decided that the frequency response of the beam would be measured using the self-sensing circuit. This would demonstrate two things, that the MFC was capable of providing an accurate sensing signal and that the self-sensing bridge circuit was balanced. The self-sensing MFC was used to excite the beam from 0 to 1000 Hz while also recording the response. The measured frequency response is shown in Figure 2.9. Looking at Figure 2.9 it is clear that the MFC is effective as a sensor and can work in a self-sensing circuit. However, referring back to the previous section outlining the effects of an unbalanced circuit and comparing it to the figure, it can be seen from Figure 2.9 that the matched capacitance is slightly larger than the capacitance of the MFC. This is realized because the anti-resonance occurs before the resonant frequency rather than after it.

Design of Positive Position Feedback Controller

The Positive Position Feedback (PPF) controller is constructed using two equations, one to describe the structure and a second to describe the compensator:

$$\text{Structure:} \quad \ddot{\xi} + 2\zeta\omega\dot{\xi} + \omega^2\xi = gt\omega^2\eta \tag{2.1a}$$

$$\text{Compensator:} \quad \ddot{\eta} + 2\zeta_f\omega_f\dot{\eta} + \omega_f^2\eta = \omega_f^2\eta = \omega_f^2\xi \tag{2.1b}$$

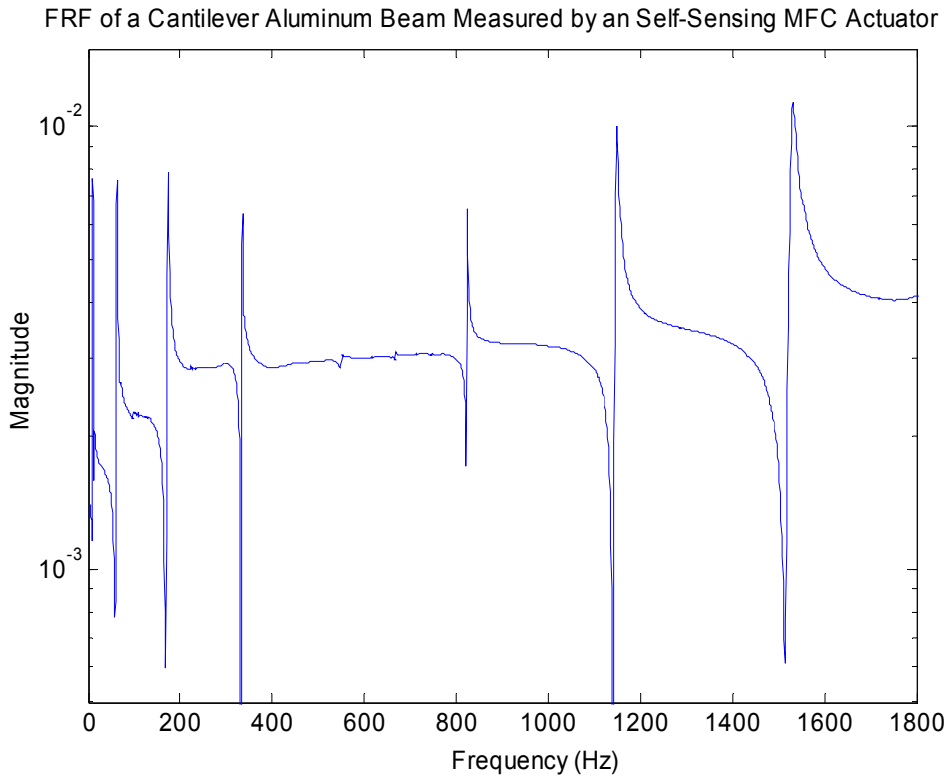

Figure 2.9: Frequency response function of a cantilever aluminum beam measured by a MFC self-sensing actuator.

where g is the scalar gain that must be positive, ξ is the modal coordinate, η is the filter coordinate, ω and ω_f are the structural and frequencies, respectively and ζ and ζ_f are the structural and filter damping ratios, respectively. The term positive position feedback comes from the fact that the position coordinate of equation 2.1a is positively fed into the filter and the structural coordinate of equation 2.1b is positively fed back into the structure (Fanson and Caughey, 1987).

This system of equations contains three parameters that can be varied to optimize the controller, ω_f, ζ_f and g. One requirement for the system to effectively control the desired frequency is that the value selected for the filter frequency lie in a close proximity to the frequency desired to be controlled. Studies have been performed to determine the optimal location of the filter frequency and other parameters. McEver (1999) proposed a method for determining the optimal placement as a function of the pole/zero spacing and compensator gain. This work led to a cookbook method of choosing the optimal values for all three parameters.

Results of Control Experiments

Once the ability of the MFC to work as a sensor was found a PPF controller was designed to suppress the vibration of the beam. A dSPACE and one self-sensing MFC actuator were used to control the beam. A monolithic piezoceramic patch was used to provide a continuous excitation signal while the controller worked to reject the disturbance. One test performed on the second mode (63.75 Hz) achieved 90% vibration reduction as shown in Figure 2.10. The MFC Patch is capable of operating at voltages as high as 1000 volts, however, the control signal supplied to the self-sensing MFC actuator was limited to 35 volts due to the size of the op-amps used and the vulnerability of the dSPACE to high voltages. If larger control voltages were used the vibration reduction would be even more substantial. The MFC self-sensing actuator was able to produce larger control forces on the beam than a PZT of equal size due to the MFC's higher electro-mechanical coupling.

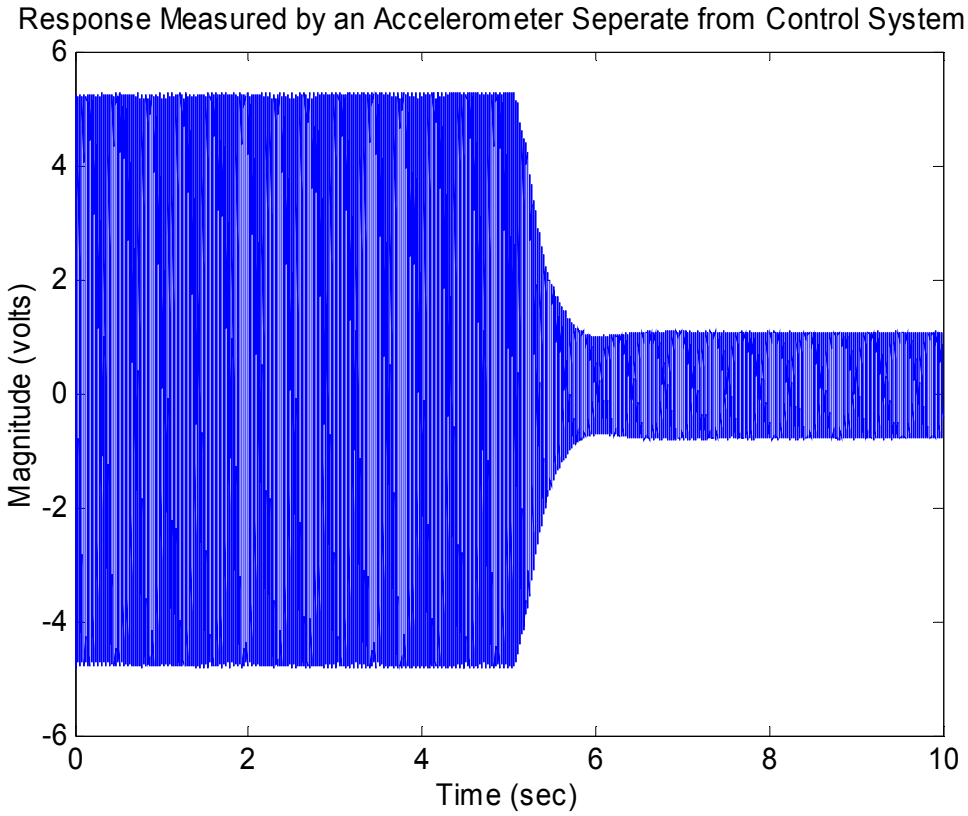

Figure 2.10: Vibration of beam measured by an accelerometer separate from the control system before and after PPF control was applied.

2.4 Chapter Summary

Chapter two has presented an investigation into self-sensing circuit particularly for use with macro-fiber composite actuator. The chapter begins by describing the development of the self-sensing actuator and a few research topics in the area. This is followed by a description of the circuit design and the principles behind how the circuit works. The major issues of self-sensing circuits have been discussed and a simulation was performed to demonstrate the effect of an unbalanced bridge circuit on the accuracy of the sensing signal generated in the circuit. The simulation shows that slight differences in capacitance values can make a significant variation in the output of the circuit. The simulation also provides a method of analyzing the balance of the circuit through the shape of the frequency response function. A simple comparison of the simulation results and a measured FRF can determine the degree of imbalance in the circuit as well as whether the matched capacitance is higher or lower than the piezoelectric's capacitance. The goal of this section was to provide the design guidelines and a detailed description of the circuitry layout such that other researches could construct the own circuitry. For instance, one of the five projects that will be performed by 2003 Los Alamos Summer Dynamic School will investigate the design issues associated with the self-sensing actuation based on initial result presented in this chapter.

The second portion of this chapter investigates the use of macro-fiber composite actuators (MFC) for use as both sensors and self-sensing actuators. Because the sensing capabilities of the MFC had never been shown before, it was necessary that its ability to do so was proven. It was decided that the sensing accuracy and the ability to use the MFC in self-sensing circuitry could all be demonstrated by measuring the frequency response function of a cantilever beam. The self-sensing MFC was shown to identify the natural frequencies and the measured FRF was analyzed using the simulation results from the previous sections to provide insight into the balance of the circuitry. After the MFC was shown to work in a self-sensing setting, a PPF controller was designed and implemented to suppress the vibration in a cantilever aluminum beam. With a low control voltage, limited by the electronic components in the circuitry and the control board used, the MFC was able to reduce the vibration by 90%, clearly showing its effectiveness.

This chapter has identified the previously unknown sensing abilities the macro-fiber composite actuator. A self-sensing circuit was designed and implemented using a MFC for

control of an aluminum beam. The results of these tests demonstrate that the MFC can perform as a monolithic piezoceramic does, although with greater ease of handling, bonding and providing more mechanical energy to the structure.

Chapter 3

Vibration Suppression of an Inflatable Structure

3.1 Introduction to Inflatable Structures

Inflated space-based devices have become popular over the past three decades due to their minimal launch-mass and volume. Once inflated, these space structures are subjected to vibrations induced mechanically by guidance systems and space debris as well as thermally induced vibrations from variable amounts of direct sunlight. Controlling the vibration and shape of space-based structures is critical to ensuring their optimal performance. However, their extremely lightweight, flexible, and high damping properties pose difficult problems in performing the vibration testing necessary to understand and characterize dynamics of the structure. The choice of applicable sensing and actuation systems suitable for use with inflated structures are somewhat limited because of their low stiffness, high flexibility and curved surfaces. In addition, excitation methods have to be carefully chosen since the extremely flexible nature causes point excitation to result in only local deformation. In early tests to determine the modal parameters of an inflated torus traditional methods of excitation were used. Griffith and Main (2000) used a modified impact hammer to excite the global modes of the structure while avoiding local excitation. Slade et al. (2001) used an electromagnetic shaker to test a torus attached to three struts with a lens. In addition, the inflated structure was tested in both ambient and vacuum conditions. It was found that the response of the structure was significantly different in ambient and vacuum conditions.

However, recent progress in the development of new piezoelectric actuators has changed the way that inflatable structures are tested. Park et al. (2001) were the first to investigate the feasibility of using smart materials, such as PVDF films, to find modal parameters and to attenuate vibration in a flexible inflated structure. Their study found that piezoelectric actuators can sufficiently excite the global modes of the inflated structure, allowing a full modal analysis to be performed. Furthermore, it was found that excitation methods using smart material do not interfere with the suspension modes of the free-free torus as other methods do. Since the work of Park et al. (2001, 2002) piezoelectric materials have been shown to be a logical choice for sensing and actuation of inflatable structures.

3.2 Multiple MFC Sensors and Actuators for Vibration Control of an Inflatable Torus

In the following sections, it will be shown that the recently developed Macro-Fiber Composite (MFC) actuator can be used as either a sensor or actuator for global vibration suppression of an inflatable structure. The MFC is constructed using piezofibers which allow the actuator to be extremely flexible, as shown in Figure 3.1. The flexibility of the MFC allows it be integrated in an unobtrusive way into or onto the curved surface of an inflated structure. In addition to being flexible, the MFC can produce significantly more strain energy than that of a typical piezoceramic actuator due to the use of interdigitated electrodes that capitalize on the higher piezoelectric d_{33} coefficient. This additional mechanical energy allows the reduction in vibration of the structure to be far more significant than with traditional piezofilm or piezoceramic actuators. Furthermore, due to the MFC's construction using piezofibers, the overall strength of the material is greatly increased when compared to that of the base material, while affording the MFC greatly increased flexibility. In addition to the increased strength of the material, the MFC is robust and can withstand a significant amount of damage without losing its ability to produce strain energy. The robustness of the MFC actuator is granted through its construction using an epoxy and Kapton shell that allow the actuator withstand substantial damage, including cracks and impacts. The robustness is one of the foremost important characteristics for the use in space applications where the actuator cannot be easily replaced. Due to these reasons, it has been concluded that MFC are the ideal choice for use with in inflatable structures (Park et al. 2001, 2002).

Previous studies at the Center for Intelligent Material Systems and Structures have used the MFC vibration testing and control of an inflatable torus. In these studies, it was shown that one MFC patch can sufficiently excite global modes of a scaled inflated torus for a modal analysis to be performed. However, the actual inflatable satellites intended for use in space would have a diameter as large as 30 meters and it is unlikely that one actuator could excite a structure of this size. Therefore, to develop control systems that are applicable to the actual inflatable satellites, it is necessary that multiple sensors and actuators are used to suppress the vibration of the inflated structure. In addition, the inflated torus is a symmetric structure that contains repeated resonant frequencies, making it is necessary that multiple actuators be used to globally suppress the vibration. The problems associated with the control of an inflatable torus with repeated modes are discussed by Jha (2002). However, experimental implementation of multiple sensor/actuator for vibration control of inflatable structures has never been investigated.

The work presented in the following sections of this chapter develops a positive position feedback controller using two pairs of sensors and actuator. It has been found, that when using positive position feedback techniques, the relative location of the sensors and actuators influences the ability of the control system to attenuate certain modes of the structure. This causes the position of the sensors and actuators to work for one mode but not for another. To overcome this issue and allow for global control of all modes of the inflatable torus, a self-sensing circuit for collocated control is investigated. The results found the self-sensing MFC circuit to be compatible with inflatable structures and posses the ability for effective vibration supression.

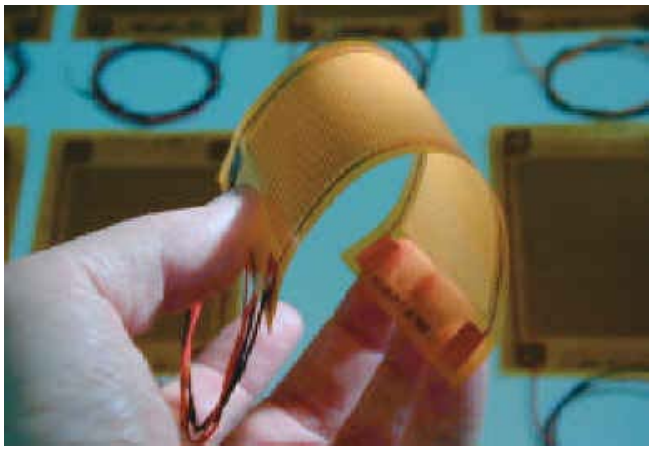

Figure 3.1: Macro-fiber composite being bent to show its flexibility.

3.2.1 Experimental Setup

The test structure is an inflatable torus made of flat sheets of polyimide film Kapton with a 1.8-meter ring diameter and a 0.15-meter tube diameter suspended in free-free boundary conditions as shown in Figure 3.2. The internal pressure of the torus was maintained at 0.5 psig using a small aquarium pump. The sensing and actuation was realized using the MFC actuator, while the disturbance excitation was introduced using an electromagnetic shaker input with a plate attached to better distribute the energy and avoid local deformation. Due to the increased flexibility of the MFC, it is able to easily conform to the toridal shape of the inflated torus. The MFC was bonded to the surface of the torus using double-sided tape, as shown in Figure 3.3. In order to ensure the response of the torus found using a MFC was accurate an accelerometer (PCB Model 352C22) sensor was attached to the torus for comparison during the tests. The accelerometer also played the role of measuring the vibration of the system before and after control was applied. The careful selection of excitation signal (specific length and bandwidth) was made to guarantee enough input energy at each excitation frequency.

Figure 3.2: Inflated torus suspended in free-free boundary conditions.

Figure 3.3: Macro-fiber composite bonded to the torus.

3.2.2 Results of Control Experiments

The first control experiment performed used an electromagnetic shaker to excite the torus and multiple MFC sensors and actuators to combat the disturbance signal. Before the control system could be implemented, the ability of the shaker to excite the global modes of the torus needed to be identified. Therefore, the torus was excited using a burst chirp signal from 0 to 100Hz and the frequency response function (FRF) was measured using MFC sensors. The choice of excitation signal greatly affects the ability to excite the global modes of the structure. This issue takes a trial and error process to find the ideal length and bandwidth signal for the range of frequencies of interest. It was found that a slow chirp signal that allowed sufficient energy to be input to the system at each frequency worked the best. In addition, to using a chirp signal it was found that the quality of the measured FRF was greatly increased when a burst signal was used. A burst signal contains two periods, during the first period the range of frequencies is swept through and during the second period nothing is sent out. This time frame when no signal is output allows the vibration of the structure to damp out and avoid leakage in the measured frequency response. Using this choice of excitation signal and a MFC as a sensor, several FRF have been measured, one of the typical results is shown in Figure 3.3. Looking at both the magnitude and coherence of the measurement, it is clear that with the correct choice of input signal the shaker is capable exciteing the structure in the frequency range of interest and the MFC

can provide an accurate sensing signal. The very high damping properties of the structure can also be seen in the magnitude of the response shown in Figure 3.4.

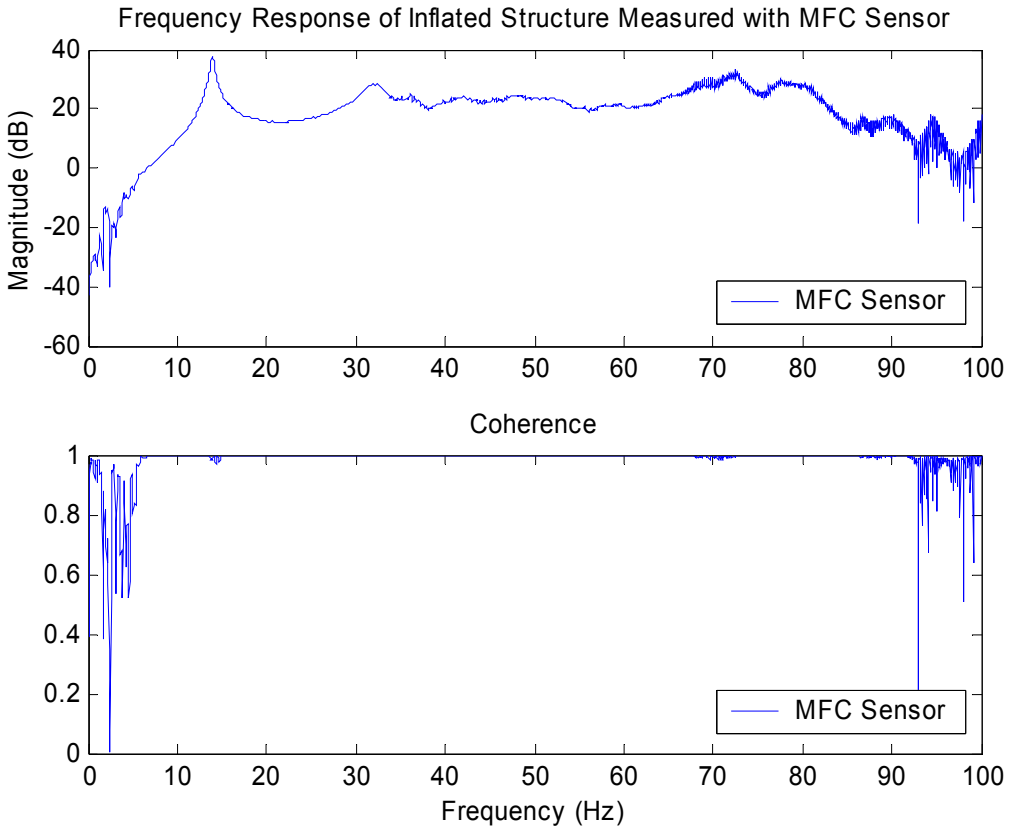

Figure 3.4: Frequency response measured from an MFC.

Once the shaker's ability to excite the structure and the MFC's sensing capabilities were realized, a multiple sensor/actuator control experiment was setup. Two pairs of sensors and actuators were applied to the torus in the configuration shown in Figure 3.5. Positive position feedback (PPF) control techniques similar to those discussed in chapter two were used since they are fairly simple and straightforward to implement in the absence of an accurate model of the system. The PPF controller was implemented and adjusted in real time using the dSpace control board model DS1102. It was found that the control systems developed using MFC as both actuators and sensors were capable of significantly reducing vibration levels of the first mode in the torus. In one experiment, a control system was designed to attenuate vibration in the first out-of-plane mode (12.8 Hz) of the torus. Figure 3.6 shows the frequency response of the system before and after control was applied. It can be seen from the figure that when one set of sensors and actuators is turned on, there is a clear reduction in vibration level of approximately 50% and

more significant vibration reduction, on the order of 70%, is achieved when both pairs of sensors and actuators are turned on. The time response of the vibration before and after the control system was applied is shown in Figure 3.7. Looking a Figure 3.7, the uncontrolled vibration is shown until the first sensor/actuator pair is turned on at 7 seconds this if followed by sensor actuator pair two turned on at 13 seconds. The top plot is the response of sensor one and the bottom plot is the response measured by sensor two. An important point that is shown in this figure is that there is a global reduction in vibration. This can be presumed because the vibration is reduced at two locations that are not in close proximity to each other. As the bonding condition improves, it is expected that the control authority over the whole structure would increase.

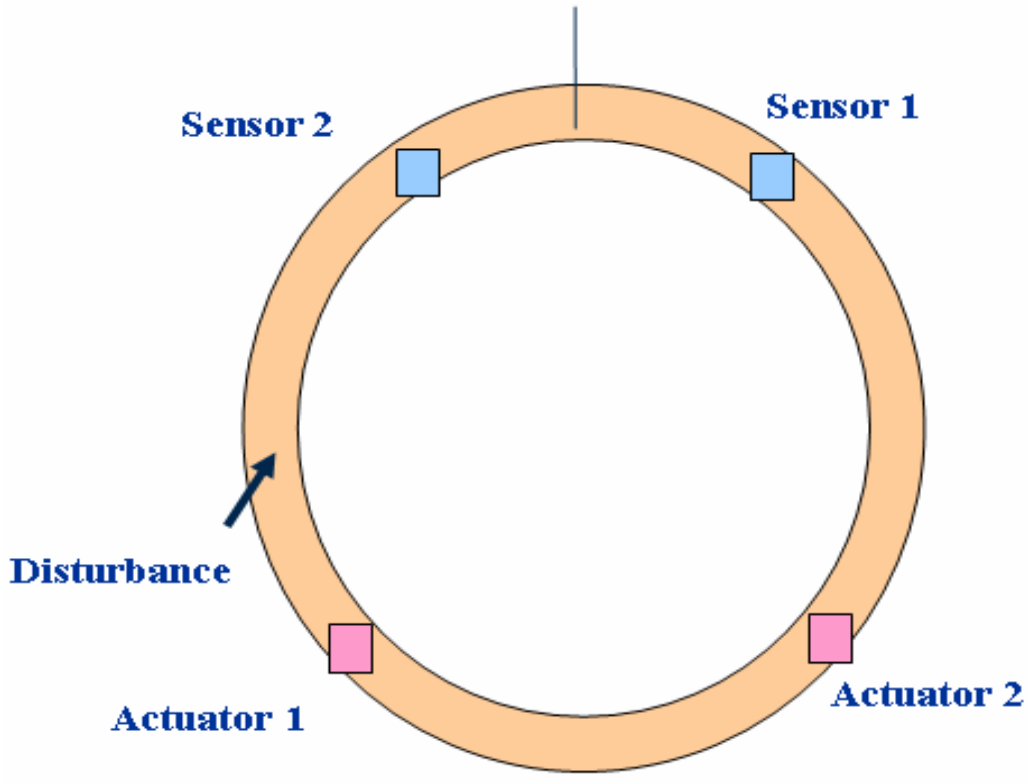

Figure 3.5: Location of disturbance input, sensor and actuator locations.

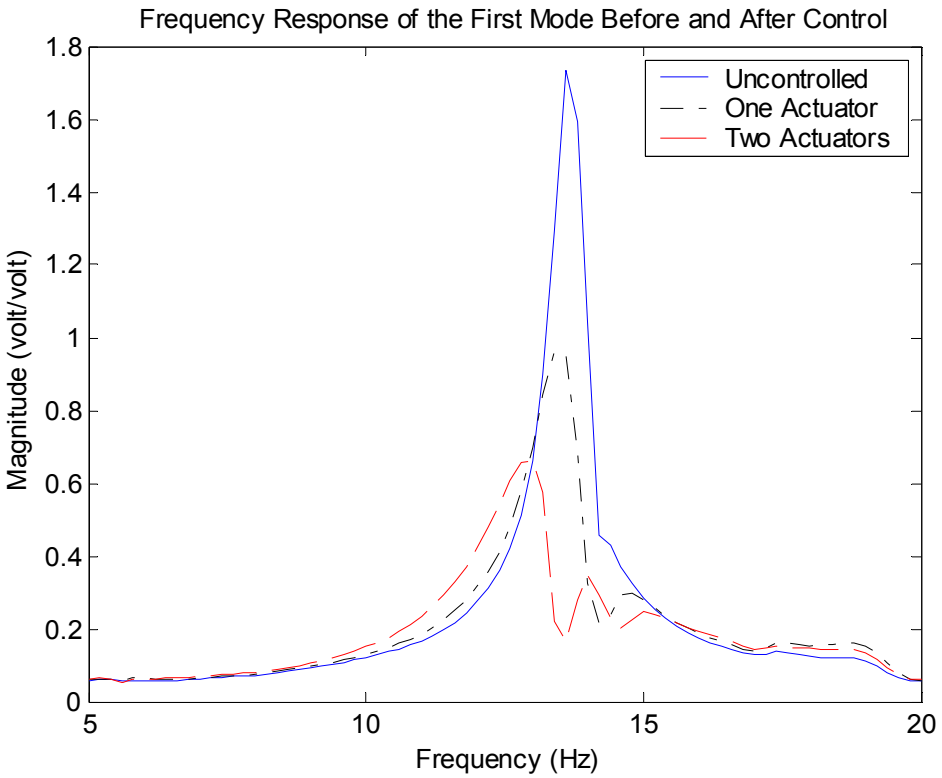

Figure 3.6: Frequency response of the first mode with no control, one actuator and two actuators.

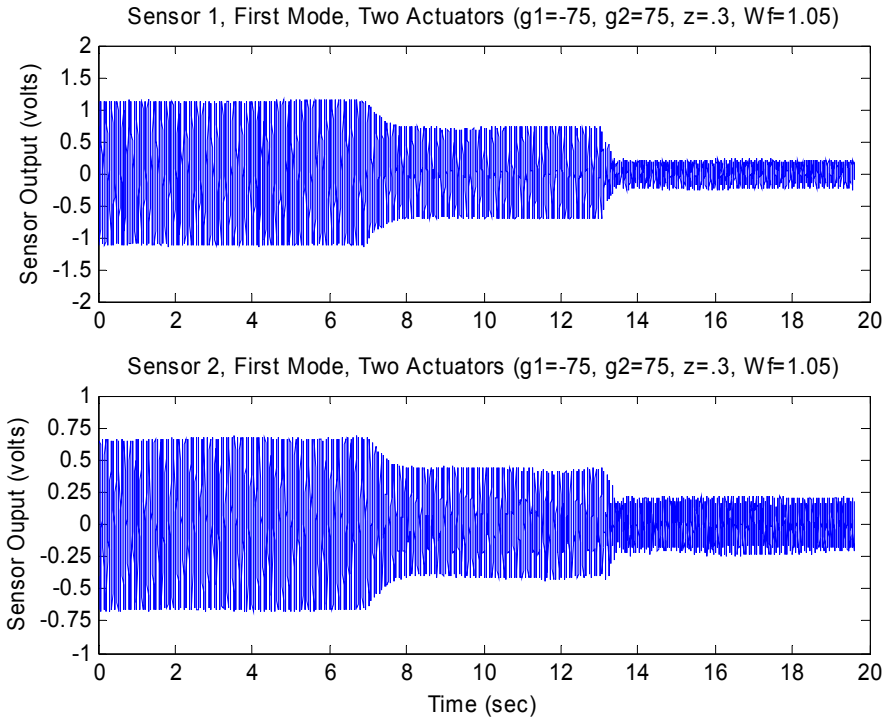

Figure 3.7: Time response of the torus before and after control was applied.

After demonstrating that the control system was capable of supplying significant vibration reduction to the first mode, our next experiment was to apply vibration control to the second mode. To do so, a similar PPF controller was designed and the same orientation of the sensors and actuators, shown in Figure 3.5 was used. However, when the control scheme was applied to the second mode, significantly different results were observed. The time response of the second mode before and after control was applied is shown in Figure 3.8. In Figure 3.8 the uncontrolled vibration is present until the first sensor/actuator pair is turned on at about six seconds, followed by the second sensor/actuator pair turned on at about 12 seconds. When the first actuator is turned on, the vibration is reduced at sensor one's location but increased at sensor two's location and likewise when actuator two is turned on. This effect clearly shows that the control system is ineffective at globally reducing the torus's second mode of vibration. This can be explained for two reasons, the relative phase of the sensor and actuator, and the existence of repeated frequencies and modes. The first reason can be seen by looking at Figure 3.9, which shows the first two out of plane mode shapes of the torus (Park et al., 2002). Recalling the setup of our control experiment from Figure 3.5, each sensor is located 180 degrees from its corresponding actuator. Now looking at Figure 3.8, the first mode has the same displacement at any two points 180 degrees apart, but in the second mode the displacement is the same at any two points 120 degrees apart. Because the sensors and actuators are located 180 degrees from one another, when controlling the first mode they are experiencing the same vibration and can be considered in phase, but at any mode higher than this the sensor and actuator are experiencing significantly different vibrations and are out of phase. Because positive position feedback techniques rely only on a filter and not a model, it is very important that the sensor and actuator be in phase and experience the same dynamics. In this case they are not in phase; the result is an ineffective controller. Therefore, this orientation of sensor and actuator with a PPF control scheme will only achieve global vibration reduction during the torus's first mode of vibration. The current setup could be made effective if an accurate model of the system was known and a different control method was used. However, the formulations of the model for a prestressed toriodal shell are nonlinear and very difficult determine, for more information on the modeling of a toroidal shell see Jha and Inman (2002). Because of the difficulties in modeling such a complex structure, control techniques that do not rely on an accurate model are all that can be performed on inflatable structure at this point.

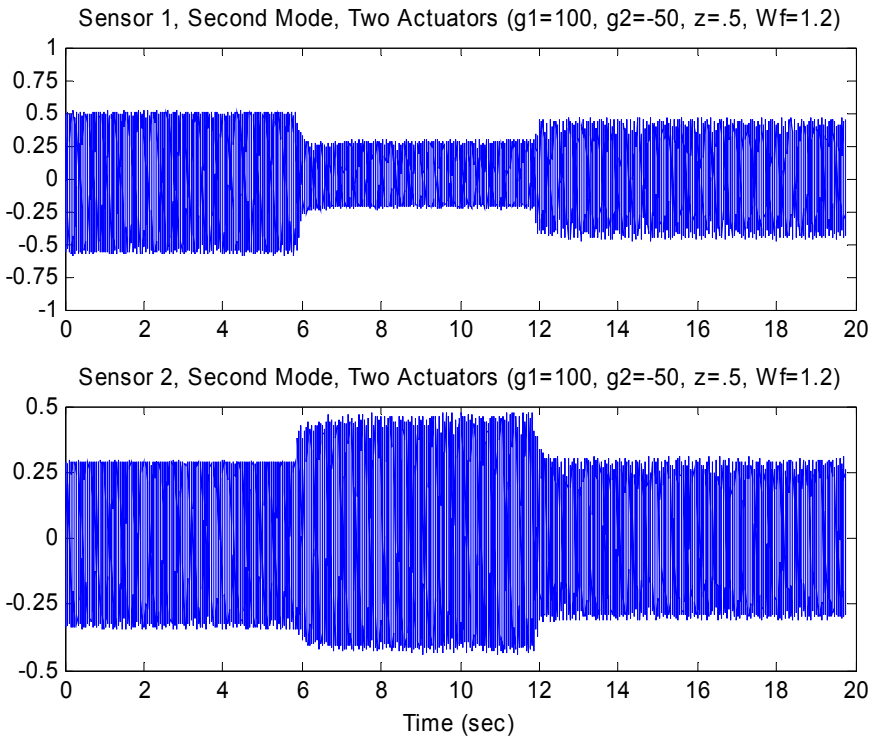

Figure 3.8: Time response of the second mode before and after control was applied.

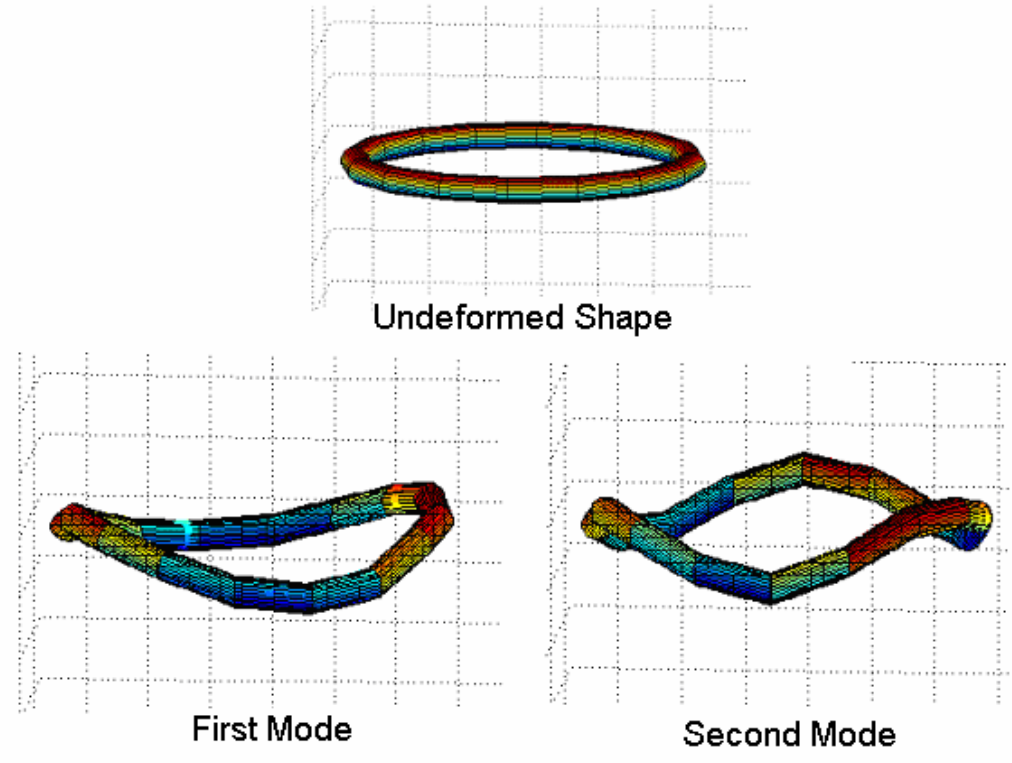

Figure 3.9: First two out of plane mode shapes of the torus (Park et al., 2002).

The second issue that arises in performing control on the toroidal structure is the presences of repeated natural frequencies and mode shapes in the symmetric structure (Jha, 2002). Because of the presence of repeated frequencies, the controller is required to have at least the same number of actuators as the number of times the frequency is repeated. In this case, the control system that was designed should have worked because there were two repeated frequencies and two actuators present. However, Because of the problems associated with the layout mentioned previously and the complication requiring two actuators, the structure was unable to be controlled. The combined effect of these two issues is that the control system allows the mode shapes to rotate around the symmetric structure instead of globally suppressing them. This effect explains why an increase in vibration occurs at one sensor and a decrease at the other. For the control experiment to work on the second mode of the inflatable structure the layout of the sensors and actuator needs to be reconfigured keeping in mind the presence of repeated frequencies that may cause spillover or perhaps additional actuators may be needed.

However, a solution simpler than determining the ideal locations of the sensors and actuators for each mode and one that would also allow the sensors and actuators to always be in phase exists. This simpler solution is to use the self-sensing control techniques described in chapter two. In this configuration the sensor and actuator would always be in phase for every mode shape because they would be perfectly collocated. In addition, if a model were used to find the ideal location of the sensors and actuators, when in orbit the changes in pressure as the satellite travels from orbital night to orbital day along with other possible changes would cause these locations to become ineffective at times. Therefore, the ideal location of both sensor and actuator that would allow for control of all modes regardless of parameter changes in the torus would be collocated, which can only be truly achieved using self-sensing actuators. Further, the use of self-sensing techniques would allow the number of actuator patches applied to the torus to be cut in half, in turn, reducing the amount of areas containing localized stiffness effects, number of patches that could be damaged and the amount of wires attached to the structure. In the following sections I will describe the tests performed on the torus to verify that self-sensing techniques are compatible with inflatable structures.

3.3 Self-Sensing MFC for Control of Inflatable Structure

In chapter two the MFC was shown to be effective as a self-sensing actuator for both measuring the frequency response and applying control to a cantilever beam. This next application of the MFC as a self-sensing actuator is to demonstrate its compatibility with an inflatable torus. The work presented in the following section does not realize control of the inflated torus, but does show that self-sensing actuators could be used for this purpose.

3.3.1 Experimental Setup

The following experiments were performed on the same inflatable torus as in the previous sections of this chapter. The MFC self-sensing actuator and the applied disturbance were positioned on the torus as shown in Figure 3.10. The active area of the MFC patch measured 87.3 x 57.4mm with a capacitance of 4.6ηF. The self-sensing circuit layout shown in Figure 2.1 of chapter two was also used for these experiments. A self-sensing circuit requires three operational amplifiers to separate the control signal from the sensing signal, for the tests performed on the inflated torus Burr Brown model OPA452 rated at 80 volts were used. These op-amps are limited to a maximum control voltage of 40 volts before they will be damaged.

3.3.2 Self-Sensing Control Results

As done before in chapter two, the frequency response of the torus was measured before the self-sensing control was applied to the torus. This was done to ensure that the self-sensing circuit was balanced and no other problems were present. The torus was excited using an electromagnetic shaker from 0 to 100Hz and the frequency response was measured using both the self-sensing MFC actuator and a PCB accelerometer model 352C22. The measurements made using the accelerometer were used to ensure that the self-sensing MFC's signal was accurate. The resulting FRF measured from the accelerometer and the MFC are shown in Figure 3.11. From the figure it can be seen that the measurements made using the self-sensing MFC are almost identical to those measured with an accelerometer, indicating that the self-sensing circuit is working properly.

Now that the MFC self-sensing actuator has been shown to be compatible with inflatable structures, and to produce an accurate measurement of the frequency response, the next step would be to demonstrate control of the torus using the self-sensing actuator. However, when designing a PPF controller, the system is subject to instabilities that can cause it to go unstable and send surge control voltages out. This would not be an issue in a normal control system but when working with self-sensing actuators the circuit provides a direct path surge voltage into the dSpace control board. In the event that a control voltage higher than the circuit's capacity is sent out, it is unlikely that the circuit could cancel it out, potentially damaging the controller. Due to these limitations in the circuitry and the vulnerability of the control board used, vibration control could not be safely applied to the torus. Instead, an experiment was performed to show that if the correct equipment were available then vibration suppression could be achieved. To do this, the torus was excited using an electromagnetic shaker from 0 to 100Hz and a 10 volt control signal was fed into the MFC. The self-sensing circuit was then used to distinguish between the applied control signal and the sensing signal while measuring an accurate frequency response. Figure 3.12 shows both the frequency response measured by the self-sensing MFC actuator attached to the torus and an accelerometer. It is clear from the Figure that the circuit was able to measure an accurate frequency response. In chapter two it was shown that if the MFC self-sensing actuator could measure an accurate sensing signal then it could control the vibration of a beam. In the previous sections of this chapter it has been shown that the MFC can effectively suppress the vibration of the torus. Therefore, since it has been shown that when the self-sensing MFC measures an accurate sensing signal, regardless of the control signal applied, it can be used for control and the MFC has been shown to suppress the vibration of an inflatable torus, then with the necessary test equipment a self-sensing MFC actuator could be used to attenuate the vibration of the torus. These results show that the potential for using self-sensing actuators for vibration control of inflatable structures exists.

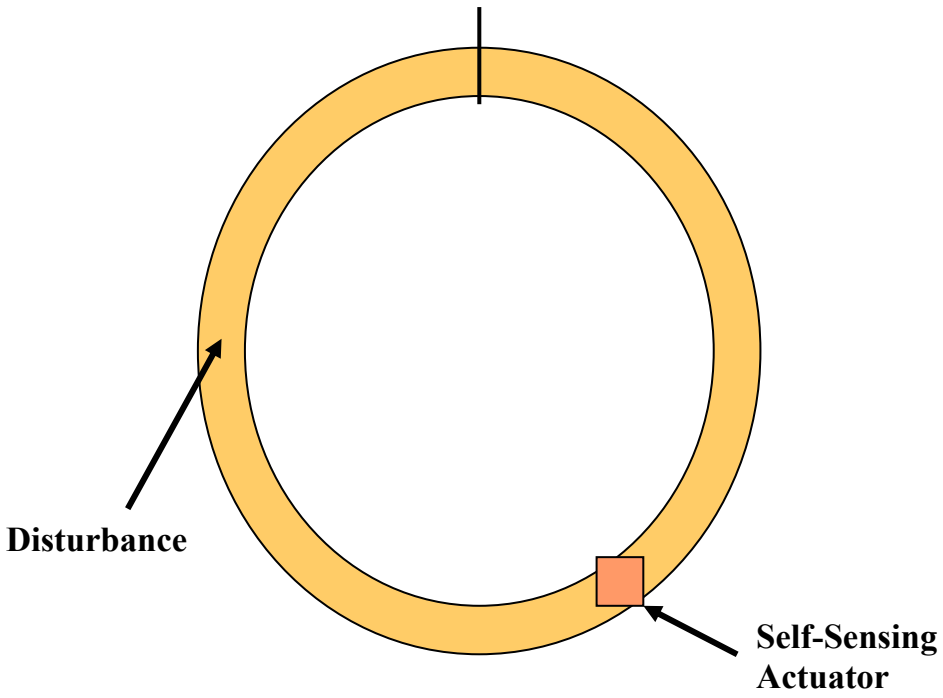

Figure 3.10: Location of disturbance and self-sensing actuator of inflatable torus.

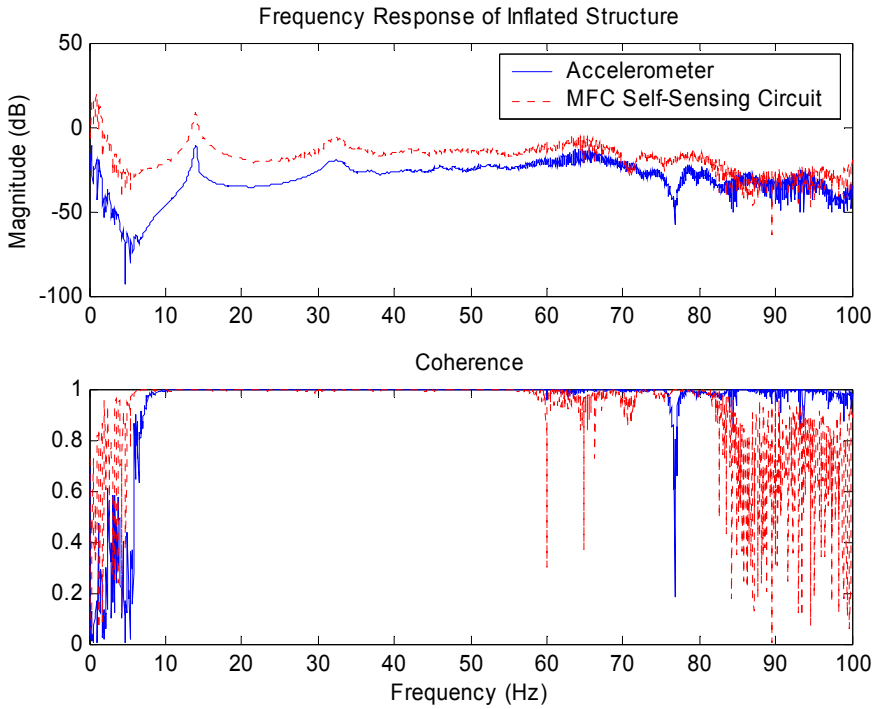

Figure 3.11: Frequency response of the inflated torus measured with a self-sensing circuit and an accelerometer.

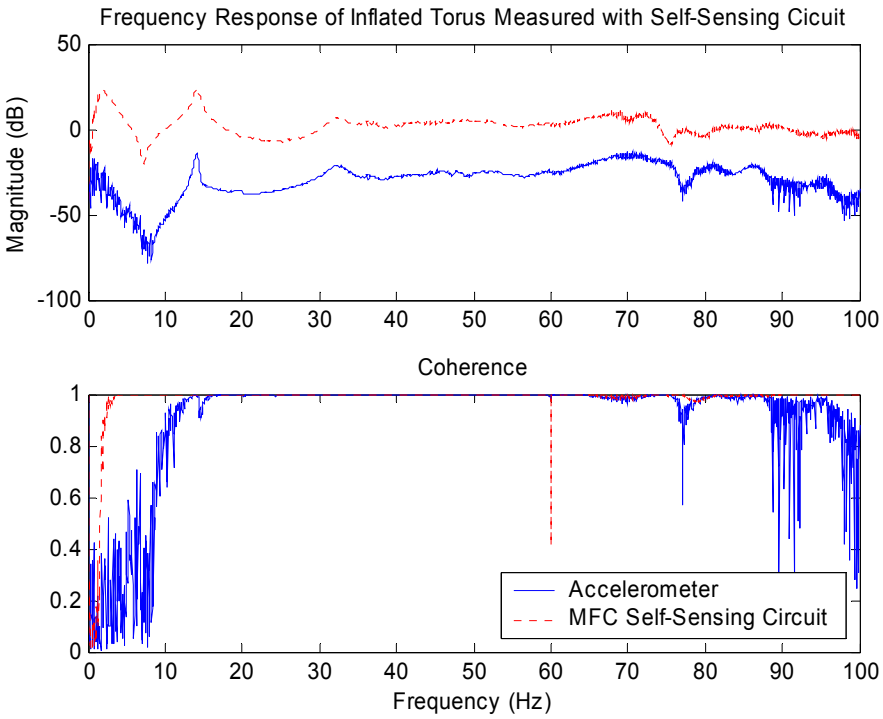

Figure 3.12: Frequency response of inflated torus found using self-sensing circuit with a disturbance signal applied to the MFC.

3.4 Chapter Summary

Chapter three investigates the use of multiple sensors and actuator for vibration suppression of an inflatable torus. Inflated satellite have become popular over the last few decades because of their extreme lightweight and flexible nature allows them to be packaged while in the cargo bay of the shuttle. While this type of structure holds many advantages for use as a satellite, it poses certain difficulties for vibration testing and control. Traditional methods actuation result in only local deflection and are not suitable for control actuators. However, smart materials have recently been shown to be effective as mechanisms for applying control to inflatable structures. The macro-fiber composite (MFC) actuator is the most suited of the smart materials for this application and in previous studies one MFC actuator has been shown to globally excite a scaled inflatable torus. While this method worked well for a scaled torus an actual inflated torus intended for use in space would have a diameter as large as 30 meters it is highly unlikely one actuator could globally excite these immense structures intended for space.

Therefore, it is necessary to develop methods of vibration control using multiple sensors and actuators.

The first portion of the work presented in this chapter designed and implemented a control system to suppress the vibration of an inflated torus. An inflated torus was outfitted with two sets of sensors and actuators and a positive position feedback controller was built to use both pairs separately for vibration control of the torus. It was found that the configuration of sensor and actuator used was very effective for the first mode and that the use of two actuators significantly increased the vibration suppression. However, the layout used and the existence of repeated frequencies in the torus cause the controller to be ineffective at the second mode causing the modes shapes to rotate around the symmetric structure. Because the optimal location of the sensors and actuators was not the same for every mode, self-sensing control was investigated. The use of self-sensing actuators would allow every mode of the torus to be controller while reducing the number of MFC applied to the torus by half.

To show that self-sensing techniques are compatible with inflatable structures a control signal was applied to an MFC self-sensing actuator and the frequency response of the torus was measured. Although the procedure did not directly show that control could be applied to the torus it does show that collocated control could be applied to the torus. Control was not fully realized because of the limitations in the control board used and the operational amplifiers used in the circuit. This experiment shows the possibility of control because in chapter two it was shown that if the self-sensing actuator could measure an accurate sensing signal then it could suppress the vibration of a beam, and in this chapter it was shown that the MFC actuator is capable of attenuating vibration of the torus. Therefore, with the results of previous tests it can be concluded that had the correct equipment been available self-sensing control would have been achieved. The experimental investigation of self-sensing actuation will be performed one the required hardware is available, and will be left for future work.

Chapter 4

Model of Piezoelectric Power Harvesting Beam

4.1 Introduction to Power Harvesting

Piezoelectric materials can be used as mechanisms to transfer mechanical energy usually ambient vibration into electrical energy that can be stored and used to power other devices. With the recent advances in wireless and MEMS technology, sensors can be placed almost anywhere necessary. Since these devices are wireless it becomes necessary that they have their own power supply. This power supply in most cases is the conventional battery, however problems can occur when using batteries because of there finite life span. When the battery is extinguished of all its power, the sensor must be retrieved and the battery changed. Because wireless sensors are developed so that they can be placed in remote locations such as structural sensors on a bridge or GPS tracking devices on animals in the wild, obtaining the sensor simply to replace the battery can become a very expensive task. Therefore, if a method of obtaining the untapped energy surrounding these sensors was implemented, significant life could be added to the power supply. One method is to use piezoelectric materials to obtain energy lost due to vibrations of the test specimen. This captured energy could then be used to prolong the life of the power supply or in the ideal case provide endless energy for the sensor's lifespan.

It has been found that a piezoelectric device attached to a beam with cantilever boundary conditions provides an effective configuration of capturing transverse vibrations and converting

them into useful electrical power. This configuration has proven itself to be effective in several experiments carried out at the Center for Intelligent Materials Systems and Structure (CIMSS) at Virginia Tech, which will be discussed in the following chapter. The work that will presented in the subsequent sections will concentrate on developing a model of a beam with piezoelectric elements attached that will provide an accurate estimate of the power generated through the piezoelectric effect. The model detailed in this chapter is based off of a more general one developed by Hagood et al. (1990) to estimate the performance of piezoelectric shunt damping circuits for active control. In addition, the model developed in Crawley et al. (1990) was used to develop the actuation equations for piezoelectric devices and the constitutive equations of bimorph actuators were obtained from Smits et al. (1991). An important addition to the combination of these models that is made to accommodate power harvesting, which was neglected in previous models, was to add material damping; if excluded the model can predict significantly more energy generation that actually developed in the real system. The following sections will develop a model of the piezoelectric power harvesting device. This model would simplify the design procedure necessary for determining the appropriate size and vibration levels necessary for sufficient energy to be produced and supplied to the desired electronic devices. An experimental verification, of the model is also performed to ensure its accuracy. Following the model verification the effects of power harvesting on the dynamics of a structure are compared to those brought on from shunt damping.

4.2 Piezoelectric Power Harvesting Beam

The following sections will develop a model to provide the amount of energy generated in the piezoelectric elements attached to a beam experiencing vibration energy. The model will be verified on a composite piezoelectric bimorph cantilever beam. This structure used to verify the model has a complicated piezoelectric layout and a composite makeup, demonstrating that the model can produce accurate results independent of the layout or complexity of the beam. The last section of this chapter will make a comparison between the dynamic effects of power harvesting and shunt damping.

4.2.1 Model of Piezoelectric Power Harvesting Beam

The following derivation will use energy methods to develop the constitutive equations of a bimorph piezoelectric cantilever beam for power harvesting. To begin the deviation we will start with the general form of Hamilton's Principle. This states that the variational indicator must be zero at all time, as shown below in equation 4.1:

$$\text{V.I.} = \int_{t_1}^{t_2} \left[\delta T - \delta U + f\delta x\right] dt = 0 \tag{4.1}$$

where T, U and $f\delta x$ terms are defined by:

$$U = \frac{1}{2}\int_{V_S} \underline{S}^T \underline{T}\, dV_s + \frac{1}{2}\int_{V_P} \underline{S}^T \underline{T}\, dV_p - \int_{V_P} \underline{E}^T \underline{D}\, dV_p \tag{4.2}$$

$$T = \frac{1}{2}\int_{V_S} \rho_s \dot{\underline{u}}^T \dot{\underline{u}}\, dV_s + \frac{1}{2}\int_{V_P} \rho_s \dot{\underline{u}}^T \dot{\underline{u}}\, dV_p \tag{4.3}$$

$$f\delta x = \sum_{i=1}^{nf} \delta \underline{u}(x_i) \cdot \underline{f_i}(x_i) - \sum_{j=1}^{nq} \delta \underline{v} \cdot \underline{q_j} \tag{4.4}$$

where U is the potential energy, T is the kinetic energy, $f\delta x$ is the external work applied to the system, S is the strain, T is the stress, E is the electric filed, D is the electric displacement, V is the volume, u is the displacement, x is the position along the beam, v is the applied voltage, q is the charge, ρ is the density f is the applied force and the subscripts p and s, represent the piezoelectric material and the substrate, respectively. Before the variational indicator can be used to solve for the equations of motion the piezoelectric constitutive equations need to be introduced into the potential energy term and the variation of both the potential and kinetic energy must be found. First the piezoelectric constitutive equations will be introduced, which are:

$$\begin{bmatrix} \underline{T} \\ \underline{D} \end{bmatrix} = \begin{bmatrix} c^E & -e^T \\ e & \varepsilon^S \end{bmatrix} \begin{bmatrix} \underline{S} \\ \underline{E} \end{bmatrix} \tag{4.5}$$

where c is the modulus of elasticity, ε is the dielectric constant and the superscript, $(\,)^S$, signifies the parameter was measured at constant strain and the superscript, $(\,)^E$, indicates the parameter was measured at constant electric field (short circuit). These constitutive equations relate the electrical and mechanical properties of the piezoelectric element. The specification of these relationships will allow electromechanical interaction to be included in the model. The term e is the piezoelectric coupling coefficient and relates the stress to the applied electric field. The piezoelectric coupling coefficient can be written as shown in equation 4.6 in terms of the more commonly specified coupling coefficient d by:

$$e = d_{ij} c^E \tag{4.6}$$

where c is the d_{ij} is the piezoelectric coupling coefficient with the subscript i and j referring to the direction of the applied field and the poling, respectively. Now we can incorporate the piezoelectric properties in the potential energy function:

$$\begin{aligned} U = \frac{1}{2}\Big[& \int_{V_S} \underline{S}^T c_s \underline{S}\, dV_S + \int_{V_P} \underline{S}^T c^E \underline{S}\, dV_p \\ & - \int_{V_P} \underline{S}^T e^T \underline{E}\, dV_P - \int_{V_P} \underline{E}^T e \underline{S}\, dV_P \\ & - \int_{V_P} \underline{E}^T \varepsilon^S \underline{E}\, dV_P \Big] \end{aligned} \tag{4.7}$$

Taking the variation of the kinetic energy from equation 4.3, and the potential energy term containing the piezoelectric properties of equation 4.7, yields:

$$\begin{aligned} \delta U = & \int_{V_S} \delta \underline{S}^T c_s \underline{S}\, dV_S + \int_{V_P} \delta \underline{S}^T c^E \underline{S}\, dV_p \\ & - \int_{V_P} \delta \underline{S}^T e^T \underline{E}\, dV_P - \int_{V_P} \delta \underline{E}^T e \underline{S}\, dV_P \\ & - \int_{V_P} \delta \underline{E}^T \varepsilon^S \underline{E}\, dV_P \end{aligned} \tag{4.8}$$

$$\delta T = \int_{V_S} \rho_s \delta \dot{\underline{u}}^T \dot{\underline{u}}\, dV_s + \int_{V_P} \rho_p \delta \dot{\underline{u}}^T \dot{\underline{u}}\, dV_p \tag{4.9}$$

The variations found in equations 4.4, 4.8 and 4.9 can be substituted into equation 4.1 to obtain the variational indicator:

$$
\begin{aligned}
V.I. = \int_{t_1}^{t_2} \Bigg[& \int_{V_S} \rho_s \delta \underline{\dot{u}}^T \underline{\dot{u}} \, dV_s + \int_{V_P} \rho_p \delta \underline{\dot{u}}^T \underline{\dot{u}} \, dV_p \\
& - \int_{V_S} \delta \underline{S}^T c_s \underline{S} \, dV_S - \int_{V_P} \delta \underline{S}^T c^E \underline{S} \, dV_p \\
& + \int_{V_P} \delta \underline{S}^T e^T \underline{E} \, dV_P + \int_{V_P} \delta \underline{E}^T e \underline{S} \, dV_P \\
& + \int_{V_P} \delta \underline{E}^T \varepsilon^S \underline{E} \, dV_P + \sum_{i=1}^{nf} \delta \underline{u}(x_i) \cdot \underline{f}(x_i) - \sum_{j=1}^{nq} \delta \underline{v} \cdot \underline{q_j} \Bigg]
\end{aligned}
\tag{4.10}
$$

This equation can now be used to solve for the equations of motion of any mechanical system containing piezoelectric elements. In order to solve equation 4.10 for the cantilever beam with bimorph piezoelectric elements some assumptions must be made. The first assumption follows the Rayleigh-Ritz procedure, which says that the displacement of the beam can be written as the summation of modes in the beam and a temporal coordinate[16]:

$$
u(x,t) = \sum_{i=1}^{N} \phi_i(x) r_i(t) = \underline{\phi}(x) \underline{r}(t) \tag{4.12}
$$

where $\Phi_i(x)$ is the assumed mode shapes of the structure which can be set to satisfy any combination of boundary conditions, $r(t)$ is the temporal coordinate of the displacement and N is the number of modes to be included in the analysis. The second assumption made is to apply the Euler-Bernoulli beam theory. This allows the stain in the beam to be written as the product of the distance from the neutral axis and the second derivative of displacement with respect to the position along the beam. Once the strain is defined in this way equation 4.11 can be used define the strain as follows:

$$
\underline{S} = -y \frac{\partial^2 u(u,t)}{\partial x^2} = -y \phi(x)'' r(t) \tag{4.13}
$$

The third and last assumption is that the electric potential across the piezoelectric element is constant. This assumption also indicates that no field is applied to the beam, which in latter equations designates the beam to be inactive material:

$$\underline{E} = \psi(y)v(t) = \begin{cases} -v/t_p & t/2 < y < t/2 + t_p \\ 0 & -t/2 < y < t/2 \\ v/t_p & -t/2 - t_p < y < -t/2 \end{cases} \tag{4.14}$$

The previous assumption is for a beam with bimorph piezoelectric elements on the top and bottom of the beam as shown in Figure 4.1. The beam in Figure 4.1 also shows the notation for the geometry of the beam that is used throughout the derivation.

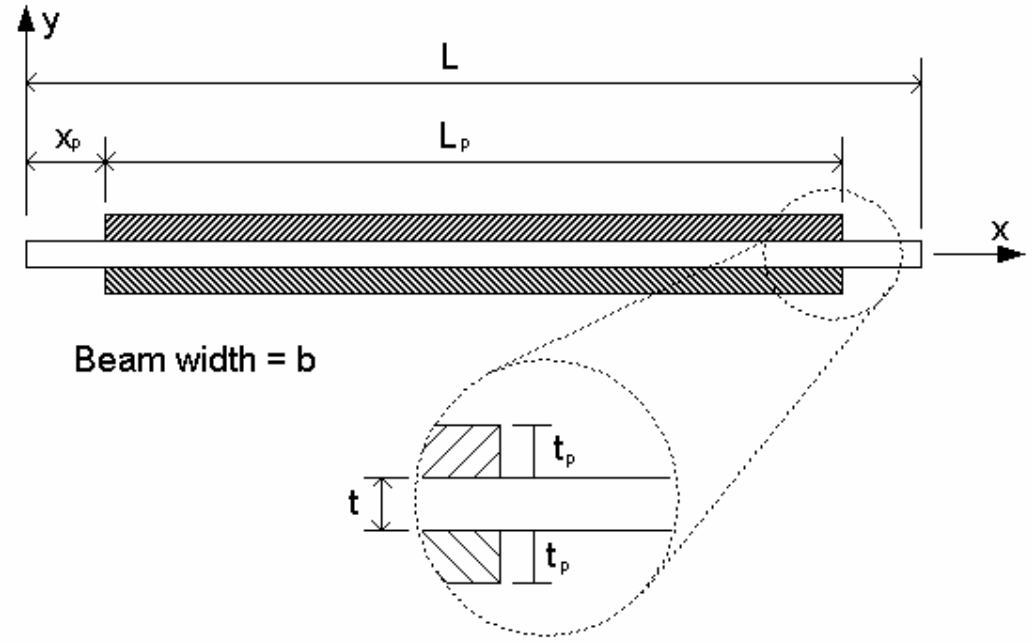

Figure 4.1: Schematic of beam describing the variables.

Using the previous assumptions we can simplify the variational indicator to include terms that represent physical parameters. By doing this the equations describing the system become more recognizable when compared to those of a typical system and help give physical meaning to the parameters in the equations of motion. The mass matrices for the system can be written as:

$$M_s = \int_{V_S} \rho_s \underline{\phi}^T(x)\underline{\phi}(x)dV_s$$

$$M_p = \int_{V_P} \rho_p \underline{\phi}^T(x)\underline{\phi}(x)dV_p \tag{4.15}$$

The stiffness matrices can be written as:

$$K_s = \int_{V_S} y^2 \underline{\phi}^T(x)'' c_s \underline{\phi}(x)'' dV_s$$

$$K_p = \int_{V_P} y^2 \underline{\phi}^T(x)'' c^E \underline{\phi}(x)'' dV_p \tag{4.16}$$

The electromechanical coupling matrix, Θ, and the capacitance matrix, C_p, are defined by:

$$\Theta = -\int_{V_P} y \underline{\phi}^T(x)'' e^T \psi(y) dV_p$$

$$C_p = \int_{V_p} \psi^T(y) \varepsilon^S \psi(y) dV_p \tag{4.17}$$

The parameters defined in equations 4.15, 4.16 and 4.17 can be substituted into variational indicator of equation 4.10. This substitution allows the variational indicator to be written as:

$$\begin{aligned} \text{V.I.} = \int_{t_1}^{t_2} \Big[& \delta \underline{\dot{r}}^T(t)(M_s + M_p)\underline{\dot{r}}(t) - \delta \underline{r}^T(t)(K_s + K_p)\underline{r}(t) \\ & + \delta \underline{r}^T(t)\Theta v(t) + \delta v(t)\Theta^T \underline{r}(t) + \delta v(t) C_p v(t) \\ & + \sum_{i=1}^{nf} \delta \underline{r}(t)\phi(x_i)^T f_i(t) - \sum_{j=1}^{nq} \delta \underline{v} q_j(t) \Big] dt = 0 \end{aligned} \tag{4.18}$$

where δ() indicates the variation of the corresponding variable. Taking the integral of the variational indicator leaves two coupled equations. The two equations shown below are coupled by the previously defined electromechanical coupling matrix Θ. The top equation defines the mechanical motion and the bottom equation defines the electrical properties of the system:

$$(M_s + M_p)\underline{\ddot{r}}(t) + (K_s + K_p)\underline{r}(t) - \Theta v(t) = \sum_{i=1}^{nf} \phi(x_i)^T f_i(t)$$

$$\Theta^T r(t) + C_p v(t) = q(t) \tag{4.19}$$

These equations now represents the electro-mechanical system and can be used to determine the motion of the beam, however this system of equations does not contain any energy dissipation. Because the model is intended to represent a power harvesting system that must be removing energy, this form is not suitable for our needs, as it does not account for energy lost through the structure. In addition, the energy removed from the system through energy harvesting must be accounted for. To incorporate energy dissipation into the equation we can use ohm's law and add a resistive element between the positive and negative electrodes of the piezoelectric. The resistive element will provide a means of removing energy from the system. If we do this the electrical boundary condition becomes:

$$v_i(t) = -R\dot{q}(t) \tag{4.20}$$

In addition to this, the system should have some type of additional mechanical damping that needs to be accounted for. If only the electrical damping is accounted for the model will over predict the actual amount of power generated. The amount of mechanical damping added to the model was determined from experimental results. This is done using proportional damping methods and the damping ratio that is predicted from the measured frequency response function. With the damping ratio known, proportional damping can be found from (Inman, 2001):

$$C = \alpha\left(M_s + M_p\right) + \beta\left(K_s + K_p\right) \tag{4.21}$$

where α and β are determined from:

$$\zeta_i = \frac{\alpha}{2\omega_i} + \frac{\beta\omega_i}{2} \quad i = 1,2,...n \tag{4.22}$$

where ζ_i is the damping ratio found from the frequency response of the structure. Incorporating equations 4.20 and 4.21 into equation 4.19, results in the final model of the power harvesting system:

$$\left(M_s + M_p\right)\ddot{\underline{r}}(t) + C\dot{\underline{r}}(t) + \left(K_s + K_p\right)\underline{r}(t) - \Theta v(t) = \sum_{i=1}^{nf} \phi(x_i)^T f_i(t)$$

$$R\dot{q}(t) - C_p^{-1}\Theta^T r(t) + C_p^{-1} q(t) = 0 \tag{4.23}$$

Equation 4.23 shown above provides an accurate model of the power harvesting system. The $\dot{q}(t)$ term provides the current output of the piezoelectric element and can be directly related to the power output of the piezoelectric through the load resistance *R*.

The last portion of our model left undefined is the forcing function. The system that we are investigating as mentioned earlier is a cantilever beam that is excited by transverse vibrations of the structure that it is clamped to; therefore no force is directly applied to the beam. Instead the clamped end of the beam is experiencing base motion and transferring that energy to the beam through its own inertia. The standard boundary conditions of the clamped end of the beam say that the slope and displacement are zero at all time. For the condition of base motion the zero displacement condition would not be held and a new set of mode shapes would need to be generated. Rather than doing this, it was decided that a force corresponding to the inertia of the beam when subjected to the base motion could be used and the clamped-free mode shapes would still be valid. The forcing function used to model the inertia of the beam is:

$$f(t) = \int_0^L \int_0^b \int_0^t \rho A \omega^2 \sin(\omega t) dz dy dx \tag{4.24}$$

With the forcing function defined everything necessary to simulate the power harvesting system is included in the model. The following sections of this chapter will describe the experimental procedures and results, in order to demonstrate the accuracy of this model.

4.2.2 Experimental Setup for Model Verification

The accuracy of the model is tested on a Midé Technology Corporation Quick Pack model QP40N, although, it could be used to model any beam with a piezoelectric attached. The QP40N is a bimorph actuator with dimensions and properties shown in Figure 4.2. The Quick

Pack is a piezoelectric actuator that is constructed from four piezo wafers embedding in a Kapton and epoxy matrix. The experiments were performed to test the amount of power generated from this device when subjected to transverse vibrations of varying frequency and amplitude. As mentioned previously we were interested in the quick Pack being mounted with cantilever boundary conditions. To provide the transverse vibration we mounted the Quick Pack actuator to an electromagnetic shaker as shown in Figure 4.3.

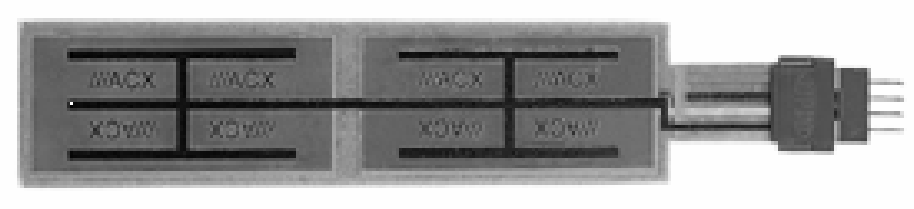

Device size (mm): 100.6 x 25.4 x 0.762
Device weight (g): 9.52
Active elements: 2 stacks of 2 piezos
Piezo wafer size (mm): 45.974 x 20.574 x 0.254
Full scale voltage range (V): ±200

Figure 4.2: Midé Technology Corporation Quick Pak model QP40N (from Midé Technology Corporation).

One complication arose when modeling the Quick Pack actuator due to its composite structure and the piezoelectric wafers not spanning the entire length of the beam, which can be seen in Figure 4.2. Because the area of the beam with no piezoelectric wafer consisted of only Kapton and epoxy, it contained a localized area containing a lower modulus of elasticity. Midé Technology Corporation could not specify a value for the effective modulus of the complete beam. Therefore, the setup shown in Figure 4.4 was constructed to measure the stiffness of the Quick Pack. To obtain a value for the stiffness the force applied to the beam and its corresponding deflection needed to be measured. The experimental setup constructed to do this consisted of a Transducer Techniques 100 gram load cell model GSO-100C and a polytec laser vibrometer. The load cell was mounted on a lead screw to allow a steady force to be applied at the tip of the beam. The result of this test found the modulus of the beam to be 2.5 GPa. The reason for this value being so low is due to the area at the mid-span of the beam that consisted of only the Kapton and epoxy. When the static tests were performed on the beam it was apparent

that the majority of the bending was occurring at this location. Therefore, it was concluded that the experimental tests performed had actually measured the modulus of elasticity corresponding to the Kapton and epoxy portion of the beam. This still left the overall modulus of the beam unknown. The value calculated for the overall the modulus of the beam was found by simply averaging the modulus of the piezoelectric material, that was supplied by Midé and the experimentally found modulus for the Kapton and epoxy matrix according to their individual percent of the cross sectional area. The resulting modulus of elasticity and the other piezoelectric properties used are shown in Table 4.1.

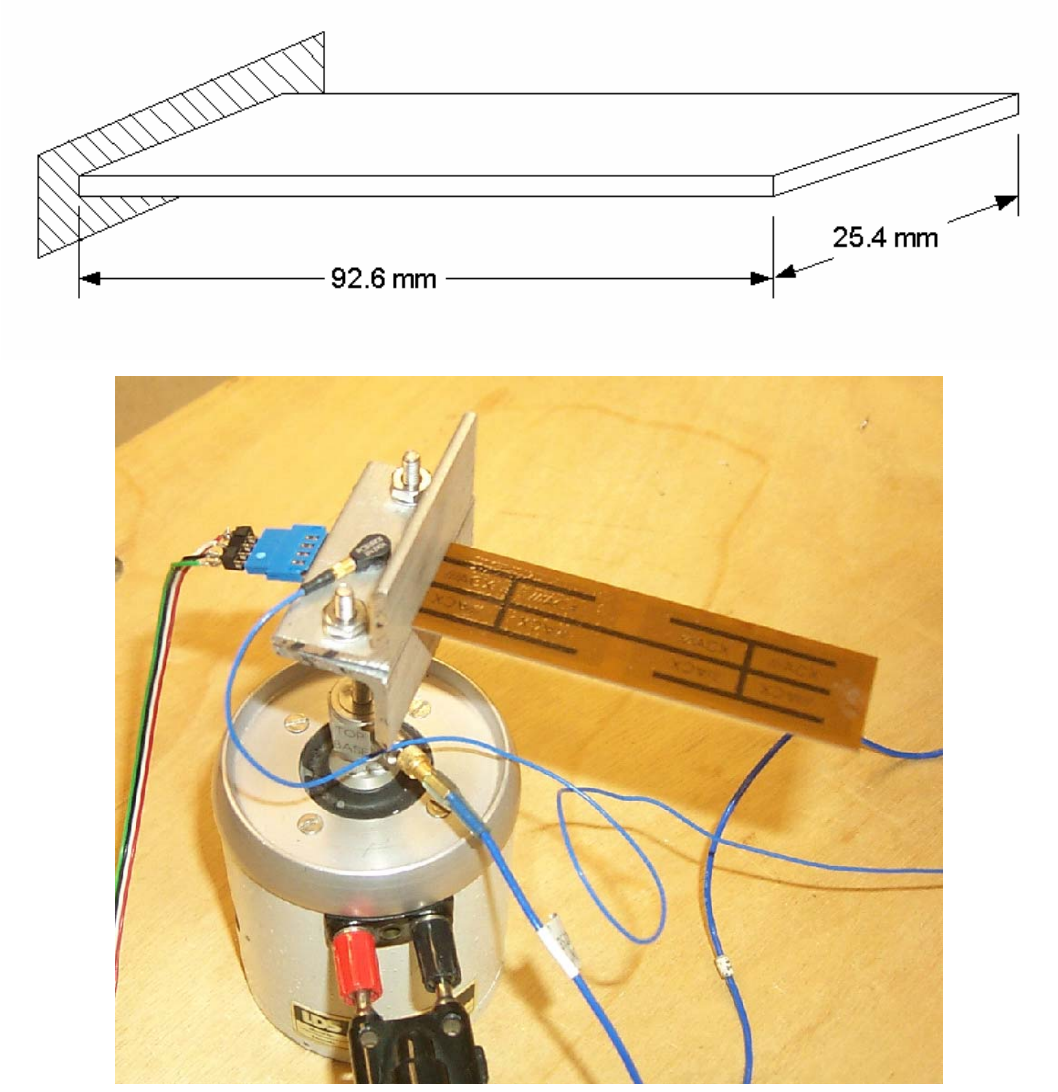

Figure 4.3: Quick Pack QP40N attached to the shaker and dimensions of beam when one end is clamped.

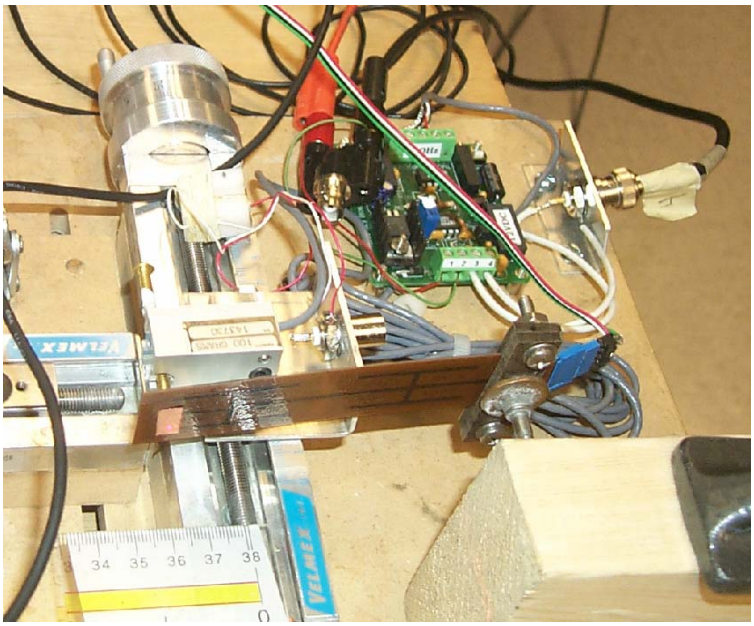

Figure 4.4: Experimental setup used to find the elastic modulus of the Kapton-epoxy matrix.

Table 4.1: Properties of the Quick Pack

Property	Symbol	Value
Dielectric Constant	k_3^T	1800
Piezoelectric Strain Coefficient	d_{13}	-179x10^{-12} m/volt
Modulus of Piezoelectric	c^E	63 GPa
Modulus of Kapton-epoxy	c_s	2.5 Gpa
Modulus of Quick Pack	c_b	35.17 GPa
Density of Piezo Material	ρ	7700 kg/m^3
Density Composite Matrix	ρ	2150 kg/m^3

4.2.3 Model Verification

The accuracy of the model was compared against experimental results to demonstrate the ability of the model to accurately predict the amount of power produced by the Quick Pack when subjected to transverse vibration. The code used to simulate the model can be found in Appendix

B. To ensure that the model and experimental tests were subjected to the same excitation force an accelerometer was used to calculate the amplitude of the sinusoidal force applied to the beam through:

$$a = A\omega^2 \sin(\omega t) \Rightarrow A_{\max} = \frac{a}{\omega^2} \tag{4.25}$$

where a is the acceleration of the clamped end of the beam. The beam was excited by a sinusoidal input and the steady state power output was measured across several different resistors. The frequency response of the model and the experimentally tested Quick Pack are shown in Figure 4.5. The differences in the two responses are attributed to the Quick Pack's composite structure resulting in coupled modes and the nonlinear properties of the Kapton material, especially its modulus of elasticity that varies nonlinearly with frequency. It is expected that a beam constructed of a homogeneous material with a piezoelectric mounted to is surface would produce a more accurate frequency response.

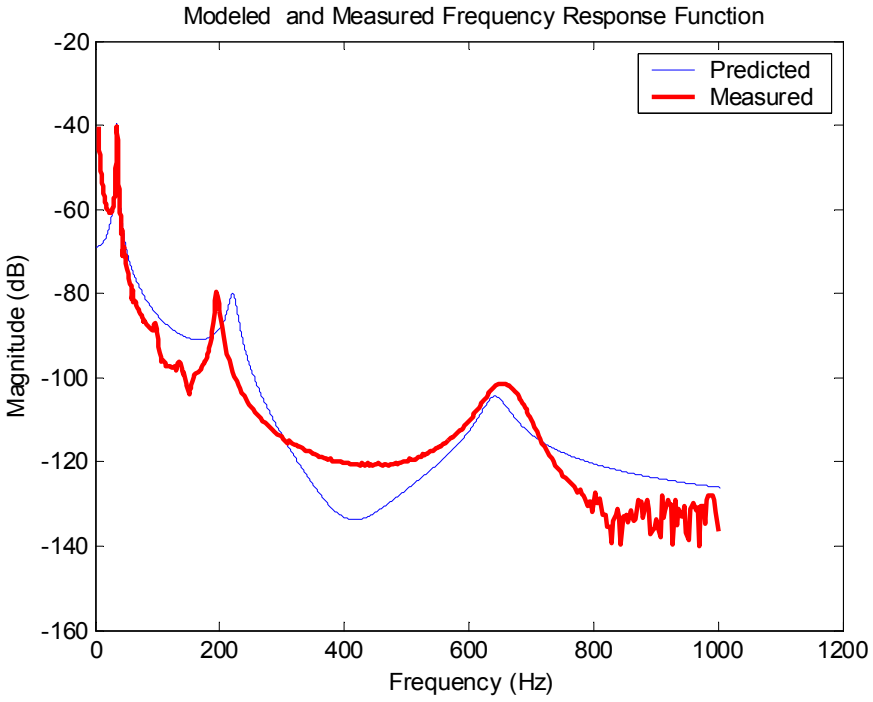

Figure 4.5: Frequency response of the model and the experimental data.

The output current of the Quick Pack was compared to the output current of the model with respect to time for various frequencies. The output current across a 10 kΩ resister for several frequencies of the model and the measured current obtained through experiments are shown is Figure 4.6, 4.7 and 4.8. Figures 4.9 and 4.10 show the output current across a 100Ω load resistance at 25 and 50Hz, respectively, and Figures 4.11 and 4.12 show the output current across a 100kΩ load resister at 25 and 50Hz, respectively. In the Figures the model shows a transient response for a small period of time, while the experimental results were recorded at steady state vibration. Therefore, the small period of time before the models settles down to steady state should not match. These Figures demonstrate that the model provides a very accurate measurement of the power generated at various frequencies and resistive loads. This shows that the model would be effective as a design tool for determining the ideal size and excitation level necessary to provide the desired power.

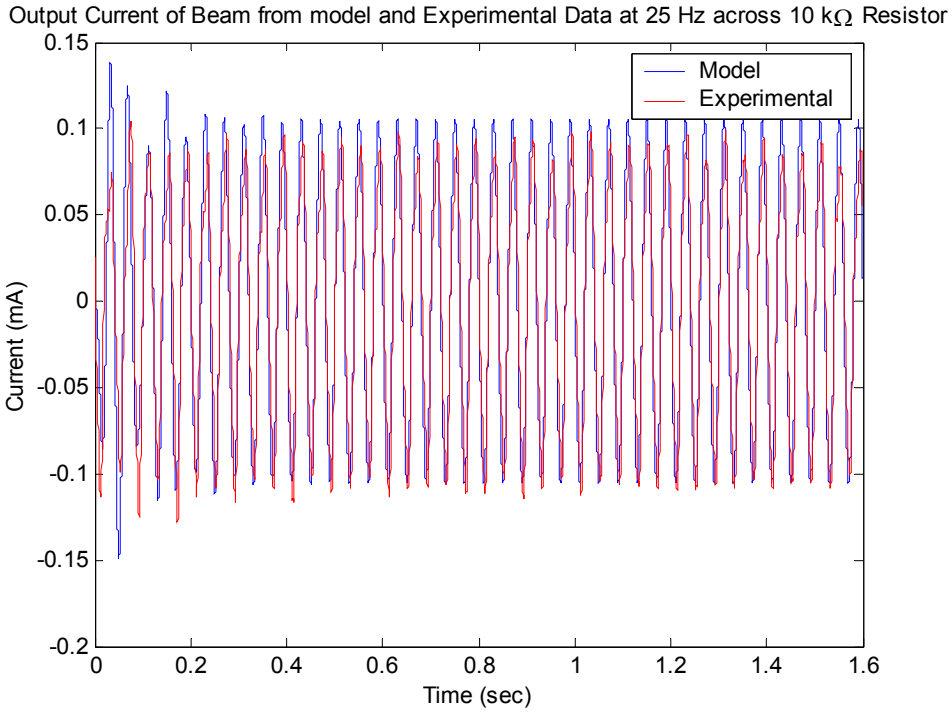

Figure 4.6: Output current predicted by model and measured across a 10KΩ resistor at 25Hz.

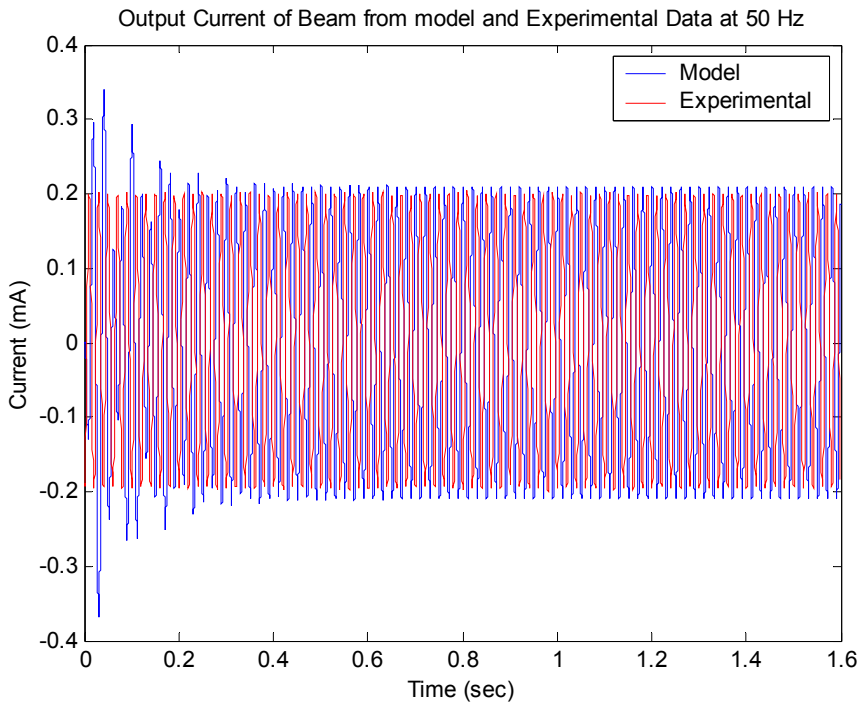

Figure 4.7: Output current predicted by model and measured across a 10KΩ resistor at 50Hz.

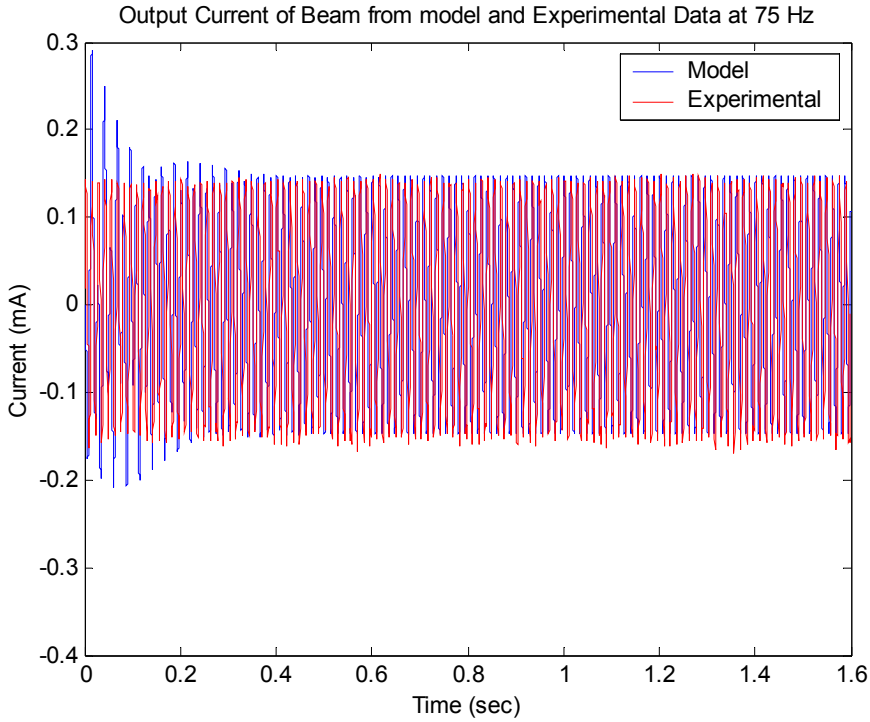

Figure 4.8: Output current predicted by model and measured across a 10KΩ resistor at 75Hz.

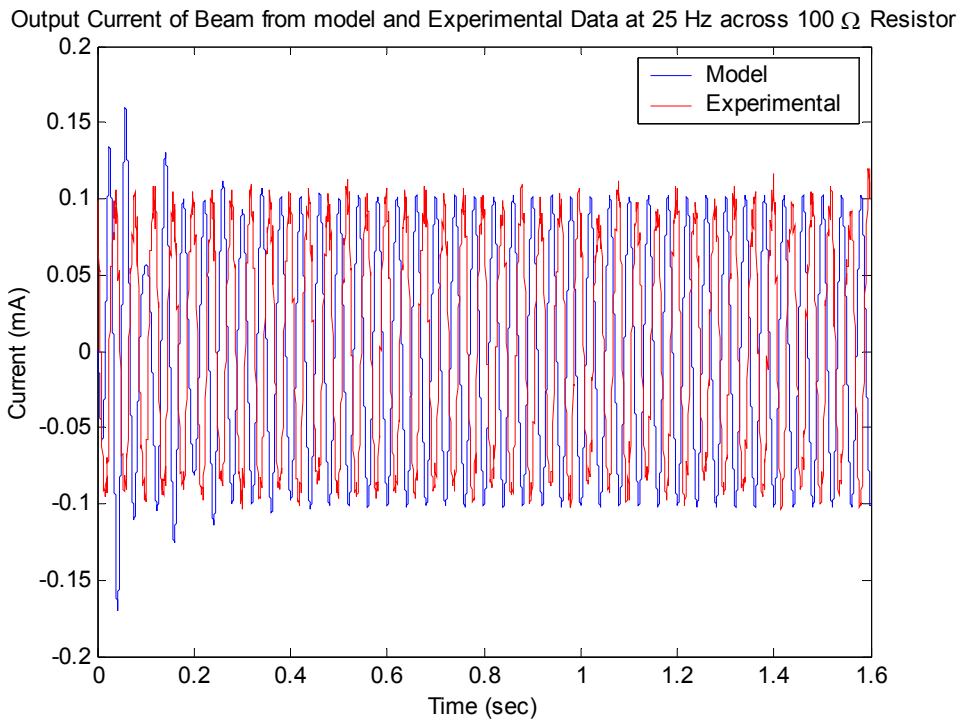

Figure 4.9: Output current predicted by model and measured across a 100Ω resistor at 25Hz.

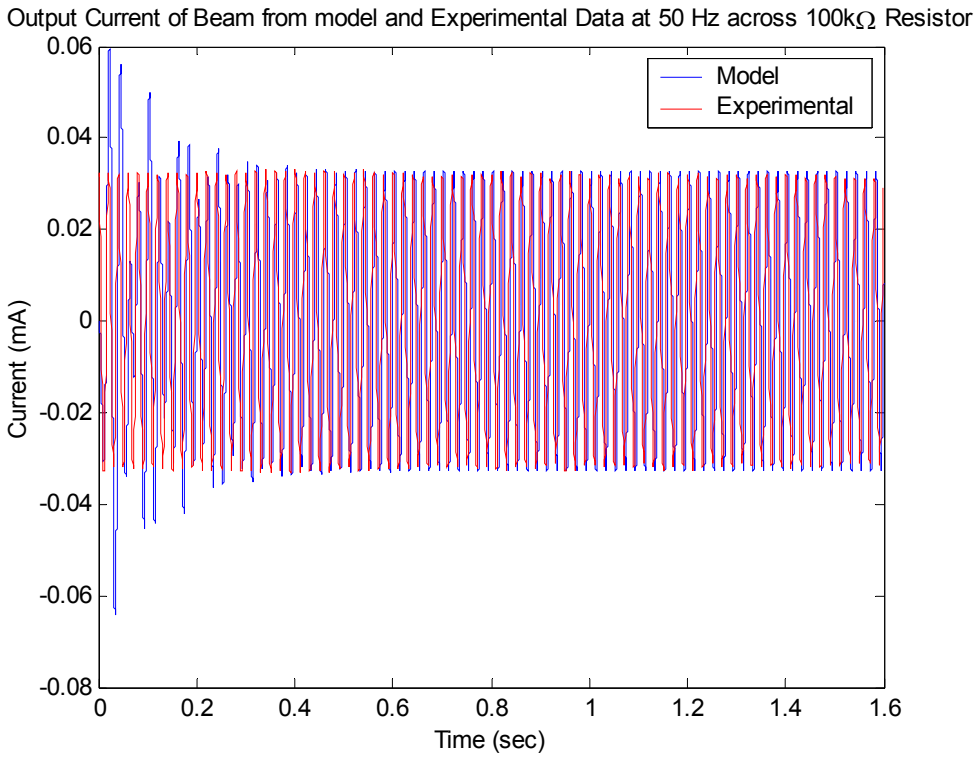

Figure 4.10: Output current predicted by model and measured across a 100KΩ resistor at 50Hz.

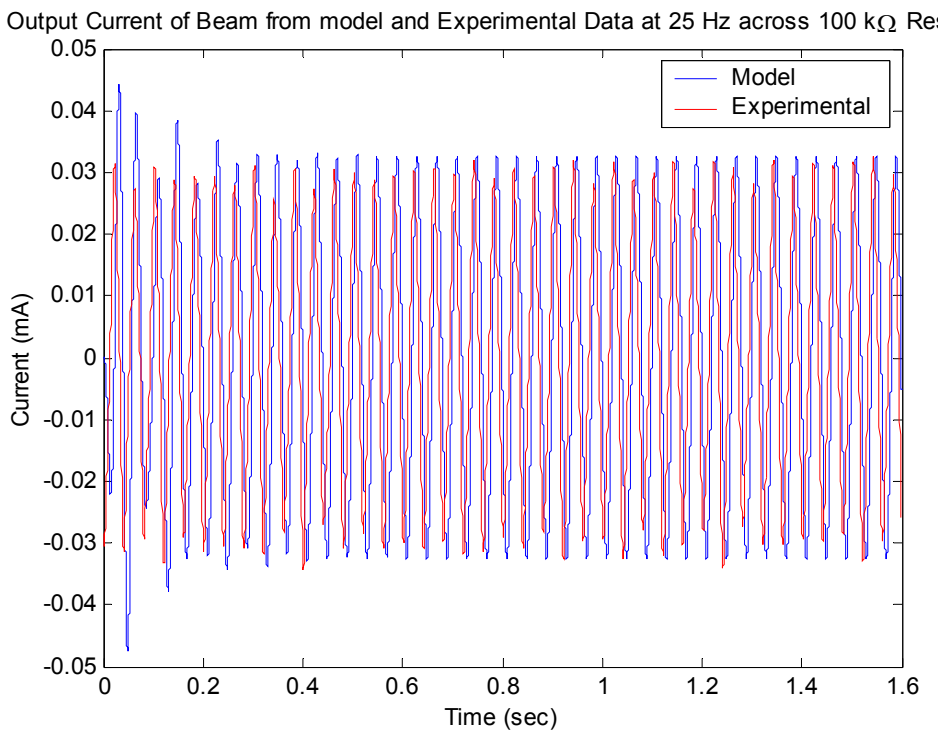

Figure 4.11: Output current predicted by model and measured across a 10KΩ resistor at 50Hz.

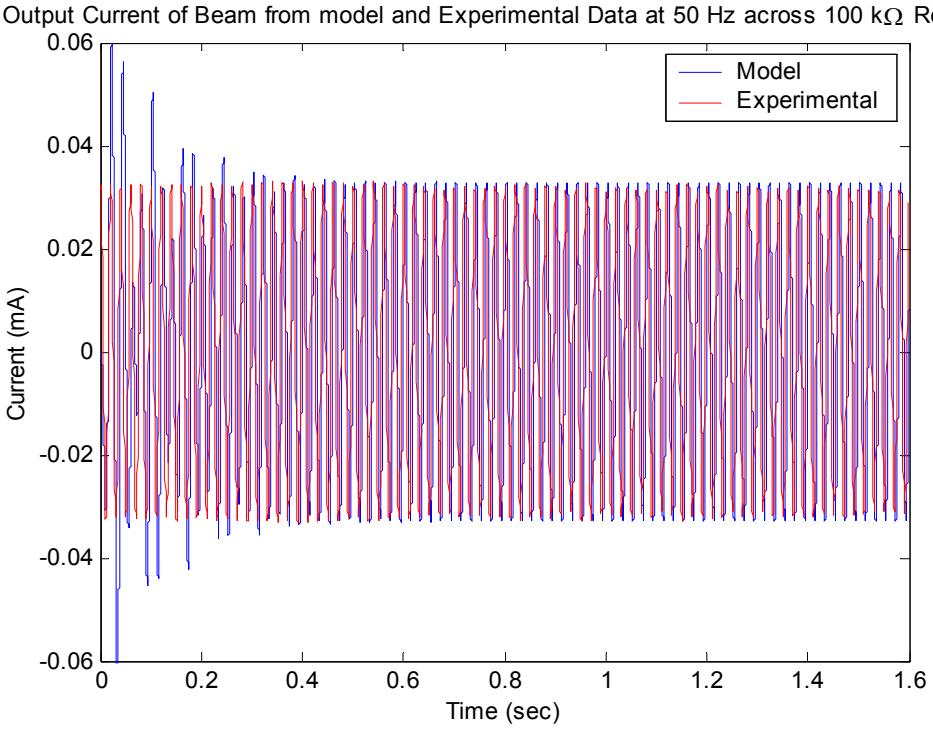

Figure 4.12: Output current predicted by model and measured across a 100KΩ resistor at 50Hz.

4.3 Disscusion of Power Harvesting and Shunt Damping

In addition to providing an accurate estimate of the of the power generated by a beam with complicated piezoelectric layout and a non-homogeneous material composition, the model also shows that power harvesting works much like a shunt damper. In the presences of a power harvesting circuit energy is taken for the system and supplied to the electrical components causing a damping effect. The damping effect is caused by the removal of energy from the system, which by definition of conservation of energy, must cause the reduced oscillation of the beam. This effect is very similar to one of the original uses of the model developed in Hagood et al. (1990) which was used to show the ability of a tuned RLC circuit to effectively damp the vibration in a beam. The major difference is that in our case we are working with a load resistance which will also induce damping to the system but over a broad range of frequencies rather than the turned frequency of a RLC circuit. The damping effect of power harvesting on an impulse is shown in Figures 4.13, 4.14 and 4.15. Figure 4.13 shows the decay of the impulse response when the load resistance is at it ideal value for removing energy from the system. Now looking at Figure 4.14, the load resistance is reduced to 100Ω causing less energy to be dissipated over the resistor, resulting in an increased settling time of the beam. However, in Figure 4.15 the load resistance becomes very high, but the settling time is still longer than the case with the resistance shown in Figure 4.13. This occurs because as the resistor becomes too large it acts like an open circuit and actually resisting the flow across the resistor making it incapable of dissipating as much energy as lower values of resistance. These Figures demonstrate the effect of power harvesting on the dynamics of a cantilever beam. It is apparent that as more energy is removed from the system the impulse dies out faster until a critical level is reached, after which the resistive load of the circuit exceeds the impedance of the piezoelectric network causing lower efficiency power generation and for this example lower energy dissipation to the beam. This study shows that the effects of power harvesting on the dynamics of a mechanical system are very similar to those of shunt damping, with the major difference being that the energy is stored for use instead of dissipated.

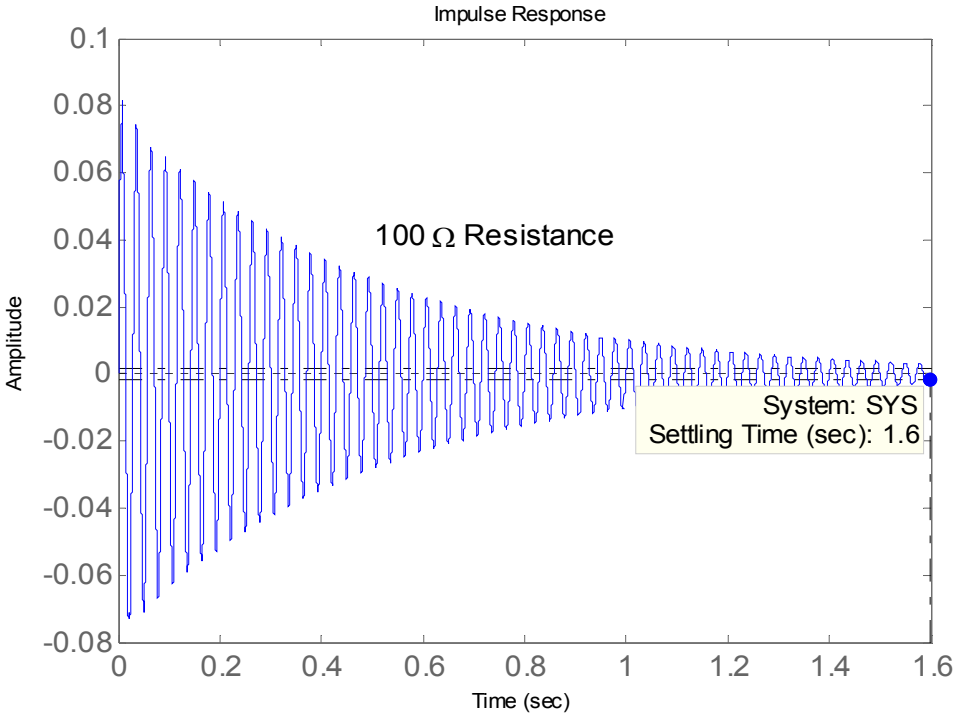

Figure 4.13: Impulse response with a 100Ω resistive load.

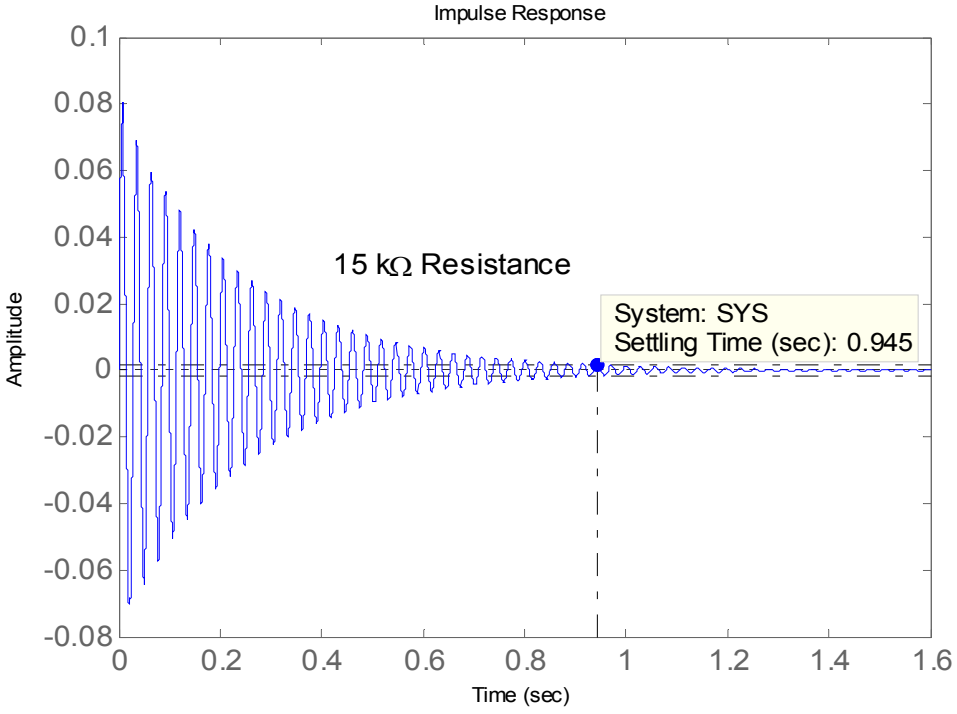

Figure 4.14: Impulse response with a 15kΩ resistive load.

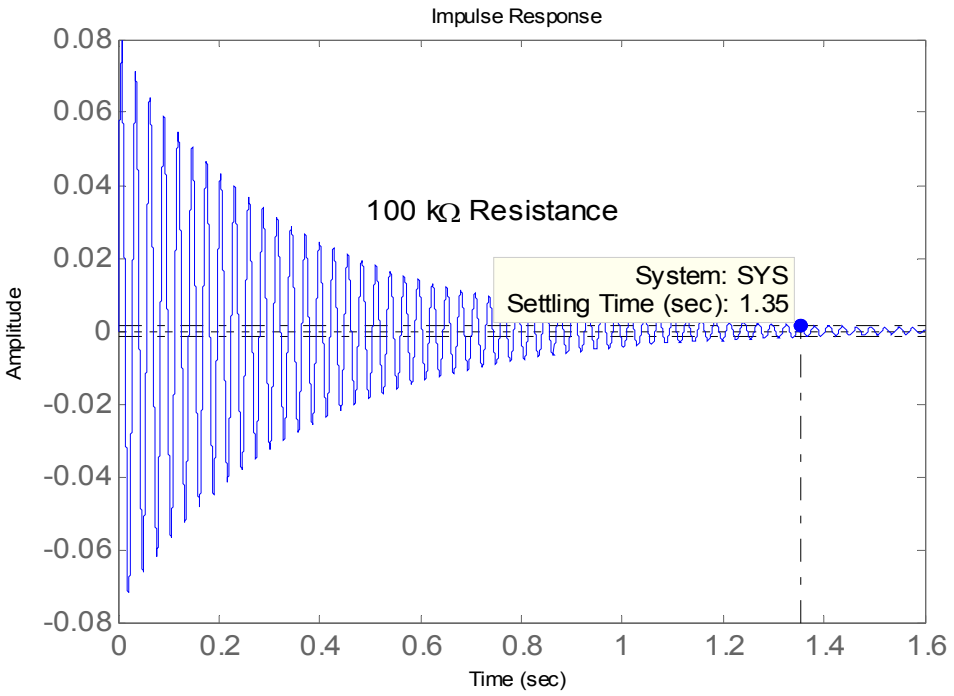

Figure 4.15: Impulse response with a 100kΩ resistive load.

4.4 Chapter Summary

One method of performing power harvesting is to use piezoelectric materials that can convert the vibration energy around them into electrical energy. This electrical energy can then be used to power other devices or stored for later use. This technology has gained an increasing large amount of attention due to the recent advances in wireless and MEMS technology allowing sensors to be placed in remote locations and operate at very low power. The need for power harvesting device is caused by the use batteries as power supplies for these wireless devices. Since the battery has a finite lifespan, once extinguished of it energy, the sensor must be recovered and the battery replaced for the continued operation of the sensor. This practice of obtaining sensors solely to replace the battery can become and expensive task because the wireless nature allows it to be place in exotic locations. Therefore, methods of harvesting the energy around these sensors must be implemented to expand the life of the battery or provide an endless supply of energy to the sensor for its lifetime.

Chapter 4 has developed a model to predict the amount of power capable of being generated through the vibration of a cantilever beam with attached piezoelectric elements. The complete derivation of the model has been provided, allowing it to be used to model a beam with any boundary conditions or layout of piezoelectric patches. The model was verified using experimental results and proved to be very accurate independent of excitation frequency and load resistance. In addition, the verification of the model was performed on a structure the contained a complex piezoelectric layout and a non-homogenous material beam, indicating that the model is robust and can be applied to a variety of different mechanical conditions. The damping effects of power harvesting were also shown to be predicted in the model and to follow that of a resistive shunt damping circuit. This model provides a design tool for developing power harvesting systems by assisting in determining the size and level of vibration needed to produce the desired level of power generation. The potential benefits of power harvesting and the advances in low power electronics and wireless sensors are making the future of this technology look very bright.

Chapter 5

Generation and Storage of Power from Piezoelectric Materials

5.1 Introduction to Power Generation and Storage

In chapter two, piezoelectric materials were shown to produce electric energy when strain energy is applied to the material. This property makes piezoelectric devices effective for obtaining energy from their surrounding, usually ambient vibration, and converting it into useful electrical power. However, the energy generated through the piezoelectric effect, is in most cases not sufficient for directly powering electronic devices. Therefore, a method of accumulating and storing the harvested energy so that it may be used in the future is an important aspect of a power harvesting system.

Several researchers have found that for the energy provided by a piezoelectric device to be of use, it must be accumulated in some way. One of the first researchers to realize the potential of power harvesting and speculate possible storage methods was Starner (1996). His research investigated the amount of power that could be generated through everyday human activity and proposed the use of capacitors and rechargeable batteries as storage devices for use with piezoelectric power harvesting devices. Umeda et al. (1997) went beyond the proposal of using a capacitor for energy storage, and tested the abilities of a circuit containing a rectifier and capacitor for storing the energy generated when a steel ball impacted a plate with piezoelectric elements attached. Shortly after the publication of this work, a power harvesting patent was

issued to Kimura (1998) for a means of storing the rectified energy from a piezoelectric device in a capacitor. However, a circuit containing only a single capacitor was not sufficient to power other electrical devices without additional circuitry. Therefore, Kymissis et al. (1998) developed a circuit to harvest the energy lost during walking; this circuit design has found use in many other researchers work. Two piezoelectric devices were located in a shoe, the first was used to absorb the impact energy of the heel and the second was used to obtain the bending energy of the sole. This circuit also used a capacitor as a storage medium, but required additional components to allow the capacitor to charge to a desired level before discharging through a transmitter. The idea of using this technology in conjunction with a transmitter opened up many doors for wireless sensors. Following this work, the interest in power harvesting for use in biological systems began to grow, and in 2000, Elvin et al. received a patent for a self-powered sensor. This patent was for a bone strain monitoring system that was self powered by the strain energy of the bone. The energy obtained from the bone was sufficient to transmit a signal containing data detailing the stain of the bone. Since these early studies in power harvesting, numerous other creative locations have been investigated for the placement of piezoelectric power harvesting devices.

While a lot of research has been devoted to the search for storage methods compatible with piezoelectric devices, other researchers have investigated using circuitry to increase the amount of power generated by the piezoelectric material. One such study was performed by Ottman et al. (2002), who used a step down DC-DC converter to maximize the power output from a piezoelectric device. It was found that at very high levels of excitation the power output could be increased by as much as 400%. However, this study did have a drawback, the additional electronic components required to optimize the power output dissipated energy. This additional circuitry required an open circuit voltage greater than ten volts for the power generated to be increased. The research that will be presented in this chapter will concentrate on power storage methods that can be used for realistic vibration levels, whereas the study performed by Ottman et al. (2002) used a resonant signal at far greater excitation levels than available in most typical structures. The realistic signal used in this chapter was generated to be comparable with that by placing an accelerometer on a car and measuring the vibration levels at a non-optimal locations.

In chapter four, a model describing a power harvesting system was formulated and shown to accurately predict the amount of energy generated during vibration of a beam. The first portion of this chapter will emphasize the methods of storing electric energy generated by a PZT. The amount of power that one particular PZT device can generate has first been estimated, and

the feasibility of the devices for recharging a battery has been studied. This research is motivated by the fact that the power generated by PZT is far smaller than required for the normal operation of most electronics in real field applications. However, when identifying the ideal storage method, the time required by PZT to charge power storage devices must be taken into account for the electronics intent to be charged. In addition, the low efficiency of both the PZT and the circuit has been identified as a critical issue in previous studies. In this study, the energy produced by the PZT is stored using two different methods. The first method tested will be the capacitor that allows for immediate access to the stored energy, this method has been commonly used by other researchers, and the second method is to charge a nickel metal hydride battery. The battery charging method provides certain advantages over the capacitor method that will be outlined in the following sections. However, the use of energy generated from piezoelectric materials has not been previously shown to be compatible with rechargeable batteries. Therefore, the ability to use this energy to do so must first be shown before other studies into this technology can be performed.

Once the ability to use energy generated by piezoelectric materials is shown to be effective for use with rechargeable batteries, the second portion of this chapter will perform a comparison of the recently developed macro-fiber composite (MFC) and the traditionally used piezoceramic material PZT. First the efficiency of each material's ability to convert applied mechanical energy into usable electric power is determined, for a random disturbance signal and at the resonance of the test specimen. Then the performance of each actuator material for recharging nickel metal hydride batteries was investigated. After testing both piezoelectric materials significant differences in their ability to produce electrical energy were found, reasons contributing to these differences will be discussed.

5.2 Piezoelectric Power Harvesting Storage Methods

This section will investigate the two previously mentioned methods of storing the power generated from the vibration of piezoelectric devices. First the use of a capacitor will be investigated and tested, followed by a study to determine if the energy from piezoelectric materials is suitable for storage in a rechargeable battery. The last portion off this section will outline the advantages and disadvantages of each method.

5.2.1 Experimental Setup

The piezoelectric device used for this portion of the study consisted of an Aluminum plate with a PSI-5H4E piezoceramic (PZT) from Piezo Systems Inc. bonded to its surface. The aluminum plate was constructed by bonding the piezoelectric material to its surface using superglue; the dimensions and plate are shown in Figure 5.1. The thickness of the aluminum plate and the PZT were 0.04 in. and 0.0105 inches respectively. The relatively thick aluminum plate was used because the piezoceramic material is extremely brittle and is susceptible to accidental breakage, when bonded to a thick substrate the likelihood of damaging the piezoelectric is greatly reduced.

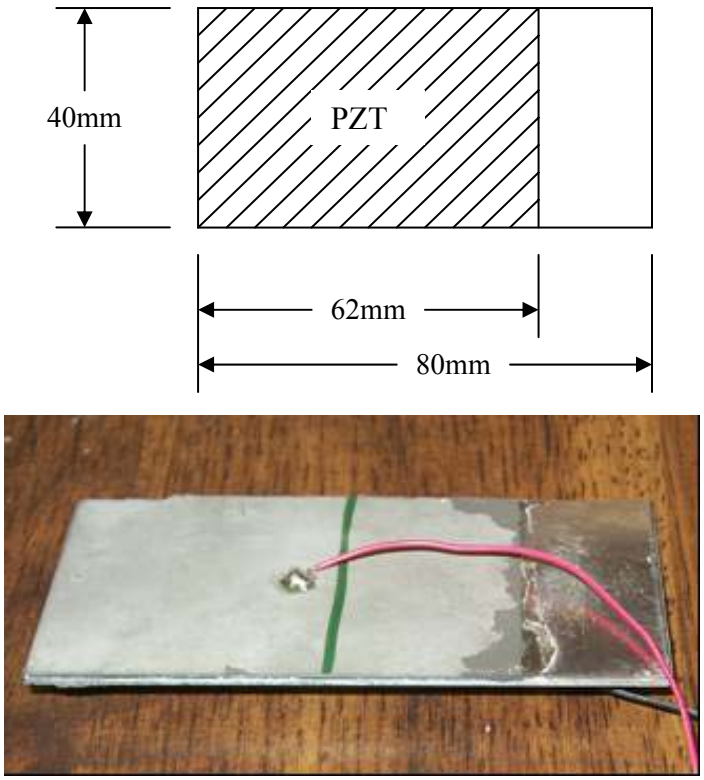

Figure 5.1: Dimensions and layout of the piezoelectric on the aluminum substrate.

The following experiment investigates the possibility of harvesting power from the vibration of a structure such as an automobile compressor. In order to simulate the vibration of an automobile compressor a PCB accelerometer, model 352C22, was attached to a random location on the compressor. The term 'random location' is used because no effort was made in optimizing the placement of the accelerometer to produce the maximum magnitude of vibration, nor is the

compressor the optimal location in the engine compartment for obtaining vibration energy. The engine was run at various speeds while the accelerometer measured the compressors response. A typical signal measured from the compressor of a Mitsubishi Eclipse had the appearance of random vibration from 0 to 1000 Hz. The aluminum plate in Figure 5.1 was attached to a ridged structure in cantilever boundary conditions (fixed-free), while a shaker applied the excitation force. The typical response showing the magnitude of vibration measured at a random location on the automobile compressor is shown in Figure 5.2, along with the input signal used for the experiment, shown in Figure 5.3. The excitation signal used in the experiments was found by placing the same accelerometer on the piezoelectric plate and adjusting the signal supplied to the shaker until it was comparable with that of the compressor. The disturbance used in the experiments had a magnitude that was 9.5% less than that of the automobile compressor, indicating that the excitation signal used was conservative in representing the vibration of an automobile compressor. The energy produced by the PZT was stored using two different methods. The first was in a capacitor that allows for immediate access to the stored energy and the second method charged a nickel metal hydride battery.

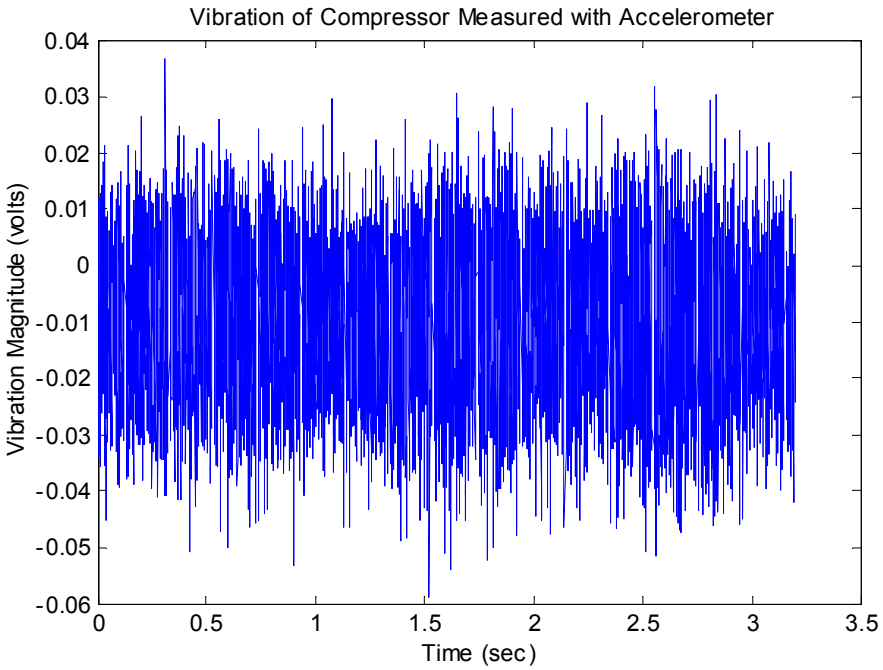

Figure 5.2: Vibration of an automobile compressor measured by an accelerometer.

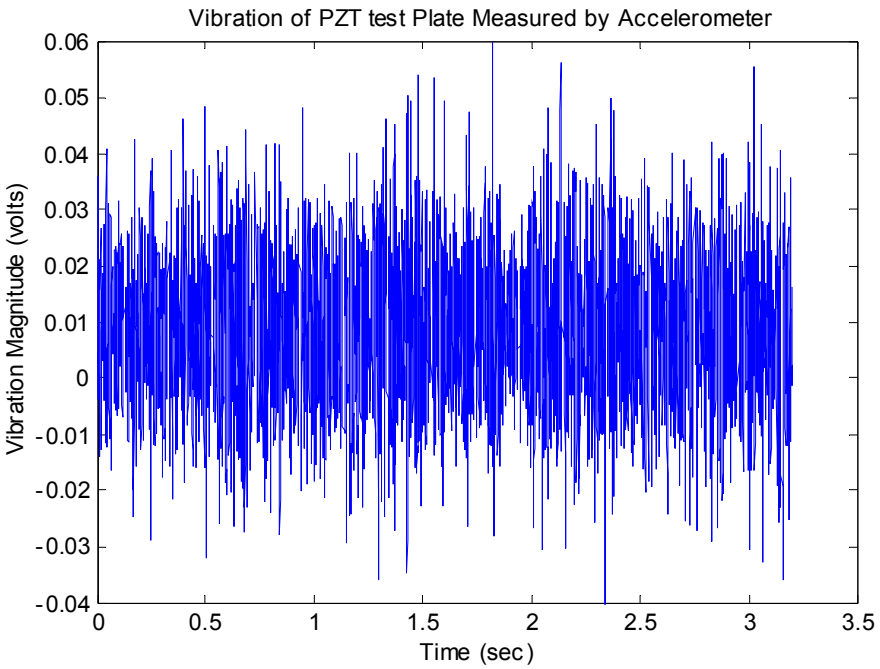

Figure 5.3: Random signal applied to the shaker as the disturbance force, with matched amplitude to the automobile compressor.

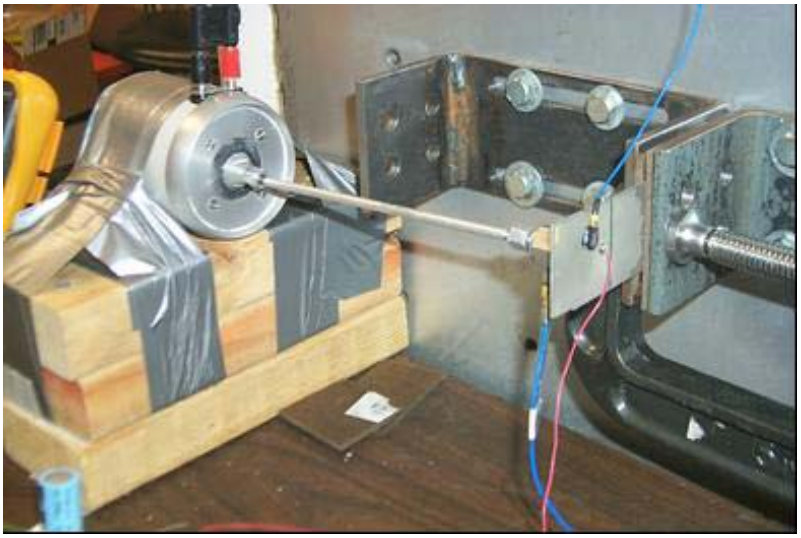

Figure 5.4: Experimental Setup used to both excite the plate and measure the vibration.

Capacitor Charging Circuit

The first method of storage used a capacitor to accumulate the energy output of the piezoelectric patch, a schematic of the complete circuit used is shown in Figure 5.5, and the circuit build on a breadboard is shown in Figure 5.6. The circuit design was modified from one used for a self-powered RF tag (Kymissis et al, 1998). The principle of operation of this circuit is as follows; first the signal from the PZT is full wave rectified and accumulated in capacitor C1. Once C1 is charged past the zener diode voltage, in this case 6.5 volts, the capacitor releases it charge, switching the BJT, Q1, to the on position, and triggering the MOSFET, Q2, to pull the ground line down allowing C1 to discharge through the circuit. The MAX666 chip is a low-power series regulator that produces a +5 volt DC signal as C1 discharges. Once C1 has discharged beyond 4.5 volts, the MAX666 sends out a negative pulse that turns the Q1, off, allowing C1 to begin the process over and recharge. In the "off" state, the circuit has a high impedance allowing C1 to charge fast.

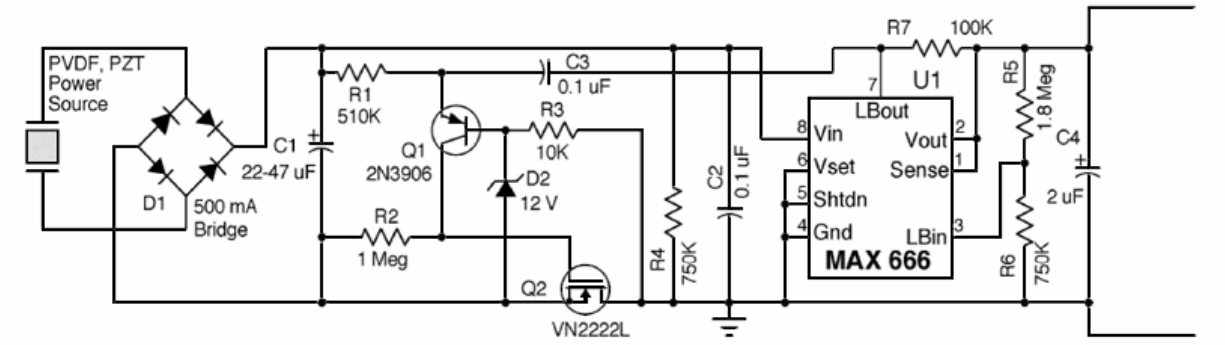

Figure 5.5: Schematic of the capacitor circuit layout (Kymissis 1998).

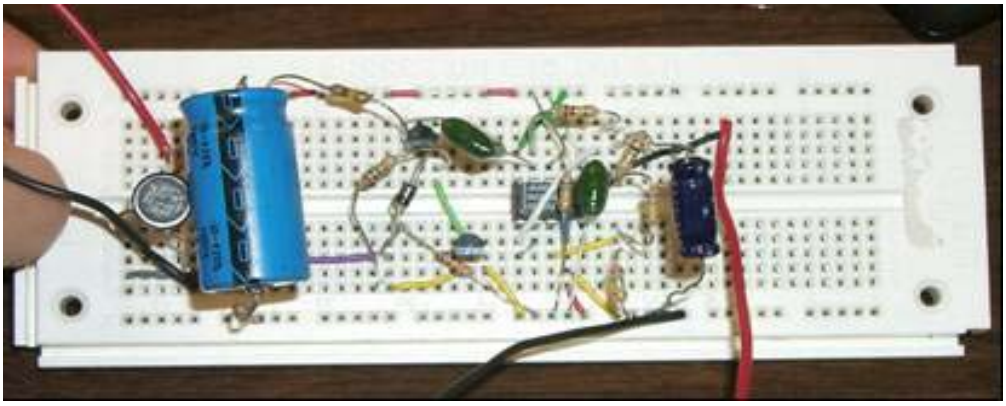

Figure 5.6: Schematic of Power Harvesting Circuit.

Battery Charging Circuit

The second method of power storage used was a circuit that charged a nickel metal hydride button cell battery. Nickel Metal Hydride batteries were used because they have a very high charge density and do not require any type of charge controller or voltage regulator to be incorporated into the circuitry. The circuit constructed to charge the battery was very simple, it consisted of a full wave rectifier, capacitor and the battery intended to be charged, as shown in Figure 5.7. The voltage produced by the PZT was first full wave rectified then accumulated in a large capacitor, typically greater than 1000μF, then the battery intended to be charged was placed in parallel with the capacitor. The simplicity of this circuit allows it to be constructed very compactly and without additional components that would result in additional power dissipation, as shown in Figure 5.8

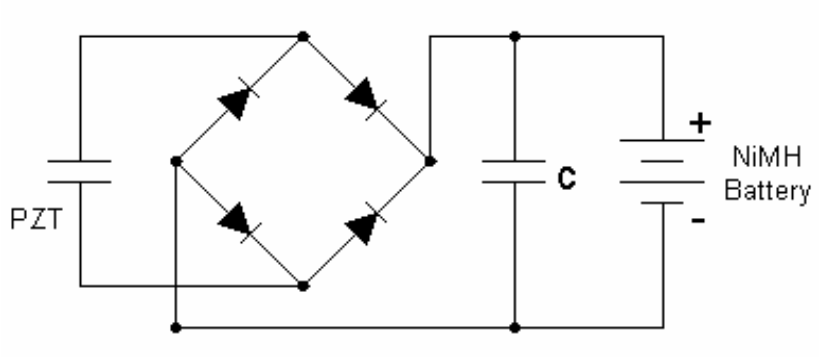

Figure 5.7: Schematic of the battery charging circuit.

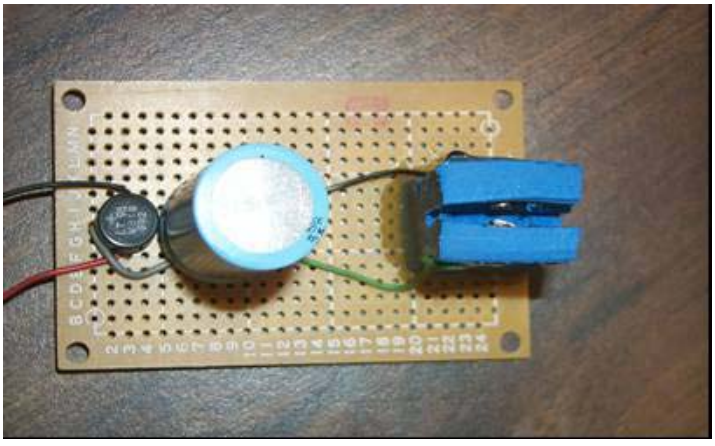

Figure 5.8: Layout of the Battery charging circuit built on a breadboard.

5.2.2 Power Generation

Before the previously mentioned circuits were used to accumulate the generated energy, the amount of power this particular device could produce was measured. The reason that I say this particular piezoelectric device, is because there are many factors that affect the power generated, such as the substrate thickness, material used, excitation strength, and load resistance used. The effect of the load resistance on the power output of a piezoelectric was discussed in chapter 4; refer back to section 4.3 for a more detail on this topic. In general, the maximum power output occurs when the impedance of the piezoelectric element and the load resistance are matched. However, this cannot always be achieved during testing because the piezoelectric is a capacitive device, which means that the impedance varies with frequency, and therefore, the optimal load resistance varies. For the following power generation results, the load resistance was set to be the impedance of the PZT at the resonant frequency of the cantilever plate.

The power generated by the PZT was obtained using the voltage drop across a 10kΩ resistor. The power is calculated using the following relation of equation 5.1 obtained using Ohm's law:

$$P = \frac{V^2}{R} \tag{5.1}$$

where P is the power and V is the voltage drop across the load resistance R. The resulting power (with a chirp input from 0-250Hz) is shown in Figure 5.9 and the voltage and current found are shown in Figure 5.10. The data presented uses a chirp signal rather than the random signal shown previously because a chirp signal allows the voltage produced at different frequencies to be visualized more easily. As can be seen in the figure, the maximum instantaneous power is identified as 2mW, which occurs at the resonance of the test plate. Three PZT plates were tested with the same configuration, and all produce a maximum power in the range of 1.5-2mW, and an average power of 0.14-0.2mW. These measurements were made with the magnitude of the chirp signal matching that of the signal measured from the automobile compressor. In addition, these measurements were made without a capacitor, which points out that this power would be immediately available for powering other devices. This estimation however does not account for the efficiencies of circuit components, such as a capacitor, diode, and voltage regulator. This

estimated power certainly would not be sufficient to operate commonly available sensors, actuators or telemetry devices in real field application, not to mention that it would require a certain period of time to charge the circuit, if a capacitor or battery is used.

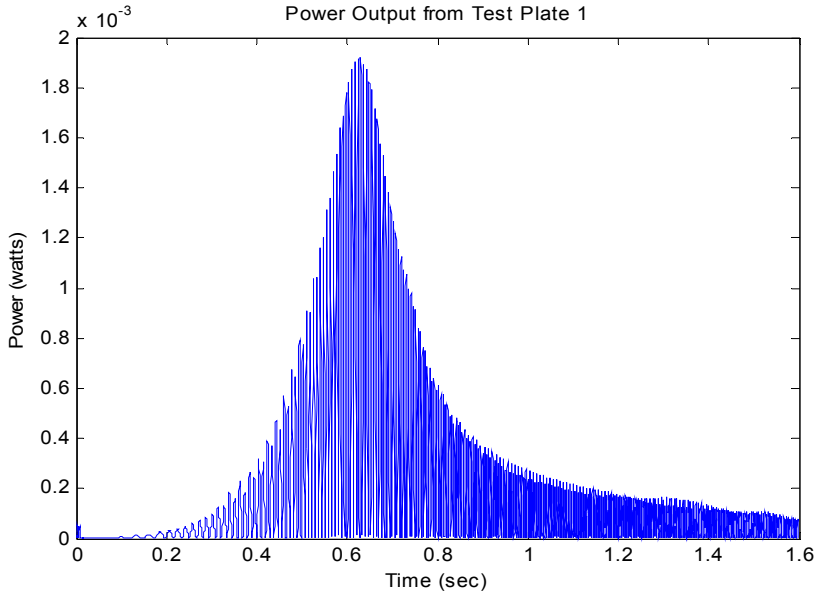

Figure 5.9: Power output from test plate with a chirp input signal.

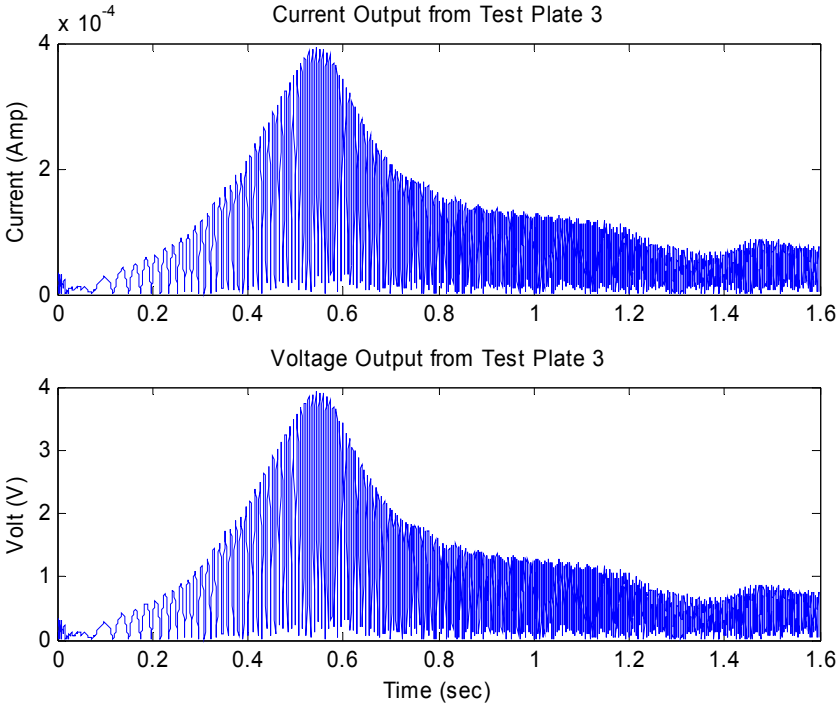

Figure 5.10: Voltage and current output from the piezoceramic test pate.

5.2.3 Capacitor Circuit

The random excitation of the plate with piezoceramic attached was able to successfully charge the capacitor and operate the circuit as expected. However, when using the high frequency excitation found on the compressor, once the capacitor reaches the charged level it discharges and charges so fast that the circuit outputs high frequency pulses corresponding to the charging and discharging of the circuit. To better show the performance of the capacitor circuit, the system was slowed down to allow the capacitor to visually discharge and recharge. Figure 5.11 shows the voltage on the capacitor and the output of the circuit with respect to time. The Figure shows that as the capacitor charges up to 6 volts, the circuitry allows it to discharge and the voltage output goes up to the regulated 5 volts. During the discharge of the capacitor, the output of the circuit stays at 5 volts until the capacitor reaches 4.5 volts, when the circuit begins to shut off, seen by the bump in the discharge of the capacitor. The process then repeats itself and the capacitor recharges. This method of collecting the energy generated by the piezoelectric allows the energy to be attained almost instantaneously. However, the circuit can only output energy for a very limited amount of time, making this method of storage impractical for powering many electronic devices, although it is effective for transmitting a short signal as done in the work by Kymissis et al. (1998).

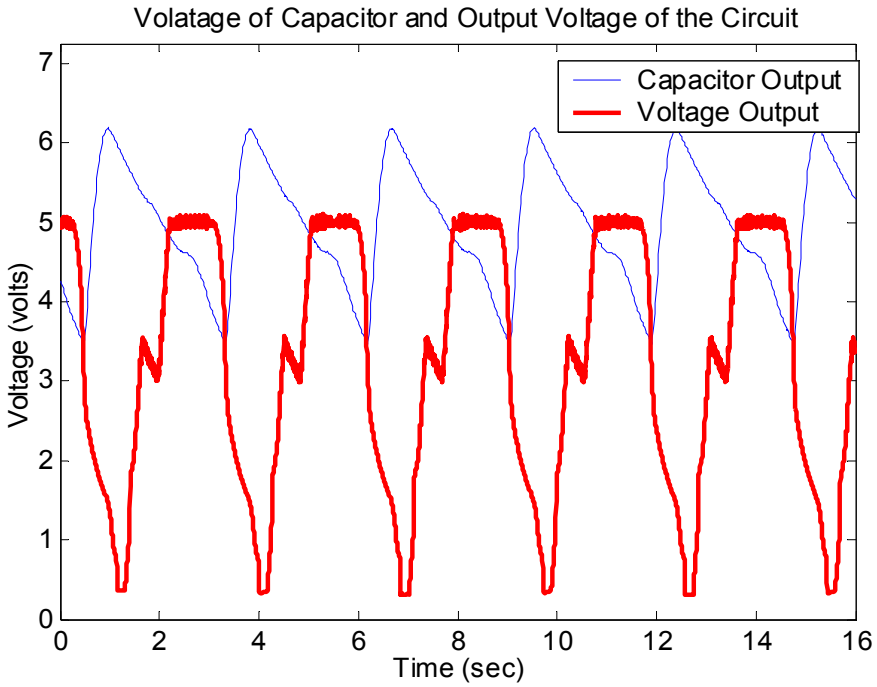

Figure 5.11: Plot of the time history of the Capacitor charging and discharging.

5.2.4 Battery Charging Circuit

In the next section, the ability of a piezoceramic and macro-fiber composite (MFC) actuator to be used as power harvesting devices for recharging batteries will be compared. However, the ability to use the energy generated during vibration of piezoelectric materials to charge a battery has not previously been performed. Therefore, the ability to use these devices for this purpose must first be shown. For this investigation into recharging batteries with piezoelectric materials, two different types of excitation signals were used to charge a 40mAh battery (the unit "mAh" stands for mille-amp-hour and is a measure of the battery's capacity, a 40mAh capacity means that the batteries will last for 1 hour if subjected to a 40mA discharge current). The first excitation signal used was a sinusoidal input at the resonant frequency of the plate, in this case 63 Hz, while the second excitation was similar to the random signal from 0-1000 Hz, corresponding to the vibration of an automobile's compressor, shown in Figure 5.3. The resonant signal was used first because compatibility of the piezoelectric output power and the charging requirements of the battery needed to be shown before other tests could be performed. Furthermore, the resonant signal had a higher probability of charging the battery due to the larger power output obtained at this frequency. Once the compatibility of the piezoelectric and battery was shown, the random excitation could be used to demonstrate that the vibration available from an automobile was capable of recharging the battery.

The first tests performed used the resonant signal to excite the plate and the time required for the battery to charge up to it cell voltage of 1.2 volts was recorded. Although the batteries charge up to values higher than 1.2 volts, this value is used for consistency. A typical time history of the battery charging at random vibration is shown in Figure 5.12. Looking at the figure it can be seen that the battery charges up to it cell voltage in slightly over 20 minutes. This Figure shows that the piezoelectric is capable of charging a nickel metal hydride battery rather quickly. Now that this previously unexploited method of storing energy generated through the piezoelectric effect has been verified, the ability to use the random excitation of a typical automobile's compressor can be tested.

The random signal was applied to the piezoelectric plate and the charge time was recorded as done with the resonant signal. The results of a typical charging test are shown in Figure 5.13. When using a random signal from 0-1000Hz the piezoelectric patch generates far

less energy because of the low strain mode shapes at these higher frequencies. However, looking at the Figure, it can be seen that even with the use of a random signal, the piezoelectric can still charge a battery in a few hours.

Numerous advantages arise when the power harvested from the vibration of a piezoelectric device is stored in batteries. First, the capacitor method requires the piezoelectric to constantly produce electrical energy the entire time the application consumes power. This is because the capacitor does not possess the power storage properties that batteries have. The power stored in batteries can be accumulated and saved for use when no vibration is present. Also the time required for a capacitor to discharge is much smaller than that of the battery, this causes the capacitor circuit to switch on and off as the capacitor charges and discharges. For applications that require a constant power supply the capacitor is not suitable, however, when using batteries, two batteries can be installed allowing one battery to be in the charging stage while the other is used to supply power. In addition, the power directly generated by piezoelectric materials would suffice to operate some micro-scale devices, but it is slightly insufficient for running typical sensors, actuators, or computing devices commonly used in real field applications. For instance, a PIC 16C71 processor from Microchip Technology requires 18mW at 4MHz (microchip Technologies Inc.), and a functional wearable computer (without communication device) can operate with a continuous power consumption of 0.5mW (Starner, 1996). By using the power generated from a PZT to charge a battery the number of applications increases significantly. The 40mAh battery that was charged in less than half an hour, contains enough energy to power a Casio LW22H watch for two years (Casio Inc.). This shows that if vibration was only present for a small amount of time when using rechargeable batteries to store the power generated by piezoelectric materials that the electronics could still receive the power needed to run for a significant amount of time.

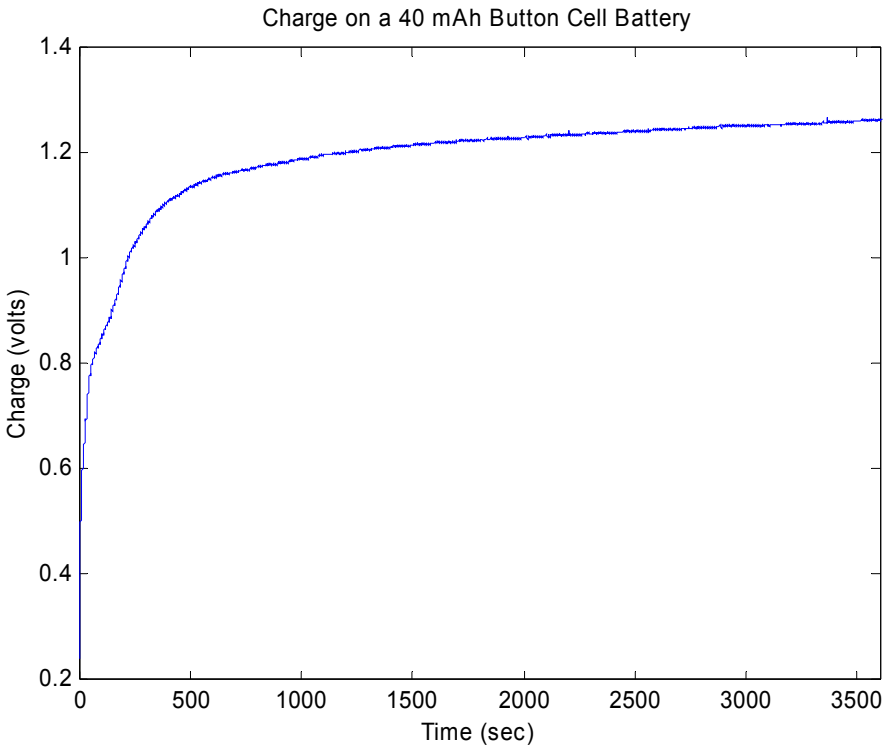

Figure 5.12: Plot showing the charge from a PZT on the battery (resonance input).

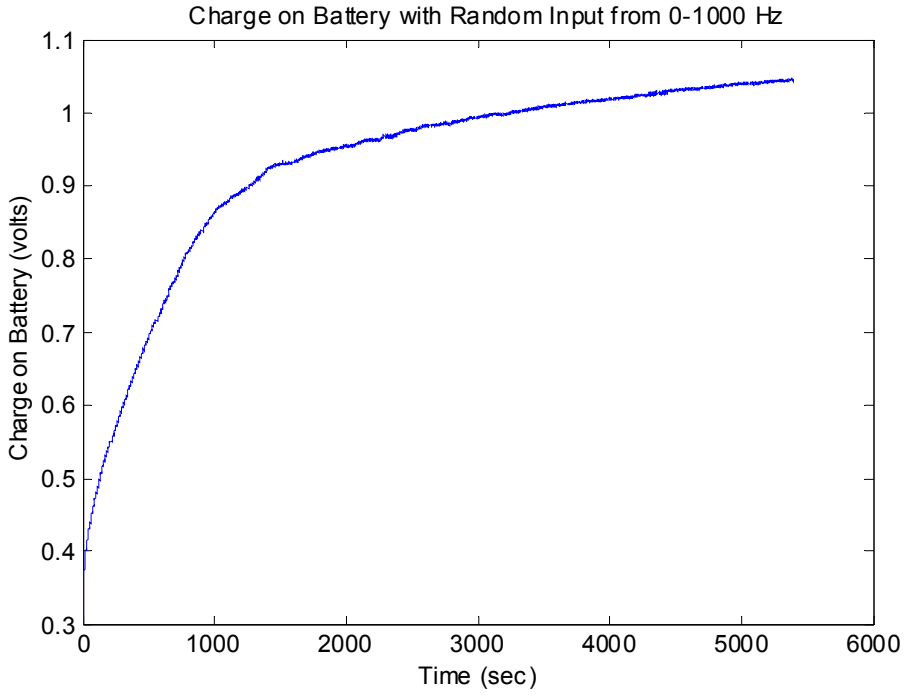

Figure 5.13: Plot showing the charge from a PZT on the battery (random input).

5.3 Comparison of Piezoceramic Materials and the Macro-Fiber Composite Actuator for Power Harvesting

The macro-fiber composite (MFC) is a new actuator that was recently developed at the NASA Langley research center. The actuator is constructed using piezofibers surrounded in an epoxy matrix and covered with a Kapton shell. The Construction of this actuator allows it to be extremely flexible, making it ideal for applications such as the inflatable satellite described in chapter 3. The flexibility of this piezoelectric device as well as the epoxy and Kapton shell, allows the actuator to be robust to damage and environmental conditions. This is a very desirable property for a power harvesting system that is intended to provide energy to electronics for an extended period of time. If the actuator were to be accidentally break as is typical with monolithic piezoelectric materials, the power harvesting capabilities of the system would reduced or become nonexistent. Furthermore, if the power harvesting device is intended for a location that is exposed to the elements, or is for use in a biological system, the power harvesting capabilities cannot be affected by such things as water causing short circuits or harsh temperatures and chemicals. The MFC is robust to all of these factors, making it an ideal candidate for a power harvesting actuator. In addition to the robust nature of the MFC, it is constructed using interdigitated electrodes that capitalize on the higher d_{33} piezoelectric coefficient, allowing for more effective exchange of mechanical and electric energy. This property should increase the efficiency of the material's ability to output electrical energy over that of the lower d_{33} coefficient found in monolithic piezoceramic (PZT) materials. The following sections will investigate the ability of this new actuator to function as a power harvesting device. The efficiency on a device level of the two power harvesting materials is calculated and compared, followed by a study to determine their effectiveness at charging batteries.

5.3.1 PZT and MFC Configuration

Two cantilever plates were constructed, one with piezoceramic and one with the macro-fiber composite, in order to compare the performance of the each as power harvesting devices. The piezoceramic plate was constructed using an aluminum shim with a PSI-5H4E piezoceramic

(PZT) from Piezo Systems Inc. bonded to its surface. The PZT and aluminum plate was constructed as shown in Figure 5.14. The thickness of the aluminum plate and the PZT were 0.0025 and 0.0105 inches respectively. The MFC plate was assembled by bonding the MFC actuator using double sided tape to a similar aluminum shim. It must be noted that due to the bonding of the MFC using double sided tape, the damping of the plate was increased and the full mechanical energy was not transmitted. The dimensions of the MFC and a picture of the plate setup are shown in Figure 5.15.

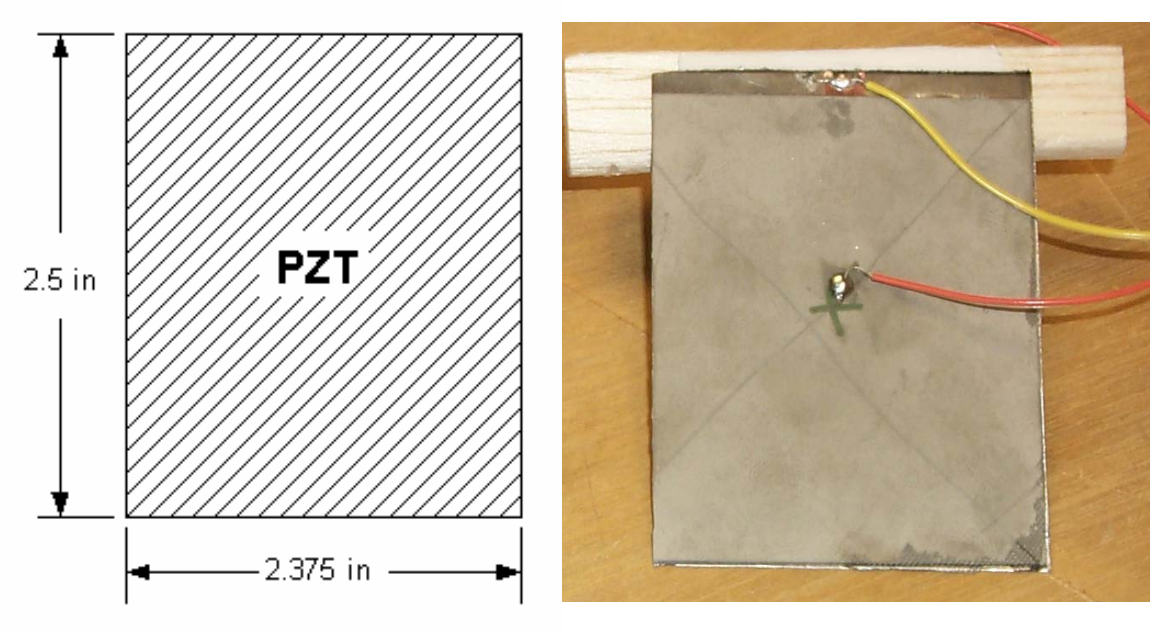

Figure 5.14: Size and layout of the PZT plate.

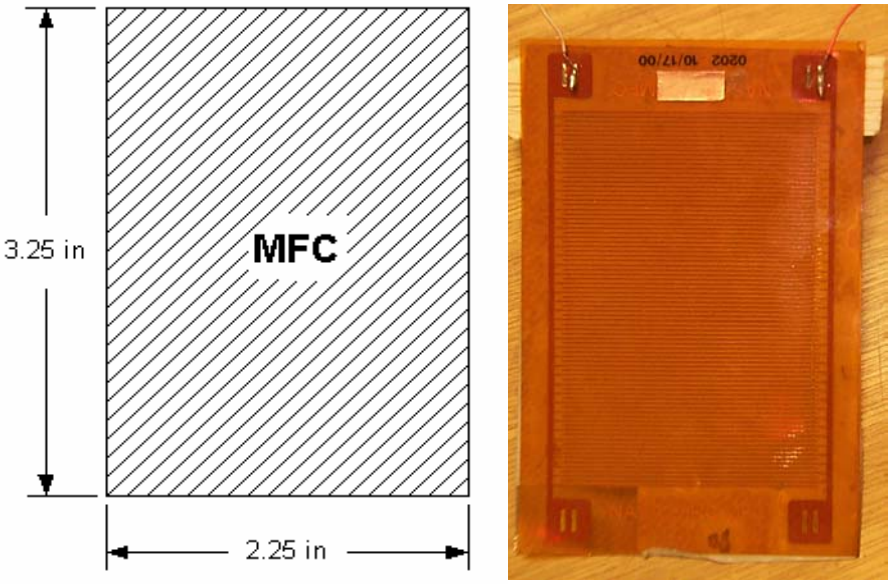

Figure 5.15: Size and layout of the MFC plate.

5.3.2 Experimental Setup

Vibration of the PZT and MFC plates was induced by an electromagnetic shaker. The two plates were configured with cantilever boundary conditions with the shaker providing base motion, as shown in Figure 5.16. The use of the shaker to provide base motion to the structure follows the same methods as the power harvesting model of chapter 4. The signal provided to the shaker was fairly low voltage as to closely follow the amplitude of the vibration around a car engine. Like the study performed in the previous section, the shaker signal adjusted using an accelerometer, until it closely resembled the excitation that would be experienced a car engine. The vibration was measured with a PCB accelerometer (model U352C22) at a random location on an automobile compressor is shown in Figure 5.2. Two different types of signals were supplied to the shaker, the first was at the resonance of the plate and the second was a random signal from 0-500 Hz. A typical random signal used to excite the cantilever plate with base motion is show in Figure 5.17, while the typical resonant signal is shown in Figure 5.18. Comparing the magnitude of the random and resonant signal of Figures 5.17 and 5.18, used to excite the plate, with the vibration measured from the automobile compressor, shows that the two are very comparable. The amplitude of the resonant signal is of lower magnitude to avoid accidental breakage of the piezoceramic element. To determine the efficiency of the setup, a Polytec Laser Vibrometer was used to measure the displacement of the plate and a PCB force transducer (model 208) was used to measure the applied force. The same simple circuit, shown in Figures 5.7 and 5.8, consisting of a capacitor and full bridge rectifier, was used to apply charge to the battery. The large capacitance, labeled C in Figure 5.7, located before the battery, was used to smooth the signal into a DC like voltage for the battery. Although more complicated circuits could be used, this circuit is simple to construct and uses passive components, therefore minimizing electrical losses.

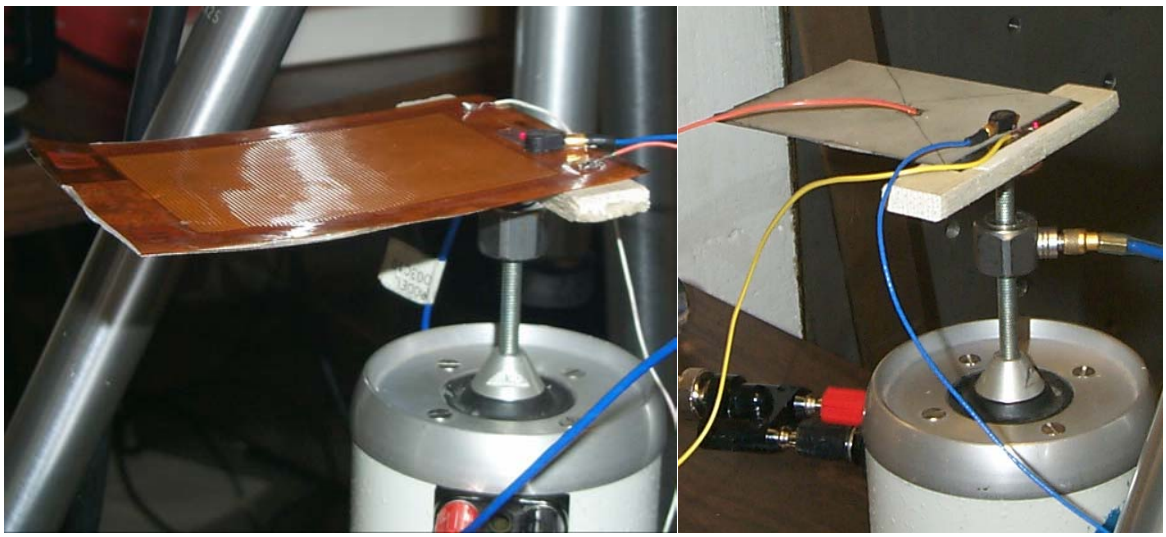

Figure 5.16: Experimental setup with the MFC plate and PZT Plate in a cantilever configuration.

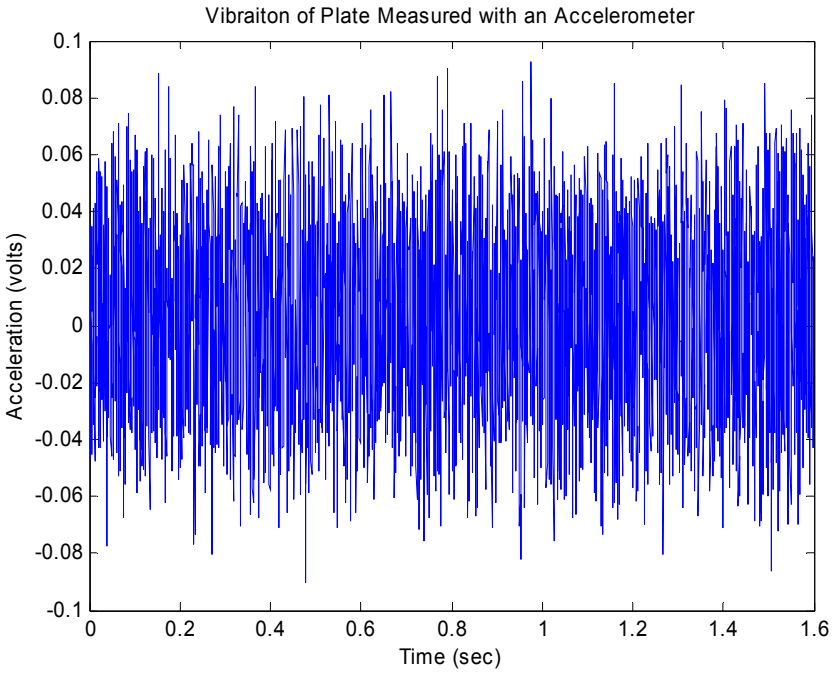

Figure 5.17: Random base vibration of the PZT and MFC cantilever plate, closely matching that of an automobile compressor.

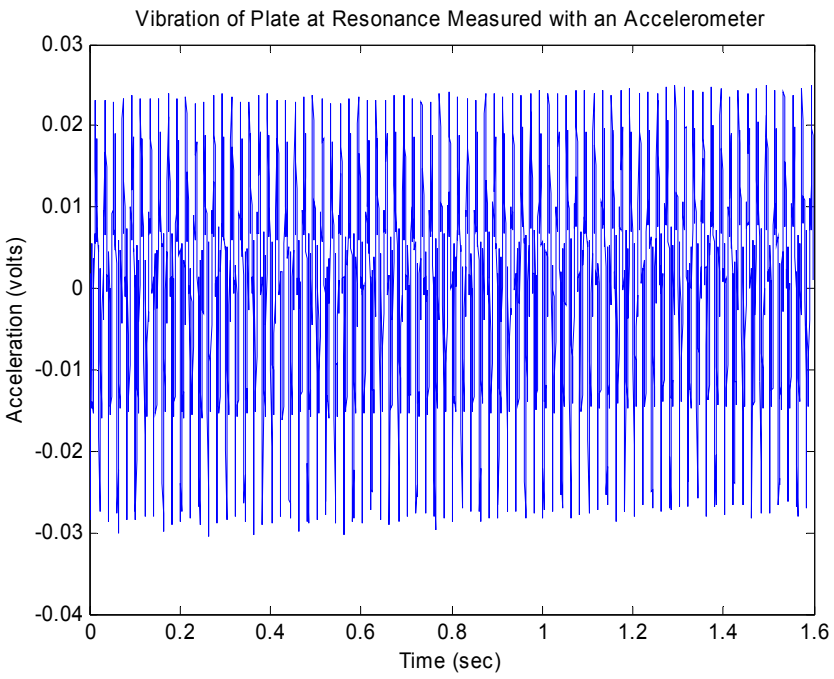

Figure 5.18: Resonant base vibration of the PZT and MFC cantilever plate, closely matching the vibration magnitude of an automobile compressor.

5.3.3 Efficiency Calculation of PZT and MFC

The first portion of the work to compare the effectiveness of the MFC and PZT for use as power harvesting devices was to determine the efficiency of each device used in our experiments. With this data obtained from the laser vibrometer, force transducer and voltage output from the piezoelectric, equation 5.2 was numerically calculated to determine the average efficiency:

$$\eta = \frac{P_{out}}{P_{in}} \times 100\% = \frac{\sum_{n=2}^{m} \frac{\left(V_n - V_{n-1}\right)^2 / R}{\left(\left(F_n - F_{n-1}\right) \cdot \left(d_n - d_{n-1}\right)\right) / \left(t_n - t_{n-1}\right)}}{m} \times 100\% \qquad (5.2)$$

where η is the efficiency, V is the voltage drop across load resistance R, F is the force applied to the base of the plate, d is the displacement of the plate, t is the time increment between data points, n is the data point index and m is the total number of data point measured. The efficiency of three input signals were calculated with the input signals being resonant, chirp and random. The resulting efficiencies are shown in Table 5.1. For each signal, three measurements were

made to show consistency. The efficiency of the PZT plate is low at resonance because the resonance frequency used was the frequency at which the voltage output was the highest, not the frequency with the best force into voltage out characteristics. This lower efficiency is shown because that is the resonance frequency used to charge the battery.

Table 5.1: Efficiency of PZT and MFC with three different inputs.

Signal	PZT Efficiency (%)	MFC Efficiency (%)
Resonant	1.1675	0.9442
	2.0777	1.0727
	1.1796	0.8782
Chirp 0-500 Hz	3.927	2.7421
	3.9388	2.5476
	3.8948	2.6285
Random 0-500 Hz	3.9369	0.7636
	3.6825	0.828
	4.2174	0.7366

While the MFC had an output voltage far larger than the PZT, the power generated was much less. This occurs because of the MFC's construction using piezofibers and interdigitated electrodes. From a power harvesting standpoint, the small pieces of piezoelectric material located between each electrode of the MFC can be considered a small power source; this is shown in Figure 5.19. Along the fiber there are numerous sections of electrodes, the majority of these small power sources are connected to one another in series. When two power sources are connected in series, the voltages add but the current does not. This concept of series connections is the reason for the low power generated by the MFC. Due to the series connection, the MFC produces a much higher voltage while the current remains far smaller than that of the PZT. The low current also causes much of the power generated to be dissipated by electronic devices, such as diodes, resulting in a lower efficiency. Additional effects of this issue will be detailed in the following section.

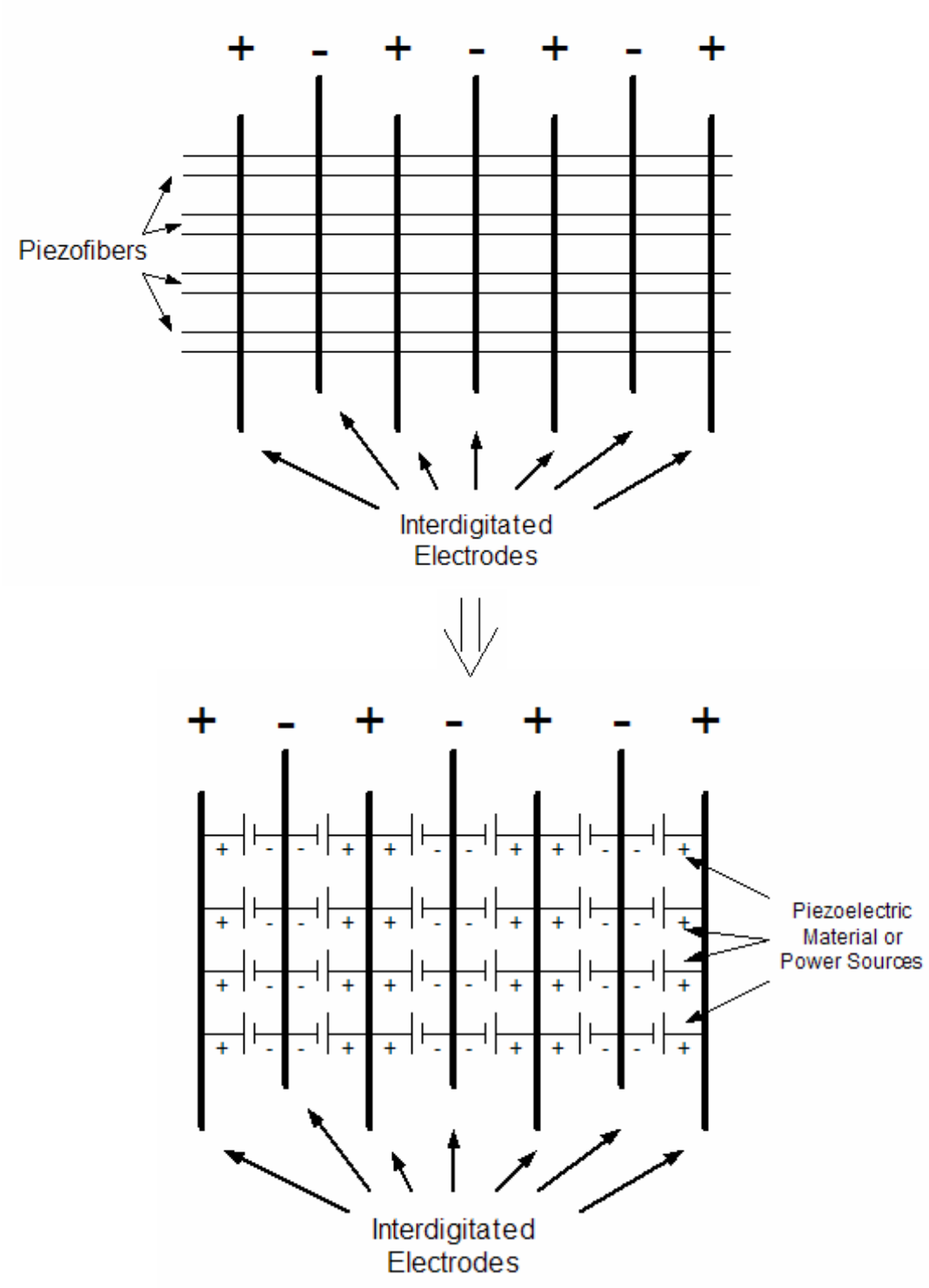

Figure 5.19: Layout of a MFC patch and the equivalent circuit layout.

5.3.4 Battery Charging Results

The tests presented in this section, investigate the ability of piezoelectric devices to charge a wide range of batteries sizes and the time required to do so. Several batteries, ranging from 40mAh to 1000mAh, were charged using the PZT and MFC. During the preliminary investigation of the compatibility of the MFC and rechargeable batteries, it was found that the MFC could not sufficiently charge even a small battery; unless the excitation signal provided by the shaker was unrealistically large (the goal of this work is to show that piezoelectric devices can charge batteries when experiencing typical levels of vibration). The MFC's inability to charge batteries can be attributed to the issue of low current discussed in the previous section. When charging a battery, the current is the most important factor. Since the MFC generates such a low current and the battery requires a current fairly high (usually one-tenth the battery's capacity or higher), the MFC actuator is not compatible with rechargeable batteries. Therefore the MFC was unable to charge the batteries and this data will not be presented.

Two signals were applied to the PZT and used to charge the batteries; the first was a resonance signal at 50Hz and the second was a random signal ranging from 0-500Hz. The resonance signal was applied at 0.8 volts peak and the random signal was applied at 1.0 volts RMS. As indicated in the previous section, the magnitude of the signals applied to the PZT plate closely resembles that of an automobile's compressor. The time required for the battery to charge past the cell voltage of 1.2 volts was measured in each case. This is not a complete charge but is about 90% full. The time required to top off the battery, is far slower than to reach this point. For this reason and the inability to detect a full charge due to the absence of a charge controller compatible with the power output from the PZT, 90% was considered a full charge.

Using the methods outlined, each battery was charged while the voltage on the battery was measured. The resulting charge time for each battery is shown in Table 5.2 and plots of the typical battery charging cycle are shown in Figures 5.20, 5.21, 5.22 and 5.23. Although the larger batteries will reach a charge level of 1.2 volts it is doubtful whether the PZT would supply sufficient current for a full charge of these batteries to be achieved. When comparing the charge times shown in Table 5.2, the resonance and random signal have similar times, this is because the voltage applied to the shaker during the resonance signal was lower than applied during a random

signal. A lower voltage signal was required during resonance to avoid over straining and breaking the PZT. This work provides a platform to build off when using piezoelectric materials to charge batteries. With the battery capacities and their corresponding charge times, this table can be used to determine the ideal battery for a specific application.

Table 5.2: Time required charging different sized batteries using a piezoelectric.

Battery Size (mAh)	**Time for Charge at Resonance**	**Time for Charge with Random Signal**
40	1.62 Hours	1.6 Hours
80	1.2 Hours	2 Hours
200	4 Hours	1.2 Hours
300	6 Hours	5.8 Hours
750	7 Hours	8.6 Hours
1000	22 Hours	32 Hours

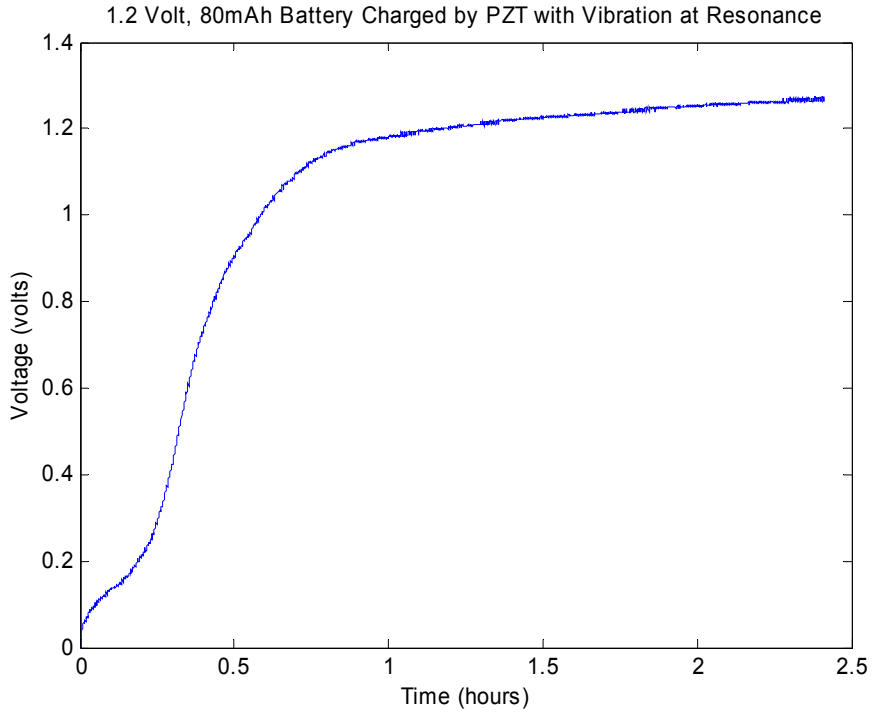

Figure 5.20: Charge history of an 80mAh battery with resonant excitation.

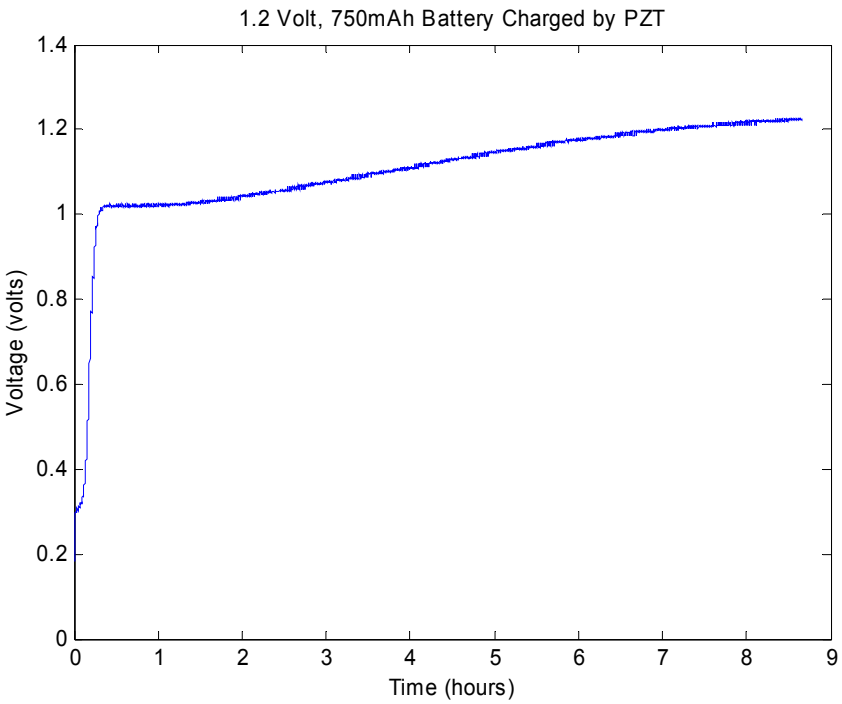

Figure 5.21: Charge history of a 750mAh battery with resonant excitation.

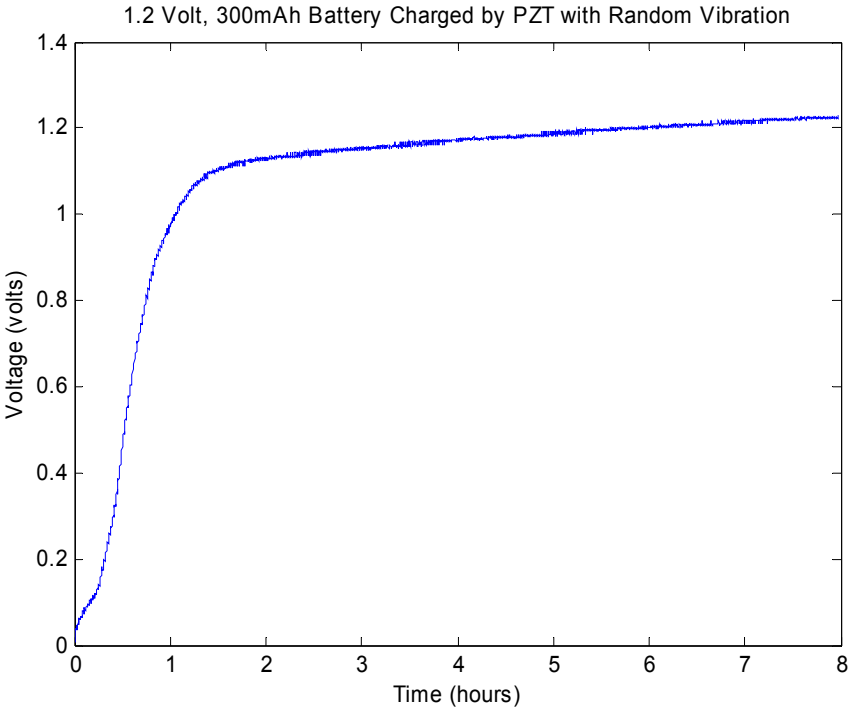

Figure 5.22: Charge history of a 300mAh battery with random excitation.

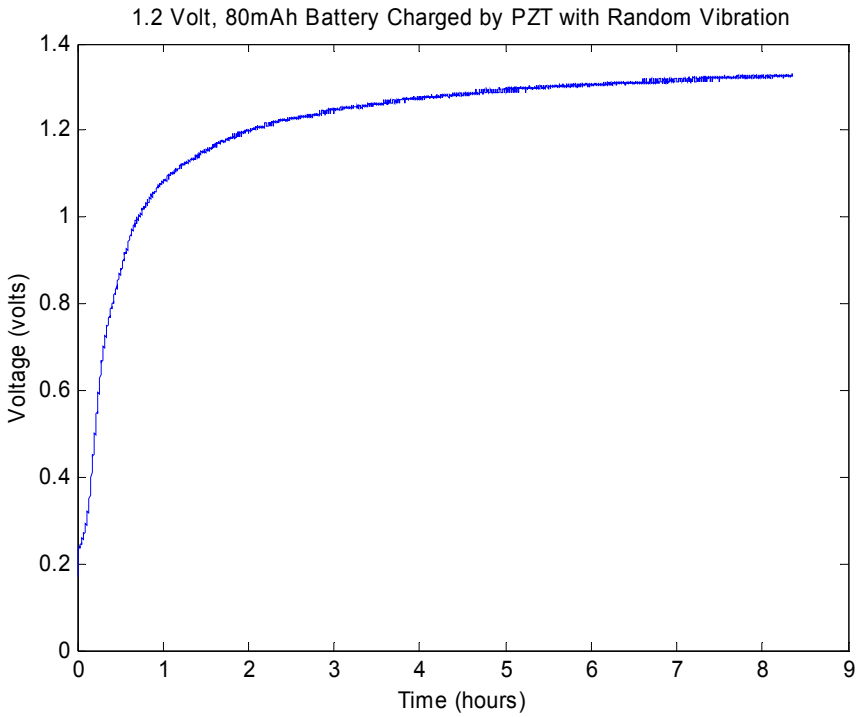

Figure 5.23: Charge history of a 300mAh battery with random excitation.

5.4 Chapter Summary

Power harvesting can be an effective way of prolonging the life of a battery or providing an endless power supply for the life of the electronic device intended to be powered. Power is generated through the piezoelectric effect which allows the material to interchange electric and mechanical energy. In this fashion, the piezoelectric material can absorb the energy around it, usually vibration, and convert it into useful electrical energy. This method of power generation can be effective, although the power supplied directly from the material is usually not normally sufficient to power most electronics. To overcome this issue, methods of accumulating the energy must be developed so that it can be used as an effective power source.

This chapter investigates two methods of storing power generated from piezoelectric materials. The first portion of this work identifies the amount of power capable of being generated from the particular power harvesting plate used. This was done to both determine the maximum power generated and to provide a means of scaling this work to other devices. The

first storage method tested was the use of a capacitor circuit and the second was a nickel metal hydride rechargeable battery. It was found the capacitor method worked well, but the high discharge rate of capacitors do not allow them to output a continuous signal, which is needed for many electronic applications. The second method of power storage tested, was to use rechargeable batteries, however, the concept of using piezoelectric materials to recharge a battery had not previously been shown. Therefore, tests were performed to demonstrate that the power output of a piezoelectric device is compatible with that required by the battery. To do this both random and resonant excitation signals were used. The amplitude of each signal corresponded to the vibration of a typical automobile compressor. Using these signals, it was found that when excited at resonance the plate could charge the battery to its cell voltage in approximately 20 minutes and the random signal could charge the battery in only a few hours. A comparison of these two methods of power storage was also given.

The second portion of this chapter compared the performance of the monolithic piezoceramic (PZT) with the macro-fiber composite (MFC) actuator for power harvesting. To perform this comparison, two plates were constructed, one with a PZT attached and the other with a MFC. The efficiency of each plate was determined and found the MFC to be less efficient than the PZT. While the MFC generates a large output voltage, the current produced is far smaller than that of the PZT; this greatly lowers its performance for power harvesting. This was followed by a detailed reason for the MFC's low current generation. The second test used to compare the two actuators, was to find the range of different capacity batteries that could be charged and the time required for each. However, when charging batteries the current is very important, this fact combined with the low current output of the MFC made it unable to charge a battery. Due to these reasons, it was found that MFC are not suitable for power harvesting. While the MFC was ineffective, the PZT's ability to charge several different size batteries was identified and the time required to charge each battery to about 90% capacity is given. This work shows that the use of rechargeable batteries with piezoelectric power harvesting devices is viable option for accumulating the energy generated to usable levels.

Chapter 6

Conclusions

This thesis has investigated the use of macro-fiber composite (MFC) actuators as sensors, actuators and power harvesting devices. The MFC actuator was recently developed at the NASA Langley Research Center and is constructed using piezoceramic fibers. The fibers are embedded in an epoxy matrix, followed by a Kapton shell. This construction allows the actuator to be extremely flexible and durable, making it ideal for applications such as inflatable satellites and other structures with flexible curved surfaces. In addition, the MFC uses interdigitated electrodes that capitalize on the higher d_{33} piezoelectric coupling coefficient. This allows the piezoelectric to more efficiently interchange electrical and mechanical energy, resulting in higher free strain and blocked force. The scope of the work presented in this thesis was to investigate the ability of the MFC to be used in various applications. This chapter will provide a brief overview of the results found and the contributions made. The chapter will end with a discussion of the future work in these areas.

6.1 Brief Summary of Thesis

The first portion of this thesis was devoted to the use of MFC as sensors and actuators for vibration suppression. Chapter two began this work by investigating the feasibility of the MFC for use in a self-sensing circuit. A self-sensing circuit allows one piezoelectric patch to be used as both a sensor and actuator simultaneously. When the piezoelectric is configured in a self-sensing circuit, the sensor and actuator are perfectly collocated, allowing it to be more effective in certain control techniques that do not require an analytical model, such as direct velocity

feedback and positive position feedback (PPF). The ability to use traditional piezoceramic materials in self-sensing circuit has been shown to be effective in numerous previous studies, but the MFC actuator had never before been shown to be compatible with self-sensing control techniques. Furthermore, the MFC was developed as an actuator, allowing its ability to be used as a sensor to go untested. Therefore, a self-sensing circuit using a MFC actuator was constructed and a PPF control scheme was implemented on an aluminum beam to show its effectiveness for both sensing and vibration suppression. The system used was able to achieve over 80% vibration reduction with an excellent settling time. In addition, a simulation was performed to show the effect of an unbalanced self-sensing circuit; the major concern for it practical use.

After determining the MFC to be an accurate sensor, in chapter 2, it was integrated onto the skin of an inflatable torus to demonstrate control of inflatable structures using multiple sensors and actuators. In previous studies at the Center for Intelligent Materials Systems and Structures (CIMSS) one MFC was shown to globally excite and effectively apply control to an inflated structure. However, these tests were performed on a scaled model of the actual inflated satellite intended for space. While one MFC patch was effective for this smaller structure, the satellites intended for use in space would have diameters as large as 30 meters, making it highly unlikely that one MFC could globally excited such an immense structure. To overcome this issue, control techniques using multiple sensors and actuators must be developed in order to ensure global vibration suppression. One such control system was developed in chapter 3, using PPF control techniques and two pairs of sensors and actuators. It was found that using PPF control and separate sensors and actuators was very efficient for control of certain modes, achieving 70% vibration reduction on the first mode, but ineffective at others due to phase differences between each sensor and actuator. Since the MFC was found to be effective as a self-sensing actuator in chapter 2, it was decided that the best way to control all modes of the structure was to use collocated control with self-sensing actuators. A self-sensing MFC was mounted onto the torus and shown to accurately measure the frequency response. However, the equipment available did not allow vibration suppression to be applied to the structure. Therefore, tests were performed to show that with the necessary equipment, self-sensing MFC actuators could be used for control of inflatable structures.

Following the investigation of MFC for sensing and control, its ability to be used as a power harvesting device was explored. Power harvesting using piezoelectric materials is accomplished by absorbing the mechanical energy around the structure, usually ambient

vibration, and converting it to useful electrical energy that can be used to power other devices. Chapter 4 develops a model to predict the amount of electrical energy produced during the vibration of a piezoelectric patch attached to a beam. The model was found to be very accurate in predicting the amount of energy generated by a composite beam with a complex layout of four piezoelectric patches. Following the development of the power harvesting model, chapter 5 performed an investigation into two methods of storing the generated energy. The motivation for this work was that the energy generated by piezoelectric materials is not sufficient to directly power most electronic devices. Therefore, the energy produced must be accumulated to allow the power harvesting system to function with typical electronics. The first method tested was a capacitor and the second was a rechargeable battery. The energy generated by the piezoelectric materials had never been previously shown to be compatible with the needs of a rechargeable battery. Therefore, tests were performed to demonstrate that they could be used to apply a charge to a battery. After it was found that both methods were compatible with the power generated by the piezoelectric, the advantages of each were discussed. Subsequent to this investigation, the efficiency of both a piezoelectric plate and a MFC plate for converting mechanical vibration into electrical energy was measured. It was found that the MFC was less efficient than the monolithic piezoceramic due to a low current output; reasons for this occurrence were also identified. Because the current output of the MFC was very low, it was unable to charge a battery because of the battery's requirement for a significant amount of current to hold a charge. Since the MFC was unable to charge the battery, only a monolithic piezoceramic was used to charge a variety of different capacity batteries while the charge times were recorded. The resulting charge time for each battery was given.

6.2 Contributions

The macro-fiber composite actuator is a piezoelectric actuator that is constructed using piezofibers embedded in an epoxy matrix with interdigitated electrodes. This actuator holds many advantages over the traditionally used piezoceramic materials. The MFC produces larger strains and blocked force, in addition to being extremely flexible. However, this actuator was recently developed and many of its benefits have not been tested or explored. This thesis has investigated some of its uses and realized some of its previously unknown abilities. The MFC's development was directed toward actuation, allowing its sensing capabilities to go unnoticed. It was found during this work that the MFC holds excellent sensing capabilities that are comparable

with that of traditionally used piezoceramic material. The topics presented in this thesis, deal with this previously unknown ability of the MFC.

The identification of the sensing abilities of the MFC actuator opens many doors for its practical use. The ability to use an MFC as a self-sensing actuator could not be performed without very accurate sensing capabilities. The first portion of this work was to realize collocated control with a self-sensing MFC actuator. This was accomplished and found to be very effective at reducing the vibration of an aluminum beam. Knowing that the MFC is an accurate sensor (comparable to that of the traditionally used piezoceramic material PZT) makes it an ideal choice for this application because of the larger control forces applied to the structure. In addition, the MFC is more easily bonded to surfaces, without the worry of accidental breakage.

Following the realization of the MFC's sensing qualities, it was used as both a sensor and actuator to apply vibration control to an inflatable torus. The work in the area of vibration control of inflatable structures has furthered the field by using multiple sensor and actuator control techniques to attenuate vibration of an inflated torus. Previous studies to suppress the vibration of inflated structures were performed on scaled models that were able to be globally excited from a single MFC patch. However, the structures intend for use in space would have diameters as large as 30 meters, making it highly unlikely that one actuator could excite it. Therefore, the use of control systems using multiple sensors and actuators must be implemented to control the vibration around these structures. The study presented in chapter 3 of this thesis, has shown that multiple sensor and actuator control systems are effective at suppressing the vibration of an inflated torus. However, it was found that the control system used could not control certain modes due to the location of the sensors and actuators not being collocated. To overcome this problem tests were performed to demonstrate that self-sensing techniques could be used with the MFC to apply collocated control of an inflatable structure.

Following the work in control, the thesis moved on to power harvesting. Power harvesting is a field that is growing very quickly due to the advances in low power electronics and wireless technology. Power harvesting using piezoelectric materials is accomplished by taking mechanical energy from around the structure, usually ambient vibration and converting it into electrical energy that can then be used to power other devices. The work presented in chapter 4 developed a model of a power harvesting system. The model was formulated using various other piezoelectric models from earlier studies. However, the model presented here

included one major difference, structural damping was accounted for. If the structural damping was not included then the system would over estimate the amount of energy produced. The addition of this parameter, allowed the model to accuracy predict the power generated from a piezoelectric. This model can be used as a design tool for developing a power harvesting system. With the model in hand, it can reveal the size and location of the piezoelectric as well as the amount of vibration required to generate the desired electrical signal.

One problem that is often encountered when using power harvesting systems is that the energy produced by the piezoelectric material is not sufficient to power most electronics. Therefore, methods of accumulating the energy so that it many be used as a power source need to be developed. The method typically used to accumulate this energy, is a capacitor. However, the capacitor has characteristic that are not ideal for many practical applications. These limitations led me to develop another method of storing the power that would not limit the type of applications that could be powered. The rechargeable battery was an option that had not been looked into by other researchers and possesses the qualities that were needed in a power harvesting system. To shown that the power generated by piezoelectric devices was compatible with rechargeable batteries, a piezoceramic plate was used to charge the battery and the time required was recorded. To charge the battery it was decided that the excitation signal supplied to the piezoelectric plate should not be of resonant nature, but rather a signal that was typical of a mechanical system. Therefore, the vibration signature of a typical automobile compressor was measured in a non-ideal location and used to actuate the piezoelectric. This study found that the vibration of a typical system could indeed recharge a dead battery. Knowing that the power output was compatible with that required by the battery we moved on to using a MFC for charging batteries. However, in doing this it was found that the MFC was incompatible with the requirements of the battery, due to a low current output. Therefore, it was determined that the MFC is not suitable for use as a power harvesting device. Following this finding, various capacity nickel metal hydride batteries were charged to determine the largest battery that could be effectively charged and the charge time for each with both a resonant and random signal. This study provides a basis for other researchers to determine the ideal size battery for there intended application based on the charge time and capacity of the battery.

The advances made from the work presented in this thesis will provide future researchers with the tools necessary to use the macro-fiber composite actuator effectively in numerous applications. The sensing capabilities of the MFC were realized and shown on to be effective as a

self-sensing actuator for collocated control, multiple sensor and actuator control techniques were used to suppress the vibration of inflatable structures allowing control to be extended to real scale satellites, the ability to use the power generated by piezoelectric materials to recharge batteries was discovered and the issues regarding the effectiveness of the MFC as a power harvesting device were discussed. In addition, a model to predict the power generation of a beam with piezoelectric patches attached was derived and shown to be very accurate on a composite beam with complicated piezoelectric layout. These contributions will certainly aid researchers in the future.

6.3 Recommendations for Future Work

While the focus of each topic investigated in this study was completed, there are a few extensions of the work that could be made. The first piece of work that could be performed to further the study in control of inflatable structures would be to obtain the equipment necessary to execute collocated control using self-sensing MFC actuators. During the period of this work, the control board available was not sufficient for the task of applying real time control, because of a 10 volt input limitation that if exceeded would jeopardize the circuitry of the board. The control voltages used to excite the torus were on the order of 700 volts. These high voltages combined with the sometimes unstable nature of the self-sensing circuitry could easily find their way into the board resulting in very expensive damage. Therefore, a method of regulating the input to the control board without jeopardizing its real time control properties must be constructed. Following this a high power self-sensing circuit must be built and used to implement collocated control on the torus.

Additional studies into power harvesting are needed to determine the efficiency of both the MFC and PZT for power harvesting on a level greater than the device level found in these studies. In addition, the studies into recharging batteries using piezoelectric devices were not able to fully charge the battery because a charge controller compatible with the power supply did not exist. Therefore, a charge controller could be constructed to allow the piezoelectric device to fully charge the batteries. This controller would have to be extremely efficient in it use of power as to not significantly reduce the electrical energy supplied to the battery. And lastly the model of a piezoelectric power harvesting beam could be extended to work with plate geometries.

Bibliography

http://www.smart-material.com

http://www.msiusa.com

http:/www.matsysinc.com

Agnes, G.S. and Rogers, J.W., 2000, "Piezoelectric Excitation of Inflatable Space Structures for Modal Testing," Proceedings of SPIE's 7th Annual Smart Materials and Structures Conference, Vol. 3985-88, Newport Beach, CA, pp. 806-819.

Bailey, T. and Hubbard Jr., J.E., 1985, "Distributed Piezoelectric-Polymer Active Vibration Control of a Cantilever Beam," *Journal of Guidance and Control*, Vol. 8, No. 5, pp. 605-611.

Baz, A., Poh, S. and Studer, P., 1987, "Optimum Vibration Control of Flexible Beams by Piezo-Electric Actuators," Proceedings of the Sixth VPI & SU/AIAA Symposium on Dynamics and Control of Large Structures, June 29th-July 1st, Blacksburg, VA, pp. 217-234.

Bent, A.A. and Hagood, N.W., and Rodgers, J.P., 1993a, "Anisotropic Actuation with Piezoelectric Fiber Composites," Presented at the fourth International Conference on Adaptive Structures, November 2-4th, Cologne, Federal Republic of Germany.

Bent, A.A. and Hagood, N.W., 1993b "Development of Piezoelectric Fiber Composites for Structural Actuation," Proceeding of the 34th AIAA/ASME/ASCE/AHS Structures, Structural Dynamics and Materials Conference, April, La Jolla, CA, AIAA Paper No. 93-1717-CP pp. 3625-3638.

Bent, A.A., Hagood, N.W. and Rodgers, J.P., 1995, "Anisotropic Actuation with Piezoelectric Fiber Composites," *Journal of Intelligent Material Systems and Structures*, Vol. 6, No. 3, pp. 338-349.

Bent, A.A., "Piezoelectric Fiber Composites for Structural Actuation," Master of Science Thesis, Massachusetts Institute of Technology, January 1994.

Bent, A. A., "Active Fiber Composites for Structural Actuation," Doctor of Philosophy Dissertation, Massachusetts Institute of Technology, January 1997.

Briand, G., Wicks, A.L. and Inman, D.J., 2000, "Vibration Testing for Control of Inflated Objects," Proceedings of the 18th International Modal Analysis Conference, San Antonio, Texas, February.

Chopra, I., 2002, "Review of State of Art Smart Structures and Integrated Systems," *AIAA Journal*, Vol. 40, No. 11, pp. 2145-2187.

Crawley, E. and Anderson, E., 1990, "Detailed Models of Piezoceramic actuation of beams," *Journal of Intelligent Material Systems and Structures*, Vol. 1, No. 1, pp. 4-25.

Crawley, E.F. and de Luis, J., 1985, "Use of Piezo-Ceramics as Distributed Actuators in Large Space Structure," Proceeding of the 26th AIAA/ASME/ASCE/AHS Structures, Structural Dynamics and Materials Conference, April 15-17th, Orlando, Florida, pp. 126-133.

Döngi, F., Dinkler, D. and Kröplin, B., 1995, "Active Panel Flutter Suppression using Self-Sensing Piezoactuators," AIAA Paper No. 95-1078, Proceeding of the 36th AIAA/ASME/ASCE/AHS/ASC Structures, Structural Dynamics and Materials Conference, April 10-13th, New Orleans, LA, pp. 2264-2272.

Dosch, J.J., Inman, D.J. and Garcia, E., 1992, "A Self-Sensing Actuator for Collocated Control," *Journal of Intelligent Materials Systems and Structures*, Vol. 3, pp. 166—185.

Elvin, N., Elvin, A., and Spector, M., 2000, Implantable Bone Telemetry Sensing System and Method," United States Patent No. 6,034,296.

Fanson, J.L. and Caughey,T.K., 1987, "Positive Position Feedback Control for Large Space Structures," AIAA Paper No. 87-0902, Proceeding of the 28th AIAA/ASME/ASCE/AHS Structures, Structural Dynamics and Materials Conference, April 9-10th, Monterey, CA, pp. 588-598.

Frampton, K.D., Clark, R.L. and Dowell, E.H., 1995, "Active Control of Panel Flutter with Linearized Potential Flow Aerodynamics," AIAA Paper No. 95-1079, Proceeding of the 36th AIAA/ASME/ASCE/AHS/ASC Structures, Structural Dynamics and Materials Conference, April 10-13th, New Orleans, LA, pp. 2273-2280.

Freeland, R.E., Bilyeu, G.D. Veal, G.R. and Mikulas, M.M., 1998, "Inflatable Deployable Space Structures Technology Summary," International Astrological Association.

Gebhardt, S. and Schönecker, A., 1999, "Fine Scale Piezoelectric 1-3 Composites by Soft-Molding" *Materials Mechanics, Fracture Mechanics, Micro Mechanics*, Preprint

Gentilman, R., McNeal, K. and Schmidt, G., 2003, "Enhanced Performance Active Fiber Composites," Proceedings of SPIE's 10th Symposium on Smart Structures and Materials Conference, March 6, 2003.

Griffith, D.T. and Main, J.A., 2000, "Modal Testing of an Inflated Thin Film Polymide Torus Structure," Proceedings of the 18th International Modal analysis Conference, San Antonio, Texas, Febuary.

Hagood, N.W., Chung, W.H. and Von Flotow, A. 1990, "Modeling of Piezoelectric Actuator Dynamics for Active Structural Control," *Journal of Intelligent Materials Systems and Structures*, Vol. 1, pp. 327-354.

Hanagud, S., Obal, M.W. and Meyyappa, M., 1985, "Electronic Damping Techniques and Active Vibration Control," Proceeding of the 26th AIAA/ASME/ASCE/AHS Structures, Structural

Dynamics and Materials Conference, April 15-17th, Orlando, Florida, AIAA Paper No. 85-0752, pp. 126-133.

Hausler, E. and Stien, E., 1984, "Implantable Physiological Power Supply with PVDF Film," *Ferroelectrics*, Vol. 60, pp. 277-282.

Inman, D.J. and Cudney, H.H., 2000, "Structural and Machine Design using Piezoceramci Materials – A Guide for Structural Design Engineers," Final Report to NASA Research Center, April.

Inman, D.J., 2001, Engineering Vibration," Prentice-Hall, Inc., Upper Saddle River, New Jersey.

Janos, B.Z. and Hagood, N.W., 1998, "Overview of Active Fiber Composite Technologies," Proceeding of the 6th International Conference on New Actuators-ACTUATOR 98, June, Berlin, Germany.

Jha, A.K., 2002, "Vibration Analysis and Control of an Inflatable Toroidal Satellite Component Using Piezoelectric Actuators and Sensors," Doctor of Philosophy Dissertation, Virginia Polytechnic Institute and State University, July.

Jha, A.K. and Inman, D.J., 2002, "Piezoelectric Actuator and Sensor Model for an Inflated Toroidal Shell," *Mechanical Systems and Signal Processing*, Vol. 16, No. 1, pp. 97-122.

Kimura, M., 1998, "Piezoelectric Generation Device," United States Patent Number 5,801,475.

Kymissis, J., Kendall, D., Paradiso, J. and Gershenfeld, N., 1998, "Parasitic Power Harvesting in Shoes," Second IEEE International Conference on Wearable Computing, August, pp. 132-336.

Lee, C.K., Chiang, W.W. and O'Sullivan, T.C., 1989, "Piezoelectric Modal Sensors and Actuators Achieving Critical Active Damping on a Cantilever Plate," AIAA Paper No. 89-1390-CP, Proceeding of the 30th AIAA/ASME/ASCE/AHS Structures, Structural Dynamics and Materials Conference, Mobile, Alabama, April 3-5th, pp. 2018-2026.

Leigh, L., Hamidzadeh, H., Tinker, M. and Slade, K.N., 2001, "Dynamic Characterization of an Inflatable Concentrator for Solar Thermal Propulsion," AIAA Paper No. 2001-1406, Proceeding of the 42nd AIAA/ASME/ASCE/AHS/ASC Structure, Structural Dynamics, and Material Conference and Exhibit, Seattle, WA, April 16-19.

McEver, M.A., 1999, "Optimal Vibration Suppression Using On-Line Pole/Zero Identification," Masters Thesis, Virginia Polytechnic Institute and State University.

Nishigaki, T. and Endo, M., 2000, "A Self-Sensing Actuator Using Piezoelectric Films with Different Thickness Control of Curved Structures," Proceedings of the 11th International Conference on Adaptive Structures and Technologies, October 23-26th,

Okugawa, M. and Sasaki, M., 2002, "System Identification and Design of a self-Sensing Piezoelectric Cantilever Structure," Journal of Intelligent Material Systems and Structures, Vol. 13, No. 4, pp.241-252.

Ottman, G.K., Hofmann. H., Bhatt, C.A. and Lesieutre, G.A., 2002, "Adaptive Piezoelectric Energy Harvesting Circuit for Wireless, Remote Power Supply," *IEEE Transactions on Power Electronics*, Vol. 17, No. 5, pp. 1-8.

Park, G., Kim, M.H. and Inman, D.J., 2001, "Integration of Smart Materials into Dynamics and Control of Inflatable Space Structures," Journal of Intelligent Materials Systems and Structures, Vol. 12, No. 6, pp. 423-433.

Park, G., Ruggiero, E. and Inman, D.J., 2002, "Dynamic Testing of Inflatable Structures Using Smart Materials," *Journal of Smart Materials and Structures*, Vol. 11, pp. 1-9.

Preliminary Mission Report, "Spartan 207/Inflatable Antenna Experiment Flown on STS-77," Spartan Project, Code 740.1, NASA Gaddard Space Flight Center, Greenbelt, MD, Febuary 14, 1997.

Ruggiero, E., Park, G., Inman, D.J. and Main, J.A., 2002, "Smart Materials in Inflatable Structure Applications," AIAA Paper No. 2002-1563, Proceeding of the 43rd

AIAA/ASME/ASCE/AHS/ASC Structures, Structural Dynamics, and Materials Conference, AIAA Gossamer Spacecraft Forum, April 22-25, Denver, CO.

Slade, K.N., Tinker, M.L., Lassiter, J.O. and Engberg, R., 2001, "Dynamics of an Inflatable Structure in Vacuum and Ambient Conditions," *AIAA Journal*, Vol. 39, No. 5, pp. 894-901.

Smits, J., Drake, S., and Cooney, T.K., 1991, "The Constitutive Equations for Piezoelectric Bimorphs," *Sensors and Actuators*, Vol. 28, pp. 41-61.

Starner, T., 1996, "Human-Powered Wearable Computing," *IBM Systems Journal*, Vol. 35, pp. 618-629.

Tinker, M.L., 1998, "Passively Adaptive Inflatable Structure for the Shooting Star Experiment," AIAA paper No. 98-1986, pp. 2320-2326.

Umeda, M., Nakamura, K. and Ueha, S., 1996, "Analysis of Transformation of Mechanical Impact Energy to Electrical Energy Using a Piezoelectric Vibrator," *Japanese Journal of Applied Physics*, Vol. 35, Part 1, No. 5B, pp. 3267-3273.

Umeda, M., Nakamura, K. and Ueha, S., 1997, "Energy Storage Characteristics of a Piezo-Generator Using Impact Induced Vibration." *Japanese Journal of Applied Physics*, Vol. 35, Part 1, No. 5B, pp. 3146-3151.

Vipperman, J.S. and Clark, R.L., 1996, "Complex Adaptive Compensation of Nonlinear Piezoelectric Sensoriactuator," AIAA Paper No. 96-1266, Proceeding of the AIAA/ASME/AHS Adaptive Structures Forum, Salt Lake City, UT, April 18-19th, pp. 1-11.

Wilkie, W.K., Bryant, R.G., High, J.W., Fox, R.L., Hellbaum, R.F., Jalink, A., Little, B.D., and Mirick, P.H., "Low-Cost Piezocomposite Actuator for Structural Control Applications," Proceedings of 7th SPIE International Symposium on Smart Structures and Materials, Newport Beach, CA, March 5-9, 2000.

Wilkie, W.K., Bryant, G.R., High, J.W. et al., "NASA-Langley Research Center Macro-Fiber Composite Actuator (LaRC-MFC): Technical Overview."

Williams, B.R., Park, G., Inman, D.J. and Wilkie, W.K., 2002, "An Overview of Composite Actuators with Piezoceramic Fibers," Proceeding of the 20th International Modal Analysis Conference.

Williams, B.R., Grimsley, B.W., Inman, D.J. and Wilkie, W.K., 2002, "Manufacturing and Mechanics-Based Characterization of Macr0 Fiber Composite Actuators," Proceedings of the ASME International Mechanical Engineering Conference and Exposition, New Orleans, Louisiana, November 17-22, 2002

Appendix A

Matlab Code and Simulink Model Used to Simulate the Effects of an Unbalanced Circuit of the Effectiveness of a Self-Sensing Actuator

```
%%%%%%%%%%%%%%%%%%%%%%%%%%%%%%%%%%%%%%%%%%%%
% This code develops the necessary parameters and functions
% to allow the Simulink program to run.
%%%%%%%%%%%%%%%%%%%%%%%%%%%%%%%%%%%%%%%%%%%%

clear all
close all

%%%%%%%%%%%%%%%%%%%%%%%%%%%%%%%%%%%%%%%%%%%%
% Define beam parameters and piezoelectric Properties
%%%%%%%%%%%%%%%%%%%%%%%%%%%%%%%%%%%%%%%%%%%%

n=10;          % Number of modes to be considered

% Beam Properties

Lb=450e-3;                  % Length of beam
wb=52e-3;                   % Width of beam
tb=3e-3;                    % Thickness of beam
Eb=6.9e10;                  % Modulus of beam
rhob=2.7e3;                 % Density of beam
Ab=tb*wb;                   % Area of beam
Ib=tb^3*wb/12;              % Area moment of inertia


% PZT Properties

d31=-190e-12;               % PZT coupling coefficient use PZT 5H
Ep=50e9;                    % Modulus of PZT
wp=20.574e-3;               % Width of PZT
tp=0.127e-3;                % Thickness of PZT
Llp=45.974e-3;              % Length of PZT
g31=-11.6e-3;                       % Voltage constant
Cpo=d31*Llp*wp/tp/g31;              % Original capacitance of PZT
```

```
Cp=Cpo+0.011*Cpo;                    % Percent change in capacitance to cause imbalance

% Define the actuator and sensor location, they are collocated

PZTloc=[17e-3; 17e-3+Llp; 17e-3; 17e-3+Llp];

% Define Electric components of the self-sensing circuit

C3=Cpo;
C2=.28e-6;
R=1.6e6;

% Weighted natural frequencies of a clamped-free long slender beam

Bn=[1.87510407 4.69409113 7.85475774 10.99554073 14.13716839]/Lb;

% Loop generates the weighted frequencies higher than the first five
if n>5;
  for k=6:n
    Bn(k)=(2*k-1)*pi/(2*Lb);
  end
end

% The natural frequencies of the beam are calculated
Bn=Bn(1:n);
wn=Bn.^2*sqrt(Eb*Ib/(rhob*Ab));     % Natural Frequencies

% Define the Mode shapes and set them to be Orthogonal

syms x real

modes= (sin(Bn*x)-sinh(Bn*x)).*(sin(Bn*Lb)-sinh(Bn*Lb))+ ...
      (cos(Bn*x)-cosh(Bn*x)).*(cos(Bn*Lb)+cosh(Bn*Lb));
```

```
Intmodes=double(int(modes.^2,x,0,Lb));        % Integrate the mode shapes along
                                              % the length of the beam

An=sqrt(1./Intmodes);                 % Normalized coefficient
omodes=An.*modes;                     % Orthonomal eigenvectors
omodesd=diff(omodes,x);                 % derivatives of mode shapes

% Define the sensor constants

yc=(tp/2+tb/2);
Ks=d31*yc*Ep*wp/Cp;

% Define the actuator constants

Ka=d31*Ep*wp/(2*tp)*(2*yc*tp);
Kad=-d31*Ep*wp/(2*tp)*(2*yc*tp);

%Sensor curvature

Wsn=double(limit(omodesd,x,PZTloc(2))-limit(omodesd,x,PZTloc(1)));

%Actuator curvature

Wan=double(limit(omodesd,x,PZTloc(4))-limit(omodesd,x,PZTloc(3)));

%%%%%%%%%%%%%%%%%%%%%%%%%%%%%%%%%%%%%%%%%%%%%%%%%%%%
Formulate the state space matrix defining the vibration of the beam
%%%%%%%%%%%%%%%%%%%%%%%%%%%%%%%%%%%%%%%%%%%%%%%%%%%%

zeta=0.005;               % Assumed modal damping

A=[zeros(n) eye(n); -diag(wn.^2) diag(-2*zeta*wn)];
B=[zeros(n,1); 1/rhob/Ab*Ka*Wan'];        % For the use of w/o Simulink
B1=[zeros(n); 1/rhob/Ab*eye(n)];
```

```
C=[Ks*Wsn zeros(1,n)];
C1=[eye(n) zeros(n)];
D=zeros(size(C,1),size(B,2));
D1=zeros(size(C1,1),size(B1,2));

sys_ol=ss(A,B,C,D);        % Final model of the system detailing the dynamics
                           % of PZT and the beam

% Convert voltage to moment or strain to volts

v2m_d=[Kad*Wan'];          % For disturbance
v2m_c=[Ka*Wan'];           % For control input
s2v=[Ks*Wsn];              % Change to voltage

Fs=20000;                  % Sampling frequency in Hz
dT=1/Fs;                   % Sampling time

t1=0; tf=5-dT;             % Simulation parameters
ts=t1:dT:tf;               % Simulation parameters

NFFT=length(ts);

a=1;                       % Magnitude of the applied voltage
VVV=a*chirp(ts,0, tf, 3500);

VFc=fft(VVV,NFFT);

f=Fs*(0:NFFT/2)/NFFT;      % frequency of interest in Hz
ww=2*pi*f;
ww(1)=0.000001;

Hsys=freqresp(sys_ol,ww);
Hsys=squeeze(Hsys);
```

```
% Convert voltage to moment or strain to volt

v2m_d=[Kad*Wan'];                % for disturbance
v2m_c=[Ka*Wan'];                 % for control input
s2v=[Ks*Wsn];                    % change to voltage

znf=.3;
wnf=wn(1)*1.3;

% Set the simulation gain
g=100;
```

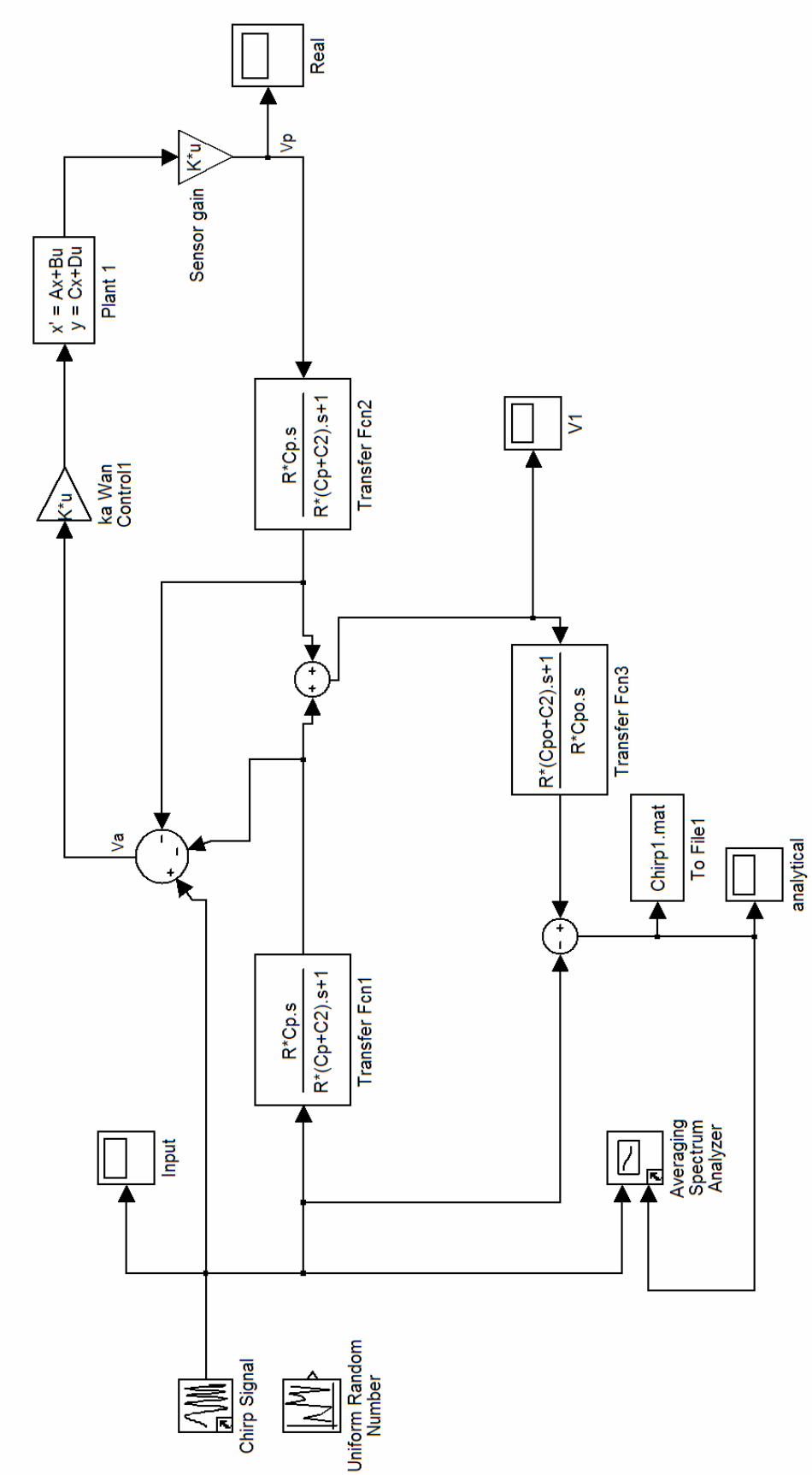
Real
Vp
K*u
Sensor gain
x' = Ax+Bu
y = Cx+Du
Plant 1
K*u
ka Wan
Control1
R*Cp.s
R*(Cp+C2).s+1
Transfer Fcn2
V1
R*(Cpo+C2).s+1
R*Cpo.s
Transfer Fcn3
Va
Chirp1.mat
To File1
analytical
R*Cp.s
R*(Cp+C2).s+1
Transfer Fcn1
Input
Averaging
Spectrum
Analyzer
Chirp Signal
Uniform Random
Number

Appendix B

Matlab Code Used to Simulate the Power Generated from a Beam with Piezoelectric Patches Attached

```
%%%%%%%%%%%%%%%%%%%%%%%%%%%%%%%%%%%%%%%%%%%%%%%%%%%%%%%
% --- Program simulates the vibration a beam with piezoelectric
% --- Patches attached, and returns the beams frequncy response,
% --- impulse response and amount of power generated
%%%%%%%%%%%%%%%%%%%%%%%%%%%%%%%%%%%%%%%%%%%%%%%%%%%%%%%

clear all
close all

% --- Define Beam Properties
wth=25.4e-3;        % width
dth=.254e-3;        % depth
Lb=92.6e-3;         % length of the beam

I=(wth*dth^3)/12;              % Moment of Inertia
AA=(wth*dth);                  % Cross-sectional Area of Beam
NuBeam=0.33;                   % Poisson's Ration
rhoBeam=4889;                  % Aluminum Beam density (kg/m^3)
EBeam=3.4*10^10;               % Modulus of Aluminum Beam
c=sqrt(EBeam*I/rhoBeam/AA);

% --- Define Piezoelectric Properties
tPZT=0.254e-3;                 % Thickness of PZT
wthPZT=20.574e-3;              % Width of PZT
K3=1800;                       % Dielectric Constant
Sigma=K3*8.85e-12;             % Dielectric Permittivity
rhoPZT=4889;                   % Piezo Density (kg/m^3)
EPZT=3.4*10^10;                % Modulus of PZT
d31=-179e-12;                  % Piezoelectric coefficient (m/v)
g31=-11.0e-3;                  % Piezoelectric Voltage Coefficient
NuPZT=0.31;                    % Poisson's Ration

% --- Weighted Natural Frequencies of a Cantilever Beam
betan=[1.87510407 4.69409113 7.85475744 10.99554073]'./Lb;
```

```
wn=betan.^2*c;          %Calculate the Undamped Natural Frequencies
n=length(betan);
freq=wn/2/pi

syms x real y z a b

SIG=[0.7340955 1.018467 0.999224497 1.0];
modes= (sin(betan*x)-sinh(betan*x)).*(sin(betan*Lb)-sinh(betan*Lb))+ ...          %Define Mode Shapes
   (cos(betan*x)-cosh(betan*x)).*(cos(betan*Lb)+cosh(betan*Lb));                  %Define Mode Shapes
Intmodes=double(int(modes.^2,x,0,Lb));
An=sqrt(1./Intmodes);                          % Normalized cofficient
omodes=An.*modes;                              % Orthonomal eigenvectors
omodesdd=diff(diff(omodes,x));

% --- Generate and Plot the Mode Shapes
xnum=0:.0001:Lb;
xnum1=Lb-45.974e-3:.000001:Lb;
xnum2=0:.000001:38.94e-3;

PhiT=omodes.';
PhiddT=omodesdd.';

i=0;
for i=1:length(PhiT)
   Phiw=subs(PhiT(1,i),xnum)';
   Phi2=trapz(xnum,Phiw);
   Phi(:,i)=Phiw;
end
plot(xnum,Phi(:,1),xnum,Phi(:,2),xnum,Phi(:,3),xnum,Phi(:,4))

%%%%%%%%%%%%%%%%%%%%%%%%%%
% --- Mass Matrices
%%%%%%%%%%%%%%%%%%%%%%%%%%
```

```
% --- Mass of Beam
Ms1=wth*rhoBeam*PhiT.'*PhiT*dth;
q=0;
p=0;
for q=1:4
   for p=1:4
      Msw=subs(Ms1(q,p),xnum)';
      Msi=trapz(xnum,Msw);
      Ms(q,p)=Msi;
   end
end

% --- Mass of Piezoelectric
Mp1=vpa(int(wthPZT*rhoPZT*PhiT.'*PhiT,y,-dth/2-tPZT,-dth/2));
Mp2=vpa(int(wthPZT*rhoPZT*PhiT.'*PhiT,y,dth/2,dth/2+tPZT));
Mp3=Mp2+Mp1;
q=0;
p=0;
for q=1:4
   for p=1:4
      Mpw1=subs(Mp3(q,p),xnum1)';
      Mpw2=subs(Mp3(q,p),xnum2)';
      Mpi1=trapz(xnum1,Mpw1);
      Mpi2=trapz(xnum2,Mpw2);
      Mpi=Mpi1+Mpi2;
      Mp(q,p)=Mpi;
   end
end

%%%%%%%%%%%%%%%%%%%%%%%%%%
% --- Stiffness Matrices
%%%%%%%%%%%%%%%%%%%%%%%%%%
```

```
% --- Stiffness of Beam
cs=EBeam;
cE=EPZT;
Ks1=vpa(int(wth*y^2*PhiddT.'*cs*PhiddT,y,-dth/2,dth/2));
q=0;
p=0;
for q=1:4
   for p=1:4
      Ksw=subs(Ks1(q,p),xnum)';
      Ksi=trapz(xnum,Ksw);
      Ks(q,p)=Ksi;
   end
end

% --- Stiffness of Piezoelectric
Kp2=vpa(int(2*wthPZT*cE*y^2*PhiddT.'*PhiddT,y,dth/2,dth/2+tPZT));
q=0;
p=0;
for q=1:4
   for p=1:4
      Kpw1=subs(Kp2(q,p),xnum1);
      Kpw2=subs(Kp2(q,p),xnum2);
      Kpi1=trapz(xnum1,Kpw1);
      Kpi2=trapz(xnum2,Kpw2);
      Kpi=Kpi1+Kpi2;
      Kp4(q,p)=Kpi;
   end
end
Kp=Kp4

%%%%%%%%%%%%%%%%%%%%%%%%%%%%%%%%%%%%%%%%%%%%%%%%%%%%%%%%%%%%%%%%%%%%%%%%%%%%
% --- Piezoelectric and Substrate Interaction Term
%%%%%%%%%%%%%%%%%%%%%%%%%%%%%%%%%%%%%%%%%%%%%%%%%%%%%%%%%%%%%%%%%%%%%%%%%%%%
T1=vpa(int(-y*wthPZT*PhiddT.'*cE*d31*(1/tPZT),y,-dth/2-tPZT,-dth/2));
```

```
T3=2*T1;
n=0;
for n=1:4;
   T41=subs(T3(n,1),xnum1);
   T42=subs(T3(n,1),xnum2);
   Theta2=trapz(xnum1,T41);
   Theta3=trapz(xnum2,T42);
   Theta1=Theta2+Theta3;
   Theta(n,1)=Theta1;
end

%%%%%%%%%%%%%%%%%%%%%%%%%
% --- Capacitance Term
%%%%%%%%%%%%%%%%%%%%%%%%%
Cp=wthPZT*(2/tPZT)*Sigma*Lb-wthPZT*(2/tPZT)*Sigma*Lb/10

%%%%%%%%%%%%%%%%%%%%%%%%%
% --- Proportional Damping
%%%%%%%%%%%%%%%%%%%%%%%%%
zeta=[0.0396; 0.0331; 0.04079; 0.0158];
Wnd=[219.91; 1240; 4209.7; 904]*2*pi;
[a,b]=solve('0.0369=a/2/219.91+b*219.91/2', '0.0331=a/2/1228.36+b*1228.36/2');
Damping1=a*(Ms+Mp)+b*(Ks+Kp);
Damping=eval(Damping1);
Damping(1,1)=Damping(1,1)-1;
Damping(2,2)=Damping(2,2)-6;
Damping(3,3)=Damping(3,3)-40;

%%%%%%%%%%%%%%%%%%%%%%%%%
% --- Forcing Term
%%%%%%%%%%%%%%%%%%%%%%%%%
R=10.01e3;              % Resistance
w=25*2*pi;              % Forcing frequency (rad/sec)
Amp=3.79e-4;            % Amplitude of Force
```

```
% --- Calculate the Effect of the Force on the Beam
F1=vpa(int(int(PhiT.'*rhoBeam*w^2*Amp,z,0,wth),y,-dth/2,dth/2));
F2=vpa(int(int(PhiT.'*rhoPZT*w^2*Amp,z,0,wth),y,-dth/2-tPZT,-dth/2)+...
   int(int(PhiT.'*rhoPZT*w^2*Amp,z,0,wth),y,dth/2,dth/2+tPZT));
F3=F1+F2;
n=0;
for n=1:4;
   F4=subs(F3(n,1),xnum);
   Force1=trapz(xnum,F4);
   Force(n,1)=Force1;
end

%%%%%%%%%%%%%%%%%%%%%%%%%%%%%%%%%%%%
% --- Define State Space Matrices
%%%%%%%%%%%%%%%%%%%%%%%%%%%%%%%%%%%%
koverm=-inv(Ms+Mp)*(Ks+Kp)+Theta*inv(Cp)*Theta';
Minv=inv(Ms+Mp);
MinvTheta=Minv*Theta;
Dam=-Minv*Damping;

A=[0 0 0 0 1 0 0 0 0; 0 0 0 0 0 1 0 0 0; 0 0 0 0 0 0 1 0 0; 0 0 0 0 0 0 0 1 0;...
      koverm Dam MinvTheta*inv(Cp);(inv(Cp)*Theta')/R 0 0 0 0 -inv(Cp)/R];

B=[0; 0; 0; 0; Minv*Force; 0];

C=[(inv(Cp)*Theta')/R 0 0 0 0 -inv(Cp)/R];                    % Matrix to output Current

C=[0 0 0 0 Phi(927,1) Phi(927,2) Phi(927,3) Phi(927,4) 0];    %Matrix to output Displacement

D=0;

%%%%%%%%%%%%%%%%%%%%%%
% --- Run Simulation
```

```
%%%%%%%%%%%%%%%%%%%%%%
SYS=ss(A,B,C,D);
t=0:.00001:1.6;
wt=w*t;

% --- Plot the Time response of Simulation and Experiment
figure(1)
Current=lsim(SYS,sin(wt),t);
plot(t,Current*1000)
hold on

% --- Load Experimental Data
load ACX_Time_25Hz_10kR_Big.vna -mat
time=SLm.tdxvec;
voltage=SLm.scmeas(3).tdmeas;
plot(time,(voltage/R)*1000,'r')
legend('Model','Experimental')
title('Output Current of Beam from model and Experimental Data at 25 Hz across 10 k\Omega Resistor')
xlabel('Time (sec)')
ylabel('Current (mA)')

% --- plot the Impulse Response
figure(2)
impulse(SYS,t)
gtext('1 k\Omega Resistance')


figure(3)
Wrange=.1:.5:6300;
[Mag,Phase]=bode(SYS,Wrange);

% --- Loop to reduce the Magnitude matrix down to plottable size
for j=1:length(Wrange)
   Mag1(:,j)=Mag(:,:,j);
```

```
end

% --- Plots the Frequency Response Function
plot(Wrange/(2*pi), 20*log10(Mag1))
hold on

% --- Load Experimental Data
load ACX_FRF_Velocity.vss -mat

% --- Plot the Experimental and Simulation Frequency Response
figure(3)
plot(Fvec,20*log10(abs(XferDat*.1124))-26.8)
```

Vita

Henry Sodano was born on October, 4 1979 to parents Henry and Peggy Sodano in Fairfax, Virginia. He graduated from Robinson Secondary School in June 1998 and began has first year of collage with a major of Mechanical Engineering at Virginia Tech in August of that year. Following four years of undergraduate study he received his Bachelors of Science in Mechanical Engineering in May of 2002. Following his undergraduate program he was invited to perform summer research at the Center for Intelligent Material Systems and Structures (CIMSS) at Virginia Tech. The work that he performed during that summer, earned him a graduate research position, and he began work on his master's degree in the fall of 2002 under the direction of Dr. Daniel J. Inman. His research focus was in vibration control of inflatable space structures and power harvesting using piezoelectric materials. In April of 2003 during the pursuit of his mater's degree, Henry was awarded a NASA Graduate Student Research Program fellowship (GSRP) to fund his efforts towards a Doctorate of Philosophy in Mechanical Engineering beginning is August of 2003.

Address: Center for Intelligent Material Systems and Structures
310 Durham Hall
Virginia Polytechnic Institute
Blacksburg, VA 24061